RECENT GEODYNAMO SIMULATIONS AND OBSERVATIONS OF THE GEOMAGNETIC FIELD

Masaru Kono
Institute for Study of the Earth's Interior
Okayama University
Misasa, Tottori-ken, Japan

Paul H. Roberts
Institute of Geophysics and Planetary Physics
University of California
Los Angeles, California, USA

Received 26 April 2001; revised 17 March 2002; accepted 5 August 2002; published 31 December 2002.

[1] In 1995, two groups [*Kageyama et al.*, 1995; *Glatzmaier and Roberts*, 1995a, 1995b] reported results of numerical integrations of fully three-dimensional, fully nonlinear dynamos. Their papers were precursors of a stream of such models that have focused particularly on the geodynamo. They provide us, in unprecedented detail, with spectacular realizations of interesting geomagnetic field behaviors, such as secular variation and even polarity reversals. The proliferation of models has, however, created some confusion and apparently conflicting results. This can be partly attributed to the different ways in which different groups have modeled the core, normalized their equations, defined their dimensionless parameters, chosen their boundary conditions, and selected their energy sources. This has made it difficult to compare the results of different simulations directly. In this paper, we first try, as far as possible, to overcome this difficulty, so that all reported results can be compared on common ground. We then review the results, emphasizing three major topics: (1) onset and evolution of convection, (2) character of the magnetic field generated, and (3) comparison with the observed geomagnetic field. Although there are large differences in the way that the simulations are defined, the magnetic fields that they generate have some surprising similarities. The fields are dominated by the axial dipole. In some models they are most strongly generated in shear layers near the upper and lower boundaries and near the tangent cylinder, an imaginary surface touching the inner core on its equator. Convection rolls occur within which a type of the α effect distorts the toroidal field lines to create poloidal magnetic field. Some features of the models are found to strongly affect the fields that they produce. In particular, the boundary conditions defining the energy flow (e.g., an inhomogeneous heat flux or distribution of buoyancy sources) are very influential and have been extensively studied. They change the frequency and the mode of magnetic polarity reversals as well as the ratio in strengths of the dipole and nondipole moments. As the ultimate goal of geodynamo simulations is to explain the features of the real geomagnetic field, it is essential that proper comparisons be made between simulation results and observations. It is remarkable that polarity reversals reminiscent of the paleomagnetically observed field reversals have already been simulated by some of the models. Other features such as drift of the field, its secular variation, and statistical properties of Gauss coefficients are discussed in this paper and are compared with observations. These comparisons are rather primitive, not only because self-consistent dynamo models are still too new and too few but also because many of the observations (and especially the paleomagnetic data) are themselves not yet reliable or decisive enough. The aim of the third part of this paper is therefore more to demonstrate the potential use of simulations than to elucidate the nature of geomagnetic field generation.
INDEX TERMS: 1510 Geomagnetism and Paleomagnetism: Dynamo theories; 1522 Geomagnetism and Paleomagnetism: Paleomagnetic secular variation; 1560 Geomagnetism and Paleomagnetism: Time variations—secular and long term; 3220 Mathematical Geophysics: Nonlinear dynamics; *KEYWORDS:* dynamo models, numerical simulation, geomagnetic field, magnetic field generation, convection in sphere

Citation: Kono, M., and P. H. Roberts, Recent geodynamo simulations and observations of the geomagnetic field, *Rev. Geophys., 40*(4), 1013, doi:10.1029/2000RG000102, 2002.

1. INTRODUCTION

1.1. Recent Geodynamo Simulations

[2] The geomagnetic field is a manifestation of the magnetic field that accompanies the flow of electricity, in this case in the Earth's core, which, being iron-rich, is a good electrical conductor. It is generally accepted that the electric currents are created by self-excited dynamo action in the Earth's fluid core; this is known as the *geodynamo hypothesis* (terms in italics are defined in the glossary, after the main text). An electric generator, or "dynamo," is a device that creates electric currents through the motion of conductors in the presence of a magnetic field. When this magnetic field is supplied solely by the electric currents themselves, the dynamo is said to be "self-excited." The core provides the moving parts of the geodynamo. It is widely believed (and will be

Table 1. Grouping of the 3-D Dynamo Simulation Results

Group	*Publications*
KS95	*Kageyama et al.* [1995], *Kageyama and Sato* [1997a, 1997b, 1997c], and *Ochi et al.* [1999]
GR95	*Glatzmaier and Roberts* [1995a, 1995b]
GR96	*Glatzmaier and Roberts* [1996a, 1996b, 1997], *Coe et al.* [2000], *Roberts and Glatzmaier* [2000a], and *Glatzmaier et al.* [1999],
KB97	*Kuang and Bloxham* [1997, 1998, 1999] and *Bloxham* [2000a, 2000b]
KAK97	*Kida et al.* [1997], *Kida and Kitauchi* [1998a, 1998b], *Kitauchi and Kida* [1998], and *Ishihara and Kida* [2000]
COG98	*Christensen et al.* [1998, 1999, 2001], *Olson et al.* [1999], and *Kutzner and Christensen* [2000]
SK99	*Sakuraba and Kono* [1999] and *Kono et al.* [2000b]
GBT99	*Grote et al.* [1999, 2000a, 2000b]
KMH99	*Katayama et al.* [1999]

assumed here) that its motion is driven by buoyancy created either by dissolved heat sources (such as ^{40}K) or by the latent heat and light constituents released at the boundary of the inner core as new material freezes onto its surface by the slow cooling of the Earth. The prime aim of geodynamo simulations is to understand the mechanisms that generate the geomagnetic field and its variation with time.

[3] Geodynamo theory and the corresponding dynamo theory for the solar magnetic field had reached a plateau by 1980. Both subjects required three-dimensional (3-D) solutions to be found to the nonlinear equations of magnetohydrodynamics (MHD), which simultaneously determine the magnetic field and the fluid motions. This *MHD dynamo* problem, sometimes also called the "dynamically self-consistent problem," required generous support on the most advanced supercomputers of the day. This was utilized by *Gilman and Miller* [1981] and *Gilman* [1983], whose findings created a marked stir in the solar physics community, as did the subsequent solar model of *Glatzmaier* [1984, 1985a, 1995b]. However, geodynamo theory did not start its upward climb from the plateau until the mid-1990s.

[4] In 1995, *Kageyama et al.* [1995] and *Glatzmaier and Roberts* [1995a, 1995b] published results of their simulations of fully 3-D nonlinear dynamos. The first of these provided insights into field-generating processes; the second was specifically designed with the Earth's magnetic field in mind and was remarkably successful in mimicking some of its observed characteristics, such as its slow *secular variation* and *polarity reversals*. These papers were perceived as the first important steps toward clarification of the physical mechanisms that generate the magnetic fields of the Earth and planets. They set in motion developments that might almost be described as explosive. For the first time in the long history of the study of the geomagnetic field, diverse dynamo models came into existence that answered dynamical questions without making any drastic ad hoc assumptions. In reviewing these developments, we shall focus only on papers that report simulations of truly 3-D and fully nonlinear dynamo models. For the sake of convenience, the papers published so far are grouped as shown in Table 1. Each paper in a group uses the same set of basic equations, the same computational scheme, and parameter values that are not widely different.

1.2. Purpose and Plan of This Review

[5] Dynamo simulations are now clarifying the physical processes on which the generation of the magnetic field depends. If the present rate of progress is sustained, we may hope to soon gain a basic understanding of the mechanisms of magnetic field generation in the planets and satellites of the solar system.

[6] For scientists working on other aspects of the magnetic field of the Earth, dynamo simulations provide a new and unparalleled opportunity of interpreting the observed features of the field in the framework of physical theory. Several models exhibit remarkable time variations (such as polarity reversals) that can be compared with the well-known facts about the actual field observed by geomagnetic and paleomagnetic techniques. It should also be pointed out that when such phenomena are described by dynamo simulations, they are given in much greater detail, both as time series and as distributions over the Earth's surface, than that provided by the actual observations of the geomagnetic field (see section 6).

[7] Comparisons between the different dynamo simulations shown in Table 1 are not completely straightforward. Some of their conclusions are in apparent conflict. The confusion mostly arises from differences in the way the models are defined. However, as dynamo simulation is quite a complex endeavor, it is difficult for nonexperts to judge which differences reflect intrinsically diverse behaviors and which are artifacts.

[8] The primary objective of the present review is to provide a basis for understanding the physical mechanism of dynamo process and to promote interactions between the dynamo theorists and the interested members of the geophysics community. Thus the emphasis throughout is on helping nonspecialists to understand the inner workings of the dynamos and to overcome the difficulties that they face when trying to resolve differences between various models. In other words, we do not aim to describe the state of the art in dynamo simulations, which is of interest mainly to specialists working

close to this branch of geophysics, for whom adequate reviews are often provided [e.g., *Busse*, 2000; *Jones*, 2000; *Roberts and Glatzmaier*, 2000b]. Instead, potential readers of this article are, for instance, paleomagnetists trying to compare the polarity reversals of dynamo models with observed records, seismologists considering the possible effect of lower mantle heterogeneity on core dynamics, and geodynamicists interested in the state of the outer and inner core and their role in the evolution of the Earth.

[9] In section 2, we present the simplest formulation of an MHD dynamo model, which includes the basic equations, the boundary conditions, and the nondimensional parameters that characterize each dynamo solution. The numerical methods used in integrating the differential equations are also briefly summarized in section 2 . Variations in the formulation are described in section 3. By examining the disparities between the reported results, we show how a direct comparison between various simulations is possible once the differences in formulation are properly accounted for. These sections are somewhat technical and may be bypassed if the reader is either already acquainted with, or not interested in, these details.

[10] Sections 4 and 5 describe the style of convection and of magnetic field generation revealed by the MHD simulations. With the knowledge gained from the Earth in mind, in section 6 we discuss what requirements are posed by the observations of the geomagnetic field and how far some of the present dynamo models satisfy them. We also discuss the types of observations needed to constrain future generations of realistic dynamo models better. The main text concludes with section 7, which reviews the present status of the subject and future challenges (see also section 1.3.3). Appendix A summarizes the notation and provides geophysically plausible estimates of the parameters relevant to simulations. The Glossary is a list of frequently used terms.

1.3. Brief Overview of Dynamo Theory

1.3.1. Kinematic Dynamo

[11] Dynamo theory has a long history. The original idea was put forth by *Larmor* [1919] to explain the origin of the strong magnetic fields of sunspots. Not long afterward, *Cowling* [1934] published his famous theorem that a dynamo cannot maintain an axisymmetric field. If we take the symmetry axis to be the polar axis, an axisymmetric field is one whose vertical and horizontal components (B_r, B_θ, B_ϕ) are independent of the longitude ϕ; here (r, θ, ϕ) are spherical coordinates. At first, Cowling's theorem made the dynamo mechanism seem unpromising as an explanation of the cosmic fields, but *Elsasser* [1946] and *Bullard* [1949] continued to have faith in it.

[12] The essential idea behind *Cowling's theorem* may be illustrated by the special case in which both the magnetic field $\bar{\mathbf{B}}$ and the fluid velocity $\bar{\mathbf{V}}$ are axisymmetric. (Axisymmetric fields are here designated by an overbar.) Let these be separated into zonal parts (i.e., $\bar{B}_\phi$ and $\bar{V}_\phi$, in the longitudinal direction) and the remaining meridional parts ($\bar{\mathbf{B}}_M$ and $\bar{\mathbf{V}}_M$. Lines of magnetic force tend to be carried with an electrical conductor as it moves. Although this tendency is imperfect because of the finite electrical conductivity of the medium, it is a useful way of picturing how the motion of a conductor modifies the field that threads it. In particular, when the rate of shear, $\omega \equiv \bar{V}_\phi/s$, is nonzero (where s is distance from the symmetry axis), the zonal motion shears the lines of force $\bar{\mathbf{B}}_M$ to create a component in the longitudinal direction; that is, it generates a zonal field $\bar{B}_\phi$ from $\bar{\mathbf{B}}_M$; this process is often called the ω *effect*. In a successful dynamo the regenerative loop has to be closed by a process that creates $\bar{\mathbf{B}}_M$ from $\bar{B}_\phi$, and no such process exists if the system is totally axisymmetric.

[13] Cowling's antidynamo theorem made it imperative to establish unequivocally that the dynamo process really can generate magnetic fields in a homogeneous electrical conductor such as the Earth's core. The problem was simplified by specifying the fluid motion. The search then became that of selecting a fluid motion that, when fast enough, can self-sustain a magnetic field, i.e., a field that neither decays nor grows in amplitude with time. In attempting to find such a *kinematic dynamo*, *Bullard and Gellman* [1954] devised a spectral method that is still widely in use today, but they were unable to demonstrate dynamo action for the particular form of motion that they selected. It is not definitely established even today whether their motion is capable of maintaining field or not, but with hindsight it is clear that they made a bad choice. Better choices were made by *Herzenberg* [1958] and *Backus* [1958], which allowed them to establish beyond doubt that spherical homogeneous dynamos can, in principle, exist. The velocity fields that they chose were, however, rather artificial. Successful kinematic dynamos that employed more realistic motions were constructed by G. O. Roberts (reported by *Roberts* [1971]), *Pekeris et al.* [1973], and *Kumar and Roberts* [1975]. The first of these showed that Cowling's theorem does not forbid kinematic dynamos in which the fluid motions are axisymmetric; such motions can maintain nonaxisymmetric (asymmetric) magnetic fields. See also *Gubbins* [1973] and *Dudley and James* [1989].

1.3.2. Mean-Field Dynamo

[14] An important insight into the workings of kinematic dynamos was made by *Parker* [1955], who pointed out that the eddies in a rotating fluid in a state of turbulent convection are likely to resemble *cyclones* and *anticyclones* in the atmosphere and that these eddies deform, and may amplify, the magnetic field in a conducting fluid. *Steenbeck et al.* [1966] provided a mathematical framework for this idea and generalized it into what became known as mean-field electrodynamics [see *Moffatt*, 1978; *Krause and Rädler*, 1980]. The idea is most easily illustrated by a two-scale system. All variables are

separated into large-scale and small-scale parts, a technique familiar in physics and especially in fluid mechanics. Consider the generation of a large-scale magnetic field $\langle \mathbf{B} \rangle$ by the interaction between the small-scale motion $\mathbf{v}'$ and the small-scale magnetic field $\mathbf{b}'$ which create an electromotive force (emf) $\varepsilon = \mathbf{v}' \times \mathbf{b}'$ that has a large-scale part,

$$\langle \varepsilon \rangle \equiv \langle \mathbf{v}' \times \mathbf{b}' \rangle, \tag{1}$$

where the angle brackets define the average over the small scales of the quantity between them. Ignoring the fact that a satisfactory theory of small-scale turbulence does not currently exist, it is nevertheless possible (following *Parker* [1955] and *Steenbeck et al.* [1966]) to argue that when the statistical distribution of small-scale motions lacks mirror symmetry, $\langle \varepsilon \rangle$ does not vanish and is approximately

$$\langle \varepsilon \rangle = \alpha \langle \mathbf{B} \rangle, \tag{2}$$

where α is generally a tensor. From the chance use of the α in equation (2), this relation became known as the α *effect*. If the small-scale motions are statistically pseudo-isotropic (meaning that they are independent of direction but change under coordinate reflection $\mathbf{x} \rightarrow$ to $-\mathbf{x}$), α is a (pseudo)scalar which is generally nonzero and is closely related to another significant (pseudo)scalar, namely, the average over the small-scale motions of the *helicity* $\mathbf{v}' \cdot \nabla \times \mathbf{v}'$ [*Steenbeck and Krause*, 1966]. The scalar form of α is the one more often adopted in applications of mean-field theory.

[15] In mean-field dynamos, $\langle \mathbf{B} \rangle$ is created not only by the emf, $\langle \mathbf{V} \rangle \times \langle \mathbf{B} \rangle$, of the large-scale fields but also by $\langle \varepsilon \rangle$. Cowling's theorem no longer applies because the regenerative loop may be closed by the emf $\langle \varepsilon \rangle$ and in particular by $\alpha \langle B_\phi \rangle$, which creates a large-scale meridional field $\langle \mathbf{B}_M \rangle$. Thus axisymmetric large-scale fields, $\langle \mathbf{B} \rangle$, may in principle be self-sustained by a simple feedback loop: In the so-called $\alpha\omega$ dynamo, the α effect creates $\langle \mathbf{B}_M \rangle$ from $\langle B_\phi \rangle$ and the ω effect produces $\langle B_\phi \rangle$ from $\langle \mathbf{B}_M \rangle$. This is not the only possibility: In the α^2 dynamo the α effect works both in creating $\langle \mathbf{B}_M \rangle$ from $\langle B_\phi \rangle$ and in producing $\langle B_\phi \rangle$ from $\langle \mathbf{B}_M \rangle$, as the meridional components of equation (2) allow in principle. Whether a mean-field dynamo is of $\alpha\omega$ or α^2 type clearly depends on whether the ω effect or the α effect is the more potent in creating $\langle B_\phi \rangle$; sometimes the term $\alpha^2\omega$ dynamo is used when both effects are influential.

[16] The powerful simplification (2) made the mean-field dynamo popular with theoreticians. Nevertheless, it should be stressed that the main applications of mean-field electrodynamics are in astrophysics, where the turbulent motions $\mathbf{v}'$ are so violent that $\langle \varepsilon \rangle$ is not negligible and may even dominate the emf $\langle \mathbf{V} \rangle \times \langle \mathbf{B} \rangle$ created by the large scales. The small-scale flows in the Earth's core are small, and their effects are mainly frictional (see section 1.3.3). It is therefore doubtful whether their α effect is significant. Nevertheless, the concepts underlying helicity and the α effect are central. They give insight into what the character of the large-scale motions $\mathbf{V}$ must be if they are to maintain a large-scale field $\mathbf{B}$ efficiently.

[17] Even when the effects of the small scales are insignificant, one may visualize that a type of large-scale α effect is at work, in which the nonaxisymmetric part, $\mathbf{V}'$, of a large-scale flow $\mathbf{V}$ creates a nonaxisymmetric field $\mathbf{B}'$ from the axisymmetric part $\bar{\mathbf{B}}$ of the large-scale field $\mathbf{B}$ and in which the emf $\mathbf{V}' \times \mathbf{B}'$ possesses an axisymmetric part,

$$\bar{\varepsilon} \equiv \overline{\mathbf{V}' \times \mathbf{B}'}, \tag{3}$$

where the overbar denotes the average over longitude, ϕ. It is the ϕ component of $\bar{\varepsilon}$ that is essential to defeat Cowling's theorem for it is this component alone that can generate $\bar{\mathbf{B}}_M$ from $\bar{B}_\phi$. If $\bar{\varepsilon}_\phi \equiv 0$, then $\bar{\mathbf{B}}$ cannot be maintained. In general, $\bar{\varepsilon}$ at a given point $\mathbf{x}$ and time t is not simply proportional to $\bar{\mathbf{B}}$ at the same $\mathbf{x}$ and t; there is no analog to equation (2). Nevertheless, the terms $\alpha\omega$ dynamo and α^2 dynamo are still used to distinguish situations in which $\bar{B}_\phi$ is created principally by the ω effect from those in which $\bar{\varepsilon}_M$ is mainly responsible.

1.3.3. MHD Dynamo

[18] The next stage in the development of dynamo theory was to attack the MHD dynamo problem. The earliest attempt was made by *Stevenson and Wolfson* [1966], but it was unconvincing because of the drastic truncations imposed by the limited computer resources of the time. Moreover, what is required are models that exploit the fact that (in a sense to be described more fully in Figure 1 and section 5.1) the Earth is a rapid rotator. In this context, *Taylor* [1963] made a very significant advance. He demonstrated that the difficulty in generating the axisymmetric components of $\mathbf{B}$ highlighted by Cowling's theorem is paralleled in a highly rotating fluid by a difficulty in determining the zonal part of $\mathbf{V}$ from $\mathbf{B}$. He proposed a way of overcoming this difficulty, defining what has become known as the *Taylor state*. A different proposal was made by *Braginsky* [1975], which rests heavily on core-mantle interaction and which he called *model Z*. Which, if either, of these concepts is more relevant to the geodynamo is unknown at present, despite further studies by *Braginsky and Roberts* [1987], *Jault* [1995], and *Walker and Barenghi* [1998] among others. This direction of research (which is called *intermediate dynamo*) has been temporarily abandoned in the stampede of 1995 onto the new plateau, the fruits of which are the main topics of this review. Nonetheless, it is already clear that a mountain lies ahead.

[19] Consider Figure 1. This shows the relation between the two nondimensional numbers that characterize MHD dynamos best: the Rayleigh number Ra and the Ekman number E. The significance of these parameters is more fully discussed in section 2.1.4 and Table 3. Here it suffices to say that the abscissa measures the speed of rotation (smaller E means more rapid rota-

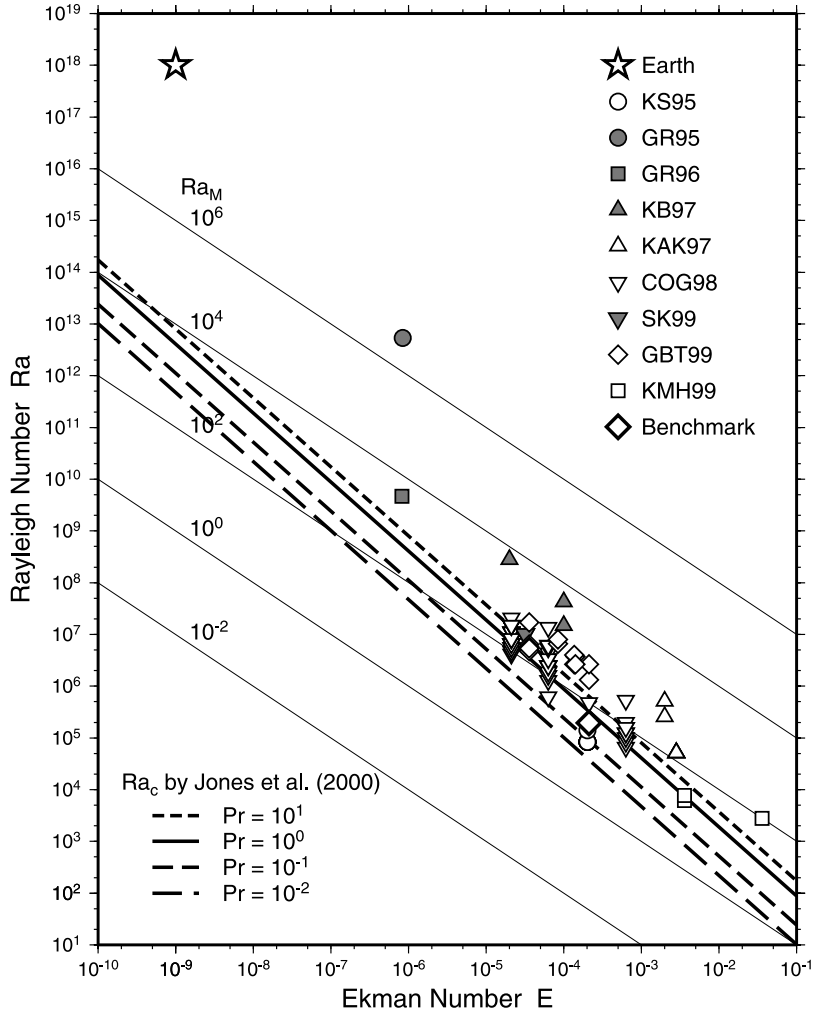

Figure 1. Relation between the Ekman number E and the Rayleigh number Ra in various MHD dynamo models. See Table 1 for the group names. Thick lines indicate the theoretical critical Rayleigh numbers determined by *Jones et al.* [2000]. Thin lines show values of the modified Rayleigh number $Ra_M = E\,Ra$. The value for the Earth is based on an eddy viscosity of 1 $m^2\ s^{-1}$. After *Kono and Roberts* [2001].

tion), while the ordinate measures the amount of energy available to the system to drive convection (larger Ra means that the system is more strongly driven). For comparison, the Ra-E relation for the onset of convection in a rotating sphere is shown for different Prandtl numbers (Pr) by the solid and dashed lines [*Jones et al.*, 2000]. It may be seen that Ra and E for the MHD dynamos studied so far are very different from what are thought to be appropriate for the Earth. It is also apparent that with the exception of the GR95 model, no simulation is very strongly driven; all other models have Ra <100 times the critical value at which convection becomes possible.

[20] Every model is at best a "large eddy simulation" (LES) of the geodynamo that encompasses only its biggest length scales and its longest timescales. Even the most highly resolved model, that of *Roberts and Glatzmaier* [2000a], deals only with scales larger than 10^4 m, and even this was possible only because E was assumed to be very much greater than is plausible for the core. Under these circumstances it is quite remarkable that such models should bear a close affinity with the geomagnetic field, but as we shall see, they do!

[21] It should be recognized that unless computer technology advances at an unprecedented rate, LES will be unavoidable for a very long time to come. This is because the spectrum of significant length scales extends from $R_0 \approx 3.48 \times 10^6$ m, the radius of the core, to plausibly $\mathcal{L}_\nu \equiv E^{1/2}R_0 \approx 0.1$ m (assuming that $E \approx 10^{-15}$, based on a molecular viscosity of 10^{-6} $m^2\ s^{-1}$).

[22] This should not occasion undue pessimism; LES is often successful. We should, however, interpret $\mathbf{V}$ and $\mathbf{B}$ in the simulations as being $\langle\mathbf{V}\rangle$ and $\langle\mathbf{B}\rangle$, now defined as the "resolved fields"; the corresponding $\mathbf{v}'$ and $\mathbf{b}'$ represent the unresolved scales, the effects of which must be incorporated into the equations governing the LES. One method of doing this is to augment the molecular diffusivities by much larger turbulent diffusivities that represent the diffusive effects of unresolved subgrid-scale motions on the resolved fields. This has been implicitly

or explicitly done for every model in Table 1. Also, in plotting the representative point for the Earth in Figure 1 we have used a turbulent viscosity rather than the molecular one. Even so, as we see from Figure 1, a chasm still exists between the simulations and the Earth. (The α effect, though also a parameterization of a subgrid-scale process that could affect the LES, is not recognized in the simulations for the reasons adumbrated above.)

[23] Much remains to be done in developing better ways of including the effects of the subgrid on the LES, ones that are faithful to the underlying MHD. Field creation by dynamo action is significant for all scales $\mathcal{L}$ greater than $\mathcal{L}_\eta \equiv \eta/\mathcal{U}$ at which the magnetic Reynolds number, $Rm = \mathcal{U}\mathcal{L}/\eta$, is O(1). Taking $\mathcal{U}$, the typical flow speed, to be 10^{-4} m s^{-1} and $\eta = 1$ m^2 s^{-1}, we see that $\mathcal{L}_\eta \approx 10^4$ m, which may be a generally attainable numerical resolution in the near future. The main dynamical effect of the magnetic field for $\mathcal{L} < \mathcal{L}_\eta$ is frictional [e.g., *Davidson*, 2001]. The principal dissipation is ohmic and occurs in the range $\mathcal{L}_\nu < \mathcal{L} < \mathcal{L}_\eta$, which will not be numerically resolved in the foreseeable future. The fabric of the unresolved scales in this "dissipation range" is strongly anisotropic, with $\mathbf{\Omega}$ and $\langle \mathbf{B} \rangle$ as preferred directions [see *Braginsky and Meytlis*, 1990; *Braginsky and Roberts*, 1995; *Matsushima et al.*, 1999; *Matsushima*, 2001]. Pancake-like structures appear [*St. Pierre*, 1996; *Shimizu and Loper*, 1997]. Evidently, the turbulent diffusivities should be similarly anisotropic, involving tensors rather than scalars. So far, no simulation has recognized this fact. Whether scalars or tensors, the diffusivities should not be constants, as has so far been assumed, but should depend on the properties of the turbulence at the point where they are required. This difficulty has also not yet been addressed.

[24] Clearly, severe difficulties lie ahead, but promising new methods have already been proposed that may allow the subgrid scale to be recognized in less ad hoc ways. In particular, we draw attention to the similarity method [e.g., *Lesieur and Metais*, 1996; *Meneveau and Katz*, 2000] and the Navier-Stokes-α method (e.g., B. J. Geurts and D. D. Holm, Alpha-modeling strategy for LES of turbulent mixing, available at http://xxx.lanl.gov/pdf/nlin.CD/0202012, 2002). However, these have not yet been applied to the geodynamo. Meanwhile, the mountain remains to be climbed.

2. FORMULATION

[25] Some simulations employ quite complicated physics, but here we shall describe in detail only the simplest type of model, which, however, contains all the ingredients basic to a successful MHD dynamo. Some of its simplifying assumptions, and especially that the core is almost uniform in density, are clearly at variance with known geophysical facts. Unfortunately, few of the key physical properties of the core demanded by geodynamo simulations are accurately determined at present, and some are very poorly known. Moreover, the numerical integrations involve approximations that are needed to obtain resolved solutions. Until mineral physics and computer technology advance further, the errors introduced by the assumption of a near-uniform core density are generally felt to be comparatively unimportant.

[26] In what follows, we shall usually employ spherical coordinates (r, θ, ϕ) rotating with the constant angular velocity $\mathbf{\Omega}$ of the mantle, which we shall take to also be that of the inner core. Sometimes we shall use cylindrical coordinates (s, ϕ, z). Here θ is colatitude, the polar axis Oz being $\theta = 0$; ϕ is longitude; r is distance from the geocenter O, and later $\mathbf{r}$ will be the radius vector from O.

2.1. Equations Governing Dynamo Process

[27] As implied in section 1, the theory of the origin of the geomagnetic field rests solidly on the geodynamo hypothesis, which supposes that the Earth's magnetism is the result of dynamo action. Undoubtedly, many other sources of magnetic field exist within the Earth (thermoelectric and electrochemical emf's, permanent magnetism, and so forth). The hypothesis presumes that these have a negligible effect. We shall also confine attention to convectionally driven dynamos and ignore the possibility (still unresolved) that the geodynamo is driven by motions resulting from the luni-solar precession [see, e.g., *Malkus*, 1968; *Vanyo*, 1991].

[28] We shall mainly consider convection and the generation of magnetic field in self-gravitating fluid spheres or spherical shells of outer radius R_0 and inner radius R_1 (which is zero in the case of the full sphere). We shall adopt the Boussinesq approximation in which all physical properties of the fluid are assumed constant, except in the buoyancy force, where variations in density created by temperature differences are taken into account. Further discussion of this approximation will be given in section 3.2.1.

2.1.1. Basic Equations

[29] The equations governing MHD dynamos are derived from the conservation laws of fluid mechanics, Maxwell's equations, and Ohm's law of electromagnetism. In the Boussinesq approximation the velocity $\mathbf{V}$ satisfies the equation of continuity for an incompressible fluid:

$$\nabla \cdot \mathbf{V} = 0. \tag{4}$$

[30] The equation of motion is obtained from conservation of momentum and is called the Navier-Stokes equation. In the dynamo problem this equation contains terms representing the effects of rotation and magnetic field:

$$\rho_0 \left[\frac{\partial \mathbf{V}}{\partial t} + \mathbf{V} \cdot \nabla \mathbf{V} \right] = -\nabla P + \rho_0 \nu \nabla^2 \mathbf{V} + \rho \bar{\mathbf{g}} - 2\rho_0 \mathbf{\Omega} \times \mathbf{V} + \mathbf{J} \times \mathbf{B}. \tag{5}$$

Here ρ is the density, ν is the kinematic viscosity, $P = p - \frac{1}{2}\rho_0|\mathbf{\Omega} \times \mathbf{r}|^2$ is the pressure modified by the inclusion of the centrifugal force, and $\bar{\mathbf{g}}$ is gravity. The left-hand side of equation (5) is the motional derivative of the momentum in a unit volume (i.e., the time derivative of $\rho_0\mathbf{V}$ following the motion of the fluid), while the right-hand side combines all the forces that cause this momentum to change. In the order of appearance, these arise from the pressure gradient, viscosity, gravity (buoyancy), rotation (the Coriolis force), and magnetic field (the Lorentz force).

[31] The simplest form of the energy conservation law is the thermal conduction equation

$$\frac{\partial T}{\partial t} + \mathbf{V} \cdot \mathbf{\nabla} T = \kappa \nabla^2 T + \epsilon, \tag{6}$$

where T is the temperature, $\kappa = k/\rho c_p$ is the thermal diffusivity, k is the thermal conductivity, c_p is the specific heat of the medium at constant pressure, and ϵ is proportional to the heat generation per unit mass created by sources, such as radioactivity, dissolved in the fluid. All of these are assumed to be constant, as are ν and the "reference density" ρ_0.

[32] The magnetic field must satisfy the solenoidal condition (Gauss's law)

$$\mathbf{\nabla} \cdot \mathbf{B} = \mathbf{0} \tag{7}$$

and the induction equation

$$\frac{\partial \mathbf{B}}{\partial t} = \mathbf{\nabla} \times (\mathbf{V} \times \mathbf{B}) + \eta \nabla^2 \mathbf{B}, \tag{8}$$

where $\eta = 1/\mu\sigma$ is the magnetic diffusivity, σ is the electrical conductivity of the fluid, and μ is the magnetic permeability; the temperature of the core is too great for μ to differ much from μ_0, the permeability of free space.

[33] In the MHD approximation, which is appropriate in most geophysical and astrophysical contexts, displacement currents are negligible, and the electric current density is given by

$$\mathbf{J} = \frac{1}{\mu_0} \mathbf{\nabla} \times \mathbf{B}. \tag{9}$$

The self-gravity of a fluid sphere of constant density ρ_0 is proportional to $\mathbf{r}$:

$$\bar{\mathbf{g}} = -g_0 \frac{\mathbf{r}}{R_0}, \qquad g_0 = \frac{4}{3}\pi G \rho_0 R_0, \tag{10}$$

where G is the universal gravitational constant and g_0 is gravity at the outer boundary. The negative sign indicates that the force is directed toward the geocenter.

[34] The system of equations is closed by an equation of state for the density ρ in equation (5). The Boussinesq approximation requires that ρ is independent of the pressure P and depends linearly on T:

$$\rho = \rho_0 [1 - \alpha(T - T_0)], \tag{11}$$

where α is the thermal expansivity (which should not be confused with the α effect considered earlier); the constant T_0 is the temperature at $r = R_0$, where the density is ρ_0. It is assumed that in all circumstances, $\alpha(T - T_0) \ll 1$, so that ρ never departs much from ρ_0. Nevertheless, g is so large that the Rayleigh number, defined in section 2.1.4, is O(1).

[35] Equations (4)–(11) define the dynamo problem in the Boussinesq approximation. If we take the scalar product of equation (5) with $\mathbf{V}$, the left-hand side becomes the rate of increase of the kinetic energy density $\frac{1}{2}\rho_0 V^2$, to which the final term on the right-hand side contributes $\mathbf{V}\cdot(\mathbf{J} \times \mathbf{B})$. This is the local rate at which magnetic energy density, $B^2/2\mu_0$, is converted into kinetic energy by the Lorentz force. If we take the scalar product of equation (8) with $\mathbf{B}/\mu_0$, we find that the first term on the right-hand side is associated with the equal but opposite term $-\mathbf{V}\cdot(\mathbf{J} \times \mathbf{B})$, giving the local rate at which the magnetic field energy grows through dynamo action. For a dynamo to function, $-\mathbf{V}\cdot(\mathbf{J} \times \mathbf{B})$ must exceed in magnitude the rate, $\mu_0\eta J^2$, at which ohmic resistance degrades magnetic energy into heat. The ratio of these terms is the magnetic Reynolds number, Rm (defined in Table 4 in section 3.4.2). A necessary condition for a dynamo to function is that $Rm > 1$, but this is far from sufficient. For instance, the sign of $-\mathbf{V}\cdot(\mathbf{J} \times \mathbf{B})$ is also significant. It cannot be consistently negative in a working dynamo, and when analyzing dynamo action in section 5, we shall be interested in knowing where in the flow $-\mathbf{V}\cdot(\mathbf{J} \times \mathbf{B})$ is positive.

2.1.2. Equations Governing Deviations From the Equilibrium State

[36] Equations (6) and (5) governing the temperature and velocity can be further reduced. We first observe that when the fluid is at rest ($\mathbf{V} = \mathbf{0}$), heat is transported by thermal diffusion alone. This defines what we may call "the equilibrium temperature distribution," $T = \bar{T}(r)$, where, by equation (6),

$$\kappa \nabla^2 \bar{T} + \epsilon = 0 \tag{12}$$

This shows that

$$\bar{T} = T_0 + \frac{\beta_0}{2R_0}(R_0^2 - r^2), \qquad \beta_0 = \frac{\epsilon R_0}{3\kappa}, \tag{13}$$

where β_0 is the (adverse) temperature gradient at the upper boundary ($r = R_0$). It may be seen from equation (13) that the equilibrium temperature gradient is directed toward the geocenter:

$$\mathbf{\nabla} \bar{T} = -\beta_0 \frac{\mathbf{r}}{R_0}. \tag{14}$$

In the preceding, we have used overbars for variables in the equilibrium state. The actual pressure and temperature are sums of their equilibrium values and the deviations from them: $P = \bar{P}(r) + P'(r, \theta, \phi, t)$, $T = \bar{T}(r) + \Theta(r, \theta, \phi, t)$. (Since $\bar{\mathbf{V}} = \bar{\mathbf{B}} = \mathbf{0}$ in the equilibrium state,

V and **B** represent deviations from that state and do not require a new notation.)

[37] In the equilibrium state, equation (5) expresses hydrostatic balance,

$$-\nabla\bar{P} + \bar{\rho}\bar{\mathbf{g}} = 0, \tag{15}$$

which may, by equation (11), be written as

$$-\nabla\bar{P} + \rho_0[1 - \alpha(\bar{T} - T_0)]\bar{\mathbf{g}} = 0. \tag{16}$$

This determines $\bar{P}(r)$, apart from an irrelevant additive constant.

[38] We may now extract from equations (5) and (6) equations governing the departures P' and Θ in pressure and temperature from their equilibrium values:

$$\frac{\partial\mathbf{V}}{\partial t} + \mathbf{V}\cdot\nabla\mathbf{V} = -\nabla\left(\frac{P'}{\rho_0}\right) + \nu\nabla^2\mathbf{V} + \alpha g_0\Theta\frac{\mathbf{r}}{R_0} - 2\boldsymbol{\Omega}\times\mathbf{V} + \frac{1}{\mu_0\rho_0}(\nabla\times\mathbf{B})\times\mathbf{B}, \tag{17}$$

$$\frac{\partial\Theta}{\partial t} + \mathbf{V}\cdot\nabla\,\Theta = \beta_0\mathbf{V}\cdot\frac{\mathbf{r}}{R_0} + \kappa\nabla^2\Theta. \tag{18}$$

These replace equations (5) and (6). It should be pointed out that equations (17) and (18) do not neglect interactions, such as $\mathbf{V}\cdot\nabla\,\Theta$, between terms representing departures from the equilibrium state. Equations (17) and (18) are therefore applicable to fully nonlinear situations.

2.1.3. Boundary Conditions

[39] The fluid is confined to the spherical shell $R_1 < r < R_0$. In the Earth's core, R_0 corresponds to the core-mantle boundary (CMB), and R_1 corresponds to the inner core boundary (ICB). Strictly, these are no-slip boundaries, also called "rigid boundaries," and they are treated as such here. Since the boundaries are stationary in our reference frame, rigid boundary conditions require that all components of the velocity vanish on them:

$$\mathbf{V} = \mathbf{0}, \qquad r = R_0, R_1. \tag{19}$$

We shall assume that the two boundaries are kept at constant temperatures given by equation (13). Hence the deviation Θ in temperature associated with the convection must vanish on the boundaries:

$$\Theta = 0, \qquad r = R_0, R_1. \tag{20}$$

[40] Since the mantle has an electric conductivity that is much smaller than that of the core, it is reasonable to assume that it is an insulator containing no sources of magnetic field, so that the magnetic field $\hat{\mathbf{B}}$ within it is of the form

$$\hat{\mathbf{B}} = -\nabla\,\Psi, \qquad \nabla^2\Psi = 0, \tag{21}$$

and Ψ is of order r^2 as $r \to \infty$. All components of the magnetic field in the core should match $\hat{\mathbf{B}}$ at the CMB:

Table 2. Units of Quantities Used for Nondimensionalization

Quantity	*Unit*	*Remarks*
Length	R_0	outer core radius
Time	R_0^2/ν	viscous diffusion time
Velocity	ν/R_0	
Pressure	$\rho_0\nu^2/R_0^2$	
Temperature	$\nu\beta_0R_0/\kappa$	
Magnetic field	$\nu(\mu_0\rho_0)^{1/2}/R_0$	

$$\mathbf{B} = \hat{\mathbf{B}}, \qquad r = R_0. \tag{22}$$

A condition similar to equation (22) holds at the ICB ($r = R_1$), and since we shall assume here for simplicity that the inner core is electrically insulating and contains no sources of magnetism, equation (21) again applies with a Ψ that is bounded throughout the inner core. The fact that the horizontal components of the electric field are also continuous at each boundary does not place a restriction on the solution (but see section 3.3.2).

2.1.4 Nondimensionalization

[41] It is a general practice in fluid dynamics to rewrite the governing equations and boundary conditions in nondimensional form because, by so doing, the system under study is characterized by a small number of nondimensional parameters. Dynamo theory is no exception, and one possible method of making the variables nondimensional is presented in Table 2.

[42] Another possible choice for the unit of length is the shell thickness $D = R_0 - R_1$, but we select the radius R_0 as the unit of length for reasons discussed in section 3.4.2. The original equations are then replaced by corresponding equations governing the nondimensional variables (for which we use the same symbols, though the prime from P' is removed):

$$\left(\frac{\partial}{\partial t} - \nabla^2\right)\mathbf{V} - Ra\,\Theta\mathbf{r} + E^{-1}\mathbf{1}_z\times\mathbf{V} + \nabla P = -\mathbf{V}\cdot\nabla\mathbf{V} - \mathbf{B}\times(\nabla\times\mathbf{B}), \tag{23}$$

$$\left(\frac{\partial}{\partial t} - Pr^{-1}\nabla^2\right)\Theta - Pr^{-1}\mathbf{V}\cdot\mathbf{r} = -\mathbf{V}\cdot\nabla\Theta, \tag{24}$$

$$\left(\frac{\partial}{\partial t} - Pm^{-1}\nabla^2\right)\mathbf{B} = \nabla\times(\mathbf{V}\times\mathbf{B}), \tag{25}$$

$$\nabla\cdot\mathbf{V} = 0, \tag{26}$$

$$\nabla\cdot\mathbf{B} = 0. \tag{27}$$

We use $\mathbf{1}_q$ to denote the unit vector in the direction of increasing coordinate q, so that $\mathbf{1}_z$ is the unit vector parallel to the rotation axis. We have collected the linear terms on the left-hand sides and the nonlinear terms on the right-hand sides.

Table 3. Nondimensional Numbers

Name	*Symbol*	*Definition*	*Ratio*
Rayleigh number	Ra	$\alpha\beta_0 g_0 R_0^4/\nu\kappa$	buoyancy versus viscous forces
Ekman number	E	$\nu/2\Omega R_0^2$	viscous versus Coriolis forces
Prandtl number	Pr	ν/κ	thermal versus viscous diffusion times
Magnetic Prandtl number	Pm	ν/η	magnetic versus viscous diffusion times
Taylor number	Ta	$(2\Omega R_0^2/\nu)^2$	Coriolis versus viscous forces
Modified Rayleigh number	Ra_M	$\alpha\beta_0 g_0 R_0^2/2\Omega\kappa$	buoyancy versus Coriolis forces
Magnetic Ekman number	E_M	$\eta/2\Omega R_0^2$	rotation period versus magnetic timescale
Diffusivity ratio	q	κ/η	magnetic versus thermal diffusion times
Magnetic Reynolds number	Rm	$V_0 R_0/\eta$	magnetic diffusion versus kinetic timescale
Elsasser number	Λ	$B_0^2/2\Omega\eta\mu_0\rho_0$	Lorentz versus Coriolis forces
Rossby number	Ro	$V_0/\Omega R_0$	inertial versus Coriolis forces

[43] Four nondimensional numbers (*Ra, E, Pr, Pm*) appear in equations (23)–(27), for which the definitions and meanings are summarized in Table 3. Table 3 also presents alternative parameters that are occasionally used. It is easy to express these by the nondimensional numbers we employ: $Ta = E^{-2}$, $Ra_M = E \cdot Ra$, $E_M = E/Pm$, and $q = Pm/Pr$. For reasons described in section 4.1.3, some authors studying magnetoconvection in rapidly rotating systems prefer to use Ra_M in place of Ra. The last three entries in Table 3 are also nondimensional but involve quantities that can be obtained only from the results of the simulation; V_0 is a typical flow speed and B_0 is a typical magnetic field strength. As is appropriate for liquid metal alloys such as the Earth's core, we shall focus below on situations in which $q \ll 1$ (or $Pm \ll Pr$).

2.2. Numerical Methods

[44] Most of the research groups listed in Table 1 have used a spectral method to solve the differential equations (23)–(27). Accordingly, the explanation below focuses on this method. Alternatives methods are discussed in section 3.5.

2.2.1. Toroidal and Poloidal Decomposition

[45] According to equation (4), one component of the fluid velocity is determined by the other two. In other words, the velocity can be specified by two independent scalar fields. This is most conveniently done by expressing the velocity as the sum of its toroidal and poloidal parts [e.g., *Bullard and Gellman*, 1954; *Chandrasekhar*, 1961; *Backus*, 1986]. Using equation (7), the same can be done for the magnetic field:

$$\begin{aligned}\mathbf{V} &= \nabla \times (V\mathbf{r}) + \nabla \times \nabla \times (U\mathbf{r}),\\ \mathbf{B} &= \nabla \times (T\mathbf{r}) + \nabla \times \nabla \times (S\mathbf{r}),\end{aligned} \tag{28}$$

where *V, T* and *U, S* are called the defining scalars of the toroidal and poloidal vectors, respectively. The requirements $\nabla\cdot\mathbf{V} = \nabla\cdot\mathbf{B} = 0$ are then automatically satisfied.

[46] In the spherical coordinates, the three components of $\mathbf{V}$ are

$$\mathbf{V} = \left(\frac{\mathcal{L}^2 U}{r}, \frac{1}{r}\frac{\partial^2(rU)}{\partial\theta\partial r} + \frac{1}{\sin\theta}\frac{\partial V}{\partial\phi}, \frac{1}{r\sin\theta}\frac{\partial^2(rU)}{\partial\phi\partial r} - \frac{\partial V}{\partial\theta}\right), \tag{29}$$

and similarly for $\mathbf{B}$. Here $\mathcal{L}^2$ is the angular momentum operator

$$\mathcal{L}^2 = \frac{\partial}{\partial r}\left(r^2\frac{\partial}{\partial r}\right) - r^2\nabla^2 = -\frac{1}{\sin\theta}\left(\sin\theta\,\frac{\partial}{\partial\theta}\right) - \frac{1}{\sin^2\theta}\frac{\partial^2}{\partial\phi^2}. \tag{30}$$

It should be noted that the radial component of a solenoidal vector involves only its poloidal scalar; also, the curl of a toroidal vector is poloidal, while the curl of a poloidal vector is toroidal, e.g.,

$$\nabla \times \mathbf{B} = \nabla \times (-\nabla^2 S\mathbf{r}) + \nabla \times \nabla \times (T\mathbf{r}). \tag{31}$$

Using equation (9), the toroidal current system determines the poloidal magnetic field and vice versa.

[47] By applying the operators $\mathbf{r}\cdot\nabla\times$ and $\mathbf{r}\cdot\nabla\times\nabla\times$ to equation (23) and $\mathbf{r}\cdot$ and $\mathbf{r}\cdot\nabla\times$ to equation (25) and rewriting $\mathbf{V}\cdot\mathbf{r}$ term in equation (24), we obtain

$$\left(\frac{\partial}{\partial t} - \nabla^2\right)\mathcal{L}^2 V = \mathbf{r}\cdot\nabla \times \mathbf{F}, \tag{32}$$

$$\left(\frac{\partial}{\partial t} - \nabla^2\right)\nabla^2\mathcal{L}^2 U + Ra\,\mathcal{L}^2\Theta = -\mathbf{r}\cdot\nabla \times \nabla \times \mathbf{F}, \tag{33}$$

$$\left(\frac{\partial}{\partial t} - Pm^{-1}\nabla^2\right)\mathcal{L}^2 S = \mathbf{r}\cdot\nabla \times (\mathbf{V} \times \mathbf{B}), \tag{34}$$

$$\left(\frac{\partial}{\partial t} - Pm^{-1}\nabla^2\right)\mathcal{L}^2 T = \mathbf{r}\cdot\nabla \times \nabla \times (\mathbf{V} \times \mathbf{B}), \tag{35}$$

$$\left(\frac{\partial}{\partial t} - Pr^{-1}\nabla^2\right)\Theta - Pr^{-1}\mathcal{L}^2 U = -\mathbf{V}\cdot\nabla\Theta, \tag{36}$$

where

$$\mathbf{F} = -E^{-1}\mathbf{1}_z \times \mathbf{V} + \mathbf{V} \times (\nabla \times \mathbf{V}) - \mathbf{B} \times (\nabla \times \mathbf{B}). \quad (37)$$

Note that the first term on the right-hand side of **F** is linear in **V**, so that the corresponding terms in equations (32) and (33) can be moved to the left-hand side and treated implicitly in numerical work. The added complexity is rewarded by an increase in the time step that can be used to advance the solution (see section 2.2.3).

[48] The original equations (23)–(27) contained eight variables, i.e., two vectors (**V** and **B**) and two scalars (T and P). After the decomposition the number of variables is reduced to five (U,V,T,S,Θ). The pressure force (as well as the gradient term arising from the identity $-(\mathbf{V}\cdot\nabla)\,\mathbf{V} = \mathbf{V} \times (\nabla \times \mathbf{V}) - \frac{1}{2}\nabla\mathbf{V}^2$) has been eliminated by taking the curl.

2.2.2. Spherical Harmonic Expansion

[49] Each of the scalar variables (U,V,T,S,Θ) is a function of time (t) and space (r, θ,ϕ). We separate them into spherical harmonic components. For instance,

$$U(r,\theta,\phi,t) = \sum_{l=0}^{L} \sum_{m=-l}^{l} U_l^m(r,t) Y_l^m(\theta,\phi), \quad (38)$$

where Y_l^m, which is proportional to $\exp(im\phi)$, is a completely normalized spherical harmonic function of degree l and order m,

$$\int_0^{2\pi} \int_0^{\pi} Y_l^{m^*}(\theta,\phi) Y_{l'}^{m'}(\theta,\phi) \sin\theta d\theta d\phi = \delta_{ll'}\delta_{mm'}, \quad (39)$$

where the asterisk denotes complex conjugation, and L is the truncation level of the expansion; in principle, the sum should be taken to $l = \infty$. Expansions of the form of equation (38) have two technical advantages: (1) when applied to the lth components of equation (38), the operator (30) becomes algebraic as shown in equation (40), and (2) the boundary conditions on **B** at an insulating boundary become simple (see equations (47)–(49)).

[50] We multiply equations (32)–(36) by $Y_l^{m^*}$ and integrate over the surface of the sphere. Because of the orthogonality of the spherical harmonics (equation (39)) and the fact that they are the eigenfunctions of the $\mathcal{L}^2$ operator with the eigenvalue $l(l + 1)$

$$\mathcal{L}^2 Y_l^m(\theta,\phi) = l(l+1) Y_l^m(\theta,\phi), \quad (40)$$

we obtain

$$l(l+1)\left(\frac{\partial}{\partial t} - \nabla_l^2\right) V_l^m = \int\int Y_l^{m^*} \mathbf{r}\cdot\nabla \times \mathbf{F} dS, \quad (41)$$

$$l(l+1)\left[\left(\frac{\partial}{\partial t} - \nabla_l^2\right)\nabla_l^2 U_l^m + Ra\,\Theta_l^m\right] = -\int\int Y_l^{m^*} \mathbf{r}\cdot\nabla \times \nabla \times \mathbf{F} dS, \quad (42)$$

$$l(l+1)\left(\frac{\partial}{\partial t} - Pm^{-1}\nabla_l^2\right) S_l^m = \int\int Y_l^{m^*} \mathbf{r}\cdot\nabla \times (\mathbf{V} \times \mathbf{B}) dS, \quad (43)$$

$$l(l+1)\left(\frac{\partial}{\partial t} - Pm^{-1}\nabla_l^2\right) T_l^m = \int\int Y_l^{m^*} \mathbf{r}\cdot\nabla \times \nabla \times (\mathbf{V} \times \mathbf{B}) dS, \quad (44)$$

$$\left(\frac{\partial}{\partial t} - Pr^{-1}\nabla_l^2\right)\Theta_l^m - l(l+1) Pr^{-1} U_l^m = -\int\int Y_l^{m^*} \mathbf{V}\cdot\nabla\Theta dS, \quad (45)$$

where $dS = \sin\theta d\theta d\phi$ is the infinitesimal solid angle and ∇_l^2 involves differentiations with respect to r alone:

$$\nabla_l^2 = \frac{1}{r^2}\frac{\partial}{\partial r}\left(r^2 \frac{\partial}{\partial r}\right) - \frac{l(l+1)}{r^2}. \quad (46)$$

Equations (41)–(45) are the differential equations to be time stepped in solving the dynamo problem.

[51] When the solutions are expanded in spherical harmonics as in equation (38), the boundary conditions (19), (20), and (22) require that

$$U_l^m = V_l^m = \Theta_l^m = T_l^m = 0, \qquad r = R_0, R_1, \quad (47)$$

while for the poloidal magnetic field, equation (22) implies that [*Bullard and Gellman*, 1954]

$$\frac{\partial}{\partial r}(rS_l^m) + lS_l^m = 0, \qquad r = R_0, \quad (48)$$

$$\frac{\partial}{\partial r}(rS_l^m) - (l+1)S_l^m = 0, \qquad r = R_1. \quad (49)$$

2.2.3. Integration of Differential Equations

[52] The variables on the right-hand side of the equations in section 2.2.1 (such as U_l^m) are functions of r and t. The r dependence is dealt with either (1) by expanding the variables in Chebyshev polynomials or (2) by defining them on a uniformly spaced grid. In the former case, we write

$$U_l^m(r,t) = \sum_n U_{l,n}^m(t) T_n(x), \qquad x = \frac{2r - R_0 - R_1}{R_0 - R_1}, \quad (50)$$

where $T_n(x)$ is the Chebyshev polynomial of degree n, and x varies between -1 and 1; the r derivatives are dealt with by recursion in n on the $U^m_{l,n}$ coefficients. In the latter case, the differential operators are replaced by finite differences:

$$\left(\frac{\partial U^m_l}{\partial r}\right)_i = \frac{U^m_{l\,i+1} - U^m_{l\,i-1}}{2\Delta r},$$
$$\left(\frac{\partial^2 U^m_l}{\partial r^2}\right)_i = \frac{U^m_{l\,i+1} - 2U^m_{l\,i} + U^m_{l\,i-1}}{(\Delta r)^2}. \quad (51)$$

[53] In equations (41)–(45), the left-hand side of each equation is linear. This part is usually solved by an implicit scheme (e.g., the Crank-Nicolson method). Their right-hand sides are spherical transforms of nonlinear functions (such as $\mathbf{r}\cdot\nabla \times (\mathbf{V} \times \mathbf{B})$), which have to be evaluated explicitly (e.g., by the Adams-Bashforth method). For this part, calculation in spectral space is not practical because $O(N \times N)$ multiplications will be needed if there are N spectral modes. Accordingly, the quantities appearing on the right-hand sides are first transformed from spectral space to physical space, the multiplications are performed in physical space, and the results are then transformed back to spectral space and used in the time stepping. This technique is often called the "pseudospectral method." Further details of this numerical technique are given by *Glatzmaier* [1984] and *Hollerbach* [2000].

3. VARIATIONS

[54] In this section, we describe some significant differences in the 3-D MHD geodynamo simulations published so far, with the aim of easing direct comparisons between them. These differences arise from the use of different equations, different boundary conditions, different definitions of nondimensional numbers, and different sources of buoyancy. Before examining them, we shall briefly describe some MHD dynamos that do not properly fit into the framework of the present review.

3.1. Not Fully 3-D Treatments

[55] *Zhang and Busse* [1988, 1989, 1990] studied the onset of convection and the generation of magnetic field in spherical shells. They assumed that the velocity and magnetic field drift in the azimuthal direction at a constant angular velocity. In other words, their solutions were steady in a frame of reference rotating about the z axis at a constant angular speed, the determination of which was part of the solution process. This ingenious idea allowed them to make progress with the limited computer resources available to them. They were able to find solutions that are fully nonlinear and three-dimensional. It has, however, become increasingly apparent during the last decade that the simple time dependence of their solutions severely limits their solution space, to the detriment of geophysical realism. For this reason, we include their model here, under the heading of "not fully 3-D treatments." (To be more precise, and regarding time as a fourth dimension, theirs is not a fully 4-D model of the type that we seek.)

[56] Another not fully 3-D model is the so-called $2\frac{1}{2}$-D dynamo [e.g., *Sarson et al.*, 1998; *Sarson and Jones*, 1999; *Fearn and Morrison*, 2001]. In these, the expansions in r and θ are as complete as they are in fully 3-D simulations, but only the axisymmetric and one (or at most a few) of the asymmetric ($m \neq 0$) modes are included. This allows forward integrations in time to be performed with limited computer resources, even with a PC, and parameter space can be explored quickly and cheaply. Although the results are usually qualitatively similar to those obtained by the fully 3-D models, the neglect of most of the nonlinear interactions between the different asymmetric modes is a matter of serious concern.

[57] As we show in sections 5.1 and 5.2, there are indeed dynamo solutions that are almost steady in a reference frame drifting in the azimuthal direction. Also, in some circumstances, dynamo solutions exist in which the amplitudes of only a few of the asymmetric modes are significant. These are, however, generally low-energy dynamos operating in a slowly rotating fluid. They belong to parameter regimes very different from those relevant to the Earth. With higher energies and higher rotation rates (large Ra and small E) the assumptions on which the models are based are quite unrealistic. For this reason, these models are not analyzed further in this review.

3.2. Basic Equations

[58] In all 3-D MHD dynamo simulations, equations (7) and (8) governing the magnetic field are the same. Differences appear in the equation of continuity, the equation of state, the buoyancy source, and the dissipative terms in the equation of motion. We summarize these in sections 3.2.1 and 3.2.2.

3.2.1. Density Changes and Source of Buoyancy

[59] Most people use the Boussinesq approximation, in which variations in density are recognized only in the buoyancy term and are simply proportional to temperature differences, as shown by equation (11). Exceptions were made by two groups: KS95 and GR96.

[60] KS95 (*Kageyama et al.* [1995] and later papers) considered situations more appropriate to the Sun and stars than to the Earth. Their working fluid is a compressible gas, and they used the full form of the continuity equation:

$$\frac{\partial \rho}{\partial t} + \nabla \cdot (\rho \mathbf{V}) = 0. \quad (52)$$

For the equation of state, KS95 employed the ideal gas law

$$P = R\rho T, \quad (53)$$

where R is the gas constant. As the convection zones in stars such as the Sun are much less massive than their radiative interiors, KS95 also assumed that self-gravity can be ignored. Since the depth of these zones is small compared with the radius of the star, they abandoned equation (10), assuming instead that g is constant across the regenerating region.

[61] GR96 (*Glatzmaier and Roberts* [1996a] and later papers) tried to model the Earth's core as faithfully as possible. Their reference state coincides with the Preliminary Reference Earth Model (PREM) of *Dziewonski and Anderson* [1981], so that $\bar{\rho}$ is a solution to the hydrostatic equation (15) at constant specific entropy S and with the gravity field $\bar{\mathbf{g}}$ that follows from $\bar{\rho}$ and Newton's law of gravitation. They replaced equation (52) with the anelastic approximation

$$\nabla \cdot (\bar{\rho}\mathbf{V}) = 0. \tag{54}$$

With equation (4) for the Boussinesq approximation, this shares the immense computational advantage of "filtering out" seismic waves, the timescales of which are too short to be relevant to the geodynamo but which (if included) would require much smaller time steps to be taken in the numerical integrations, thereby greatly increasing the computational expense. KS95 evaded this difficulty by making their velocity of sound so low that sound crosses their system in a time comparable with the timescale of field generation. Equation (54) allows the momentum density $\bar{\rho}\mathbf{V}$ to be represented by toroidal and poloidal scalars, just as $\mathbf{V}$ is in the Boussinesq approximation (see equation (28)).

[62] Despite the different physics incorporated in equations (52)–(54), the resulting simulations have the same general character as those based on the Boussinesq approximation. This may be because neither model is strongly nonuniform. For example, the density $\bar{\rho}$ in equation (54) varies by little more than 10% across the Earth's fluid core. There are, however, deeper differences between the GR96 and Boussinesq models, even though both follow the standard practice of describing convection as a deviation from a reference state that is in hydrostatic equilibrium. In the case of the Boussinesq model the reference state is also in thermal equilibrium; equation (13) satisfies the steady state thermal conduction equation (12). In contrast, $\bar{T}$ for the anelastic solution does not do so, but there is no absolute requirement that it should; a reference state is merely a mathematical convenience and need not have a precise physical significance. Conductive reference states are remote from the state of the core, which is almost isentropic. This is because convection is vigorous enough to mix the core thoroughly (except near boundaries). It is obviously very convenient to choose an adiabat as the reference state, since then the departures from that state associated with the hot rising and cold descending currents are tiny, which would not be the case if a conductive reference state were selected in its place. The pressure gradients associated with these currents are small compared with the hydrostatic pressure gradient, so that it is convenient to use equation (15) in defining the adiabatic reference state, with the paradoxical consequence that the reference state is hydrostatic even though it can only be brought into being by thorough mixing.

[63] The analogous situation for a Boussinesq system arises for large Ra, when convection is strong and creates a mean temperature profile (the horizontal average of $\bar{T} + \Theta$) that is nearly independent of depth except in boundary layers. This state differs drastically from $\bar{T}$, but (unlike the case for the compressible layer) it can still be described using the formulation of section 2.1.2, since Boussinesq theory assumes that $\alpha(T - T_0) \ll 1$, no matter how large $T - T_0$ is. Consequently, ρ never departs far from ρ_0. (Convection occurs in a Boussinesq fluid only because g is supposed to be so large that Ra is finite, despite the smallness of $\alpha\beta R_0$.)

[64] The models discussed so far do not include the nonthermal buoyancy created by differences in chemical composition in the Earth's core. The essential physics is encapsulated by the simplest two-component model in which the core is assumed to be a binary alloy of iron and some lighter constituent having a mass fraction ξ. In the Boussinesq approximation, equation (11) is replaced by

$$\rho = \rho_0[1 - \alpha(T - T_0) + \alpha^\xi(\xi - \xi_0)], \tag{55}$$

where

$$\alpha = -\frac{1}{\rho}\left(\frac{\partial \rho}{\partial T}\right)_{P,\xi}, \qquad \alpha^\xi = \frac{1}{\rho}\left(\frac{\partial \rho}{\partial \xi}\right)_{P,T}. \tag{56}$$

Equation (6) must be supplemented by a similar equation for ξ:

$$\frac{\partial \xi}{\partial t} + \mathbf{V} \cdot \nabla \xi = \kappa^\xi \nabla^2 \xi + \epsilon^\xi, \tag{57}$$

where ϵ^ξ is a source term representing the increasing proportion of light material that originates from differentiation at the inner core boundary and that then mixes into the fluid core (see also section 1.3.3). The molecular diffusivity, κ^ξ, is tiny, but when diffusion is dominated by small-scale motions, both κ and κ^ξ should be replaced by appropriate turbulent diffusivities. (See *Braginsky and Roberts* [1995], who point out that these diffusivities should be tensor quantities, although GR96 took them to be scalars.)

3.2.2. Dissipation

[65] KS95 and GR96 include in the energy balance both Joule heating

$$Q_J = |\mathbf{J}|^2/\sigma, \tag{58}$$

and viscous dissipation

$$Q_\nu = \rho_0 \nu (e_{ij} e_{ij} - \tfrac{1}{3}(\nabla \cdot \mathbf{V})^2), \tag{59}$$

where e_{ij} is the rate of strain tensor. These terms, which cannot be consistently retained in the Boussinesq approximation, are not negligibly small but seem not to be great enough to affect the solutions drastically.

3.2.3. Hyperdiffusivity

[66] In dynamo simulations it is generally found that the decay of magnetic energy density with increasing spherical harmonic degree l is quite slow. In fact, it is much slower than for the kinetic energy density in nonmagnetic convection. This means that in moderate- to high-energy dynamos the convergence is not satisfactory even at relatively high truncation levels, of order $L = 50$. One way to enhance the convergence is to increase the diffusion coefficients for the small scales artificially. Forms such as

$$(\nu,\kappa,\eta)\nabla_l^2 = \begin{cases} (\nu_0, \kappa_0, \eta_0)\nabla_l^2, & l \le l_0, \\ (\nu_0,\kappa_0,\eta_0)\,(1 + a l^n)\nabla_l^2, & l > l_0, \end{cases} \tag{60}$$

are often employed and are termed *hyperdiffusivities*. Here a, n, ν_0, κ_0, and η_0 are positive constants.

[67] As an example, GR95 used $a = 0.075$, $n = 3$, and $l_0 = 0$, which means that when l is 10 and 20, the diffusivity is 76 and 601 times its value when no hyperdiffusivity is added. Because of the high energy input to the GR95 model, the use of such large hyperdiffusivities was mandatory. SK99 also used $n = 3$ and $l_0 = 0$, but because their models were not as strongly driven, they assumed a more moderate values of $a = (1/20)^3$. The diffusivities for $l = 10$, 20, and 40 were then only 1.1, 2, and 9 times larger than for $l = 0$. They found, however, that it was necessary to impose hyperdiffusivities of this magnitude to secure good numerical convergence. Many of the COG98 models were not so strongly driven that hyperdiffusivity proved to be unnecessary. As we discuss in section 5.1, the higher the energy input the slower the decay of the energy densities with increasing l and the greater the necessity for hyperdiffusion. Although hyperdiffusivity is certainly an arbitrary assumption, it may be unavoidable for some time to come when strongly driven dynamos are studied [see *Roberts and Glatzmaier*, 2000a].

3.3. Boundary Conditions

[68] The conditions set out in section 2.1.3 are appropriate for rigid, constant temperature, electrically insulating boundaries. The resulting conditions (equations (19)–(22)) are very simple but may not match the real Earth well. As a result, other boundary conditions have been explored in an attempt to be geophysically more realistic. Some models, which may be relevant to the early Earth before the inner core formed, suppose that the core is entirely fluid. In such cases, the conditions that would have been applied at the inner core boundary are replaced by the demand that all variables are nonsingular at the geocenter.

3.3.1. Velocity

[69] Most simulations employ rigid (no-slip) conditions at both boundaries. *Kuang and Bloxham* [1997] argue, however, that in the real Earth the Ekman boundary layers are too thin to be resolvable in numerical simulations and that the viscous stress-free boundary conditions are more appropriate in simulations than the no-slip conditions. *Roberts and Glatzmaier* [2000b] point out that this is not as obvious as at first sight appears (see also section 5.4.2).

[70] At stress-free boundaries the radial component of the velocity V_r as well as the tangential components of the viscous stress tensor ($\sigma_{r\theta}$, $\sigma_{r\phi}$) must vanish. This leads to the conditions [*Chandrasekhar*, 1961]

$$V_r = 0, \qquad \frac{\partial}{\partial r}\left(\frac{V_\theta}{r}\right) = 0, \qquad \frac{\partial}{\partial r}\left(\frac{V_\phi}{r}\right) = 0, \qquad r = R_0, R_1. \tag{61}$$

[71] Condition (19) at no-slip boundaries assumes that the inner core rotates with the same angular velocity Ω as the mantle. If the inner core rotates freely, the boundary condition at the ICB should be changed to

$$\mathbf{V} = \mathbf{\Omega_1} \times \mathbf{r}, \qquad r = R_1, \tag{62}$$

where $\mathbf{\Omega}_1$ is the angular velocity of the inner core relative to the mantle. It is then also necessary to add the equation of motion of the inner core that determines $\mathbf{\Omega}_1$. This was done first by *Braginsky* [1964] and more recently for the 3-D dynamo models of GR95, GR96, and SK99.

3.3.2. Magnetic Field

[72] All components of the magnetic field are continuous at the CMB and ICB (see equation (22)). In most cases, the region above the core is assumed to be electrically insulating, and the field above the CMB is then a potential field that vanishes with increasing r (see equation (21)). To assess the effects of electromagnetic core-mantle coupling, *Glatzmaier and Roberts* [1995a, 1995b] assumed that a thin shell, of thickness $0.04D$, at the bottom of the mantle possessed the same electrical conductivity as in the core, giving it the same depth-integrated conductivity as that estimated for the mantle. In this case, the induction equation is solved including this layer, and the boundary condition is applied at $D + 0.04D$. (To be more precise, Glatzmaier and Roberts did not use the reference frame fixed to the mantle but instead used the reference frame in which the total angular momentum of the Earth is zero. By solving an equation of motion for the mantle they could then determine the small variations in the angular velocity of the mantle created by the changing electrodynamic state of the core.)

[73] *Kageyama et al.* [1995] assumed that

$$B_r \neq 0, \qquad B_\theta = B_\phi = 0, \qquad r = R_0, \tag{63}$$

as had been done previously by *Gilman and Miller* [1981], *Wang et al.* [1991], and others. This condition is simpler to apply than equations (21) and (22) when finite difference methods are employed. It has no theoretical justification but has some observational support in the case of the Sun [see *Howard and Labonte*, 1981].

[74] Instead of supposing that the inner core is an insulator, it is more realistic to assume that its electrical conductivity is similar to that of the outer core. Then the condition that the horizontal components of the electric field should be continuous at $r = R_1$ becomes important. $\mathbf{V}$ and η continuous at $r = R_1$ implies that the horizontal components of $\mathbf{J}$ are continuous. Taken with the continuity of the magnetic field, it requires that

$$T = T_i, \qquad \frac{\partial T}{\partial r} = \frac{\partial T_i}{\partial r}, \qquad S = S_i, \qquad \frac{\partial S}{\partial r} = \frac{\partial S_i}{\partial r}, \qquad r = R_1, \quad (64)$$

where T_i and S_i are defining scalars for the toroidal and poloidal field in the inner core. Conditions (64), which were used by GR95, GR96, and SK99, are required to determine how the electrodynamic state of the fluid core determines that of the inner core.

3.3.3. Energy Supply

[75] A specification of the temperature gradient β_0, or equivalently the distributed heat source ϵ, together with boundary condition (20), provides just one possible way of controlling the energy supply to a thermally driven dynamo, and this, in turn, determines the fluid density and hence the buoyancy force. There are a number of alternatives. One could set $\epsilon = 0$ but specify the temperature difference, ΔT, between the two boundaries, or one could assign the temperature gradient at the CMB, which, in turn, determines the total surface heat flow, Q_0, at the CMB.

[76] When studying the dynamo in a secularly cooling Earth, the internal energy released in the bulk of the outer and inner cores can be represented by an ϵ source [see, e.g., *Sakuraba and Kono*, 1999]. There is also a release of latent heat at the ICB associated with the progressive freezing of the inner core. This gives rise to a discontinuity in the heat flux, and therefore in $\partial T/\partial r$, at the ICB. Because the liquidus and solidus are unlikely to coincide, light material is released at the ICB during freezing, and this creates a flux of light constituent. Unlike heat, the light element cannot (we suppose) flow into the mantle, which means that

$$(\nabla \xi)_r = 0, \qquad r = R_0. \quad (65)$$

This mass fraction, ξ, in the fluid core therefore increases. In other words, conservation of mass requires that the assumed source of ξ in the fluid core is consistent with the flux of ξ or, equivalently, $\partial \xi/\partial r$, on the ICB. This flux, the release of latent heat, and the rate at which the ICB moves upward because of freezing are all proportional to one another in a unique way that has been determined by *Braginsky and Roberts* [1995] and implemented from 1996 onward by *Glatzmaier and Roberts* [1996a, 1996b, 1997]. In their approach the boundary conditions on T and ξ at the ICB, and the sources of heat and composition in the bulk of the fluid core, cannot be imposed; they are (in a cooling Earth) determined by the heat flux at the CMB.

[77] *Glatzmaier et al.* [1999] broke new ground when they studied dynamos in which the heat flux was supposed to depend on horizontal position on the CMB, i.e., to vary with θ and ϕ. This assumption seems natural when we recall that mantle convection, which controls the heat flux from the core, itself involves cold falling and hot rising motions above different areas of the CMB. From a theoretical point of view, the *Glatzmaier et al.* [1999] model was a radical departure from earlier types of dynamo model. The equitemperature surfaces, even for a stagnant conductive solution of the type we consider in section 2, were no longer horizontal and were therefore not perpendicular to $\mathbf{g}$. No matter how large the viscosity of the fluid (provided it is not actually infinite, as for a solid), the state of zero motion $\mathbf{V} = \mathbf{0}$ does not satisfy the equations of motion. The fluid must move for all nonzero *Ra*. Such a flow is often called *free convection* to distinguish it from convective stability, which concerns situations of the type we considered in section 2, in which a stagnant conductive solution exists, which is unstable only when *Ra* is large enough. Although an experimenter can take pains to ensure that the equitemperature surfaces are horizontal in his apparatus, nature is not so obliging, and free convection is the rule rather than the exception. Nevertheless, when *Ra* is sufficiently great and the flow is vigorous enough, it is hard to distinguish between free convection and convective instability.

[78] *Glatzmaier et al.* [1999] integrated several dynamo models, all with the same total heat flow into the mantle but each distributing that heat flow differently over the CMB. They demonstrated that the assignment of the heat flux over the CMB strongly affects the mode and frequency of magnetic reversals (see section 6.4.3). *Bloxham* [2000a, 2000b] also studied dynamo models in which heat flux from the CMB is horizontally varying. He concluded that this determines the dipole/quadrupole ratio (see section 6.3.3). The effect of boundary conditions on the behavior of geodynamo models is currently a hot research topic, which is being pursued by several groups.

3.4. Nondimensionalization

[79] *Glatzmaier and Roberts* [1996a, 1996b] used dimensional equations in their dynamo simulations, but most authors prefer nondimensional equations because they feel that the properties of the system can then be understood more naturally. A word of caution is in order here. It is often thought that once a set of nondimensional parameters (Rayleigh number, Ekman number,

Table 4. Use and Definition of Nondimensional Numbers in Various Groups[a]

Group	*Ra**	*E*	*Ta**	*Ro**	*Pr**	*Pm**	*q**
KS95[b]	$\alpha\beta'_0 g_0 D^4/\nu\kappa$		*Ta*		$3\nu/2\kappa$	*Pm*	
GR95	$\alpha g_0 Q_0/2k\kappa\Omega$	$\nu/2\Omega D^2$			ν/κ		η/κ
KB97	$\alpha\beta_1 g_0 R_0^2/2\eta\Omega$	$\nu/2\Omega R_0^2$		*Ro**			κ/η
KAK97	$\alpha g_0 \Delta T D^4/\nu\kappa R_0$		*Ta*		ν/κ		η/κ
COG98	$\alpha g_0 \Delta T D/\nu\Omega$	$\nu/\Omega D^2$			ν/κ	*Pm*	
SK99	$\alpha\beta_0 g_0 R_0^4/\nu\kappa$	$\nu/2\Omega R_0^2$				*Pm*	κ/η
GBT99[c]	$\alpha\beta_0 g_0 D^6/\nu\kappa R_0^2$		*Ta*		ν/κ	*Pm*	
KMH99	$\alpha g_0 \Delta T D^3/\nu\kappa$		*Ta*		ν/κ	*Pm*	

[a]Ekman number and magnetic Prandtl number are used by all the groups with the same definition, $Ta = (2\Omega D^2/\nu)^2$ and $Pm = \nu/\eta$. Magnetic Rossby number was used by KB97 as $Ro^* = \eta/2\Omega R_0^2$. Subscript 0 and 1 indicate that the values are evaluated at the top and bottom boundaries, respectively, of the fluid shell. Symbols are as follows: β' is the superadiabatic temperature gradient, and $Q_0 = 4\pi R_0^2 \kappa\beta_0$ is the total heat flow. Other symbols are defined in the text.

[b]KS95, from *Kageyama and Sato* [1977a]; *Pr** is defined to be ν/κ.

[c]GBT99, from *Grote et al.* [2000b]; the definition of *Ra** was changed to $\alpha g_0 \Delta T D^4/\nu\kappa R_0$.

etc.) for a particular experiment or simulation is known, the results are directly comparable with other experiments or simulations. This is not, however, the case for the dynamo because the equations can be, and have been, made nondimensional in several different ways.

3.4.1. Units

[80] As mentioned in section 2.1.4, the unit of length can be chosen as either the radius of the core (R_0) or the thickness of the spherical shell ($D = R_0 - R_1$). Similarly, there are three possibilities for selecting the unit of time: viscous, thermal, or magnetic diffusion times. Differences in scaling result in different definitions of the nondimensional parameters. It is easy (though tedious) to account for the differences by using, for instance, the fact that $D/R_0 \approx 0.65$ for the Earth. The three Prandtl numbers (*Pr, Pm*, and *q*) determine the ratios of the three choices of time unit (Table 3).

[81] The selection of the unit of temperature presents more difficulty. It is often taken to be the temperature contrast, ΔT, between the upper and lower boundaries, but sometimes the product of the temperature gradient at a certain place (usually the CMB) and the chosen length scale defines the unit. This variety of possibilities is accompanied by an equal number of definitions of the Rayleigh number, and comparisons between them must be performed with care.

3.4.2. Nondimensional Numbers

[82] In general, dynamo models are completely characterized by a set of four nondimensional numbers and one constant ratio. In this paper they are the Rayleigh number *Ra*, the Ekman number *E*, the Prandtl number *Pr*, the magnetic Prandtl number *Pm*, and the radius ratio $\zeta = R_1/R_0$. Other combinations are possible and Table 4 lists the four nondimensional numbers, as defined and used by different groups. (In Table 4, asterisks emphasize the fact that the numbers are as defined by each group and may be different from the ones given in Table 3.)

[83] In defining the Ekman number a factor of 2 was included by all groups except COG98; some authors prefer the alternative Taylor number *Ta*. Two of the three Prandtl numbers are nearly always defined in the same way, although *Kageyama et al.* [1995] at first added a factor of 3/2 in *Pr* but later removed it [*Kageyama and Sato* 1977a]. The third diffusivity ratio (*q*) is sometimes defined as κ/η and sometimes as η/κ.

[84] These considerations, as well as a cursory examination of Table 4, tell us that conversion from one groups' notation to another's is usually trivial, involving only a change in the unit of length, from R_0 to *D* or vice versa. Conversion of Rayleigh numbers is less straightforward and if incorrectly done can cause significant errors; different definitions may give values that disagree by more than 1 order of magnitude! *Kono and Roberts* [2001] considered this problem in detail. They pointed out that the analysis of convection in a rapidly rotating body by *Jones et al.* [2000] showed (for reasons given in section 4.2.1) that Ra_c is almost independent of *D* when $\zeta = R_1/R_0$ lies in the range that has been used by most dynamo simulators: $0.3 < \zeta < 0.5$. Thus R_0 is preferred over *D* as unit of length, and the product of the temperature gradient at the CMB and R_0 is the preferred temperature unit because it best describes the power source driving convection and generating magnetic field.

[85] *Kono and Roberts* [2001] further argued that this definition of the Rayleigh number can easily be generalized to encompass compositional buoyancy also. Then in the definition of the Rayleigh number for the thermal convection it is appropriate to replace $\alpha\beta_0$ by $\alpha\beta_0 + \alpha^\xi\beta_1^\xi\zeta^2$, where β_1^ξ is the compositional gradient at the ICB. The factor ζ^2 is included in recognition of the smaller area of that surface.

[86] Table 5 summarizes how the nondimensional numbers, as defined for the different simulations, can be converted to those used in the present paper. As can be seen from Table 5, some of the factors appearing in the conversion of the Rayleigh numbers may be quite large. For instance, $1/(1-\zeta)^6$ is 13.3 when the radius ratio is 0.35.

[87] For a rapidly rotating system such as the Earth's

Table 5. Derivation of the Nondimensional Numbers With Common Definition

Group	*Ra*	*E*	*Pr*	*Pm*
This study	$\alpha\beta_0)g_0R_0^4/\kappa\nu+ (\zeta^2\alpha^{\xi}\beta_1^{\xi})g_0R_0^4/\kappa\nu$	$\nu/2\Omega R_0^2$	ν/κ	ν/η
KS95	$Ra^*/(1-\zeta)^4$	$(1-\zeta)^2\,(Ta^*)^{-1/2}$	$2Pr^*/3$	Pm^*
GR95	$Ra^*/4\pi(1-\zeta)^2\,E^*$	$(1-\zeta)^2\,E^*$	Pr^*	Pr^*/q^*
KB97	$(1-\zeta)^2\,Ra^*/q^*\,E^*$	E^*	E^*/q^*Ro^*	E^*/Ro^*
KAK97	$\zeta Ra^*/(1-\zeta)^5$	$(1-\zeta)^2\,(Ta^*)^{-1/2}$	Pr^*	Pr^*/q^*
COG98	$\zeta Ra^*Pr^*/(1-\zeta)^4\,E^*$	$(1-\zeta)^2\,E^*/2$	Pr^*	Pm^*
SK99	Ra^*	E^*	Pm^*/q^*	Pm^*
GBT99	$Ra^*/(1-\zeta)^6$	$(1-\zeta)^2\,(Ta^*)^{-1/2}$	Pr^*	Pm^*
KMH99	$\zeta Ra^*/(1-\zeta)^4$	$(1-\zeta)^2\,(Ta^*)^{-1/2}$	Pr^*	Pm^*

core, many authors prefer a "modified Rayleigh number" that includes the angular velocity Ω. Typically, this is the product of the usual Rayleigh number and the Ekman number (see section 4.1.3).

3.5. Numerical Methods

[88] GR95 and GR96 used a slightly different method from that described in section 2.2.2. Although they represented the velocity and magnetic field in the toroidal-poloidal form (equation (28)), they did not eliminate P by taking the curl of equation (23). Instead, they applied $\mathbf{r}\cdot$, $\mathbf{r}\cdot\nabla\times$, and ∇_{H^*} (horizontal divergence) operators directly to equation (23). This avoids one of the r differentiations, the one that led to equation (33). The resulting lower-order system is solved for P, as well as for the toroidal and poloidal scalars. GR95 and GR96 also treated the terms involving the Coriolis force (the linear part of **F**) implicitly.

[89] KS95 did not use the pseudospectral method at all but employed a grid point representation of the r and θ dependencies. This approach was also adopted in the intermediate models of *Braginsky* [1975], *Braginsky and Roberts* [1987], and *Jault* [1995].

[90] The use of regular grids in spherical coordinates is difficult because the Courant condition for the stability of the computation is hard to satisfy near the polar axis, where the φ grid points crowd together. The poles present a further difficulty because the differencing scheme is singular there. *Kageyama et al.* [1995] overcame these problems by imposing regularity conditions on the scalars and vectors at the poles and by discarding fluctuations in the solutions having wavelengths that are too short [see *Kageyama et al.*, 1993].

4. CONVECTION

[91] The aim of this section is to summarize the salient properties of magnetoconvection in a rotating fluid. This serves as a preparation for section 5, in which the workings of MHD dynamos are analyzed.

4.1. Thermal Convection in a Plane Layer

[92] The classical problem of the subject is *Rayleigh-Bénard convection*; this is, in fact, where the Boussinesq approximation of section 2 originated. The top and bottom boundaries of a uniform fluid layer of infinite horizontal extent are maintained at temperatures T_0 and $T_0 + \Delta T$, respectively, where $\Delta T > 0$. It is therefore (in the usual case $\alpha > 0$) in a potentially unstable gravitational state; heavy material overlies light. Because its viscosity and thermal conductivity are finite, the fluid does not move when ΔT is small. Nevertheless, if ΔT is large enough, motion cannot be prevented, and convection commences. The driving force of this convection is buoyancy, which is the difference between the forces exerted by gravity on the lighter and heavier fluid elements.

4.1.1. Rayleigh-Bénard Convection

[93] Whether the fluid convects or not is determined by the value of a single nondimensional measure of ΔT, the *critical Rayleigh number*, Ra_c; the fluid remains at rest if $Ra < Ra_c$ and convects if $Ra > Ra_c$. In the "critical state," $Ra = Ra_c$, the flow is infinitesimally weak but has the same general character as actual convection when Ra is only modestly in excess of Ra_c. The flow consists of a circulation that carries heat from the lower to the upper boundary. Viewed from above, the motions have a tessellated pattern (such as an array of parallel rolls or an interlocking set of hexagons) having a single horizontal wavelength a_c, which is of order D^{-1}, where D is the layer depth; that is, the convection cells are "as wide as they are deep." Such motions are "preferred" since in transporting heat across the layer they expend the least possible energy on viscous dissipation.

[94] The values of Ra_c and a_c are obtained by linearizing the Boussinesq equations and by then seeking solutions in the form of Fourier modes in which every variable is proportional to $\exp(ia_x x + ia_y y + \lambda t)$, the "constants" of proportionality being functions of the vertical coordinate z. This leads to a linear eigenvalue problem for the growth rate λ. The next step is to find, for each constant a_x and a_y, the smallest value, $Ra_m(a_x, a_y)$ of Ra for which the real part of λ is zero, i.e., for

which that particular Fourier mode is marginal, neither growing nor declining with time. For some stability problems the imaginary part of λ may be nonzero, but such "overstability" does not arise here, and we may find Ra_m by setting $\lambda = 0$ from the outset [see *Chandrasekhar*, 1961]. Because of the horizontal isotropy of the layer, $Ra_m(a_x, a_y)$ depends only on the total wave number $a = \sqrt{a_x^2 + a_y^2}$, so that we may write $Ra_m = Ra_m(a)$. The final step is to determine the critical wave number a_c by finding the minimum Ra_c of $Ra_m(a)$ as a function of a. If we suppose that Ra is initially zero and is gradually increased, the first modes capable of convection are those for which $a = a_c$, and this will happen as soon as Ra reaches the value Ra_c. If Ra is increased beyond Ra_c, the previously omitted nonlinearities in the governing equations become significant and must be restored. They limit the amplitude of the convective motions, which increases with increasing Ra. Ultimately, the convective motions become irregular and finally chaotic, i.e., turbulent.

[95] The numerical values of a_c and Ra_c are controlled by several factors. These include the mode of heat transfer (either the layer is heated from below or from within or a specified amount of heat is supplied or extracted at the boundaries) and the nature of the boundaries (either no-slip, where fluid adheres completely to the boundary all the time, or stress-free, where the fluid follows the shape of the boundary but is free to move tangentially) (see section 3.3.1). Moreover, since the convective motions are associated with a vertical heat flux that varies in the horizontal direction, the assumption that the boundaries are maintained at constant temperatures implies that they are good thermal conductors. If this is not the case, the heat conduction equation must be solved in the walls and matched to the convective solution in the fluid. In short, there is scarcely an end to the varieties of situations that can be addressed, even more than were contemplated in section 3.3.3.

4.1.2. Effect of Rotation

[96] Suppose next that the bounding walls of the Bénard layer rotate about the vertical with a constantly maintained angular velocity $\mathbf{\Omega} = \Omega \mathbf{1}_z$, and let this rotation define our reference frame. In the conduction state the fluid rotates with the walls, i.e., $\mathbf{V} = \mathbf{0}$. We once more seek the critical a_c and Ra_c for which the conduction state becomes unstable.

[97] We recall here the *Proudman-Taylor theorem*: the slow, steady motion of an inviscid, incompressible fluid is two-dimensional. This is easily established. Under the stated conditions the equation of motion (17) reduces to a balance between the Coriolis force and the pressure gradient:

$$2\rho \mathbf{\Omega} \times \mathbf{V} = -\nabla P. \tag{66}$$

Operating on this with $\nabla \times$ and recalling that $\nabla \cdot \mathbf{V} = 0$, we obtain

$$(\mathbf{\Omega} \cdot \nabla)\, \mathbf{V} = \mathbf{0}, \tag{67}$$

or $\mathbf{V} = \mathbf{V}(x, y)$. Even if the buoyancy force is restored to equation (17), it still follows that $(\mathbf{\Omega} \cdot \nabla) V_z = 0$ so that by the boundary conditions on the walls, $V_z \equiv 0$, and

$$\mathbf{V} = \mathbf{V}_H \equiv V_x(x,y)\mathbf{1}_x + \mathbf{V}_y(x,y)\mathbf{1}_y. \tag{68}$$

The admissible flow is horizontal and therefore cannot transmit heat across the layer. In the case of marginal convection (in which $\mathbf{V}$ is infinitesimal), the only possibilities of breaking this "Proudman-Taylor constraint" or rotational constraint are by restoring either $\nu\nabla^2\mathbf{V}$ or $\partial\mathbf{V}/\partial t$ or both to equation (17). It can be shown [*Chandrasekhar*, 1961] that only the first of these alternatives is possible when $Pr > 1$, and we consider that case alone.

[98] When the viscosity is small ($E \ll 1$), the Coriolis forces are so large, and the implications of the Proudman-Taylor theorem are so strong, that the marginal convective circulations are almost two-dimensional, in the sense that $\partial\mathbf{V}/\partial z$ is much smaller than $\nabla_H\mathbf{V}$ almost everywhere and $a_c = O(E^{-1/3}D^{-1}) \gg O(D^{-1})$. The convection cells are much narrower than their height. Such highly sheared motions are expensive to maintain against viscous dissipation. The buoyancy forces must be correspondingly large, and this means that Ra_c must be much greater than in the nonrotating case, and in fact, $Ra_c = O(E^{-4/3})$. We conclude that rotation tends to suppress convection.

[99] A new possibility arises: subcritical convection. Let us view the convection from the inertial frame in which, in the conduction state, the vortex lines form a uniform vertical array of density 2Ω across the layer. The Proudman-Taylor theorem is related to Kelvin's theorem, which states that vortex lines are carried by an inviscid fluid in its motion. Since vortex lines have tension, they are difficult to bend and can only move horizontally as a whole, as indicated by equation (68). The net vorticity across the layer is determined by the motion of the boundaries and cannot change. One can, however, imagine convective motions that rearrange the vortex lines to crowd them together through some horizontal areas, thus leaving other areas relatively vortex-free, in which convection can therefore occur even though Ra is much less than Ra_c. In this way, subcritical states may be envisaged, i.e., states in which finite amplitude convection persists even though $Ra < Ra_c$. It is necessary that the convective motions are strong enough to prevent the vortex lines from returning to their original uniform distribution.

4.1.3. Effect of Magnetic Field

[100] Back in the corotating frame, we consider next the case in which the layer is electrically conducting and lies in a uniform vertical magnetic field $\mathbf{B}_0 = B_0\mathbf{1}_z$. The corresponding problem with a horizontal applied field has recently been comprehensively analyzed by *Roberts and Jones* [2000] and *Jones and Roberts* [2000a].

[101] We again focus on the case $E \ll 1$ of rapid

rotation. Because of the Lorentz force (see equation (5)) an additional term $(B_0/\mu_0\rho_0)\partial\mathbf{B}/\partial z$ appears on the right-hand side of equation (66), and this provides another way of defeating the rotational constraint. If the Elsasser number, Λ, is O(1), the Coriolis and Lorentz forces are of roughly the same size, and it is found that a_c is of order D^{-1}; as in the original nonrotating case, the critical convection cells are as broad as they are deep. The magnetic field has increased the scale of the convection in directions perpendicular to Ω, and this has reduced the net (viscous plus ohmic) dissipation, so that the buoyancy force does not have to work so hard to maintain convection. It is therefore not surprising that Ra_c is reduced. In fact, $Ra_c = O(E^{-1})$ which, though large, is much smaller than in the nonmagnetic case for which $Ra_c = O(E^{-4/3})$, as we have seen. Stated another way, the modified Rayleigh number, Ra_M, defined in section 2.1.4 is O(1), i.e., the critical temperature gradient β_0 for convection is independent of ν; viscosity is no longer required to break the Proudman-Taylor constraint, as it was in section 4.1.2. Its role is taken over by the magnetic field, if large enough, and this can substantially facilitate convection in the layer.

4.2. Thermal Convection in Spheres and Spherical Shells

[102] The Earth's fluid core may be modeled as in section 2 by a spherical annulus $R_1 < r < R_0$ within a self-gravitating body $r < R_0$ of uniform density ρ_0. The natural starting point for the study of convection in such a body of fluid is again the marginal stability problem for $\mathbf{\Omega = 0}$, i.e., that of determining the value, Ra_c, of Ra for which the conduction solution $T = \bar{T}(r)$ of equation (13) becomes convectively unstable. Because of the spherical symmetry, corresponding to the horizontal isotropy of the plane layer studied in section 4.1.1, the marginal Rayleigh numbers $Ra_m(l)$ depend only on the harmonic degree, l, of the convection pattern and not on its order m (see equation (38)). The objective is to find the critical value l_c of l by minimizing $Ra_m(l)$ over l.

[103] The most unstable modes are those for which the convection cells are as wide as they are deep. If the fluid fills the entire sphere ($R_1 = 0$), this gives $l_c = 1$, which means that there is only one upwelling and one downwelling. For $m = 0$, for example, the upwelling is under the north (or south) pole and the downwelling lies beneath the south (north) pole. Elsewhere, the motions have horizontal components that carry the fluid between the two, so completing the convective circulation. In a thin annulus ($D \ll R_0$), curvature effects are unimportant, and convection is essentially the same as in the plane layer. The horizontal wavelengths of the critical modes are comparable with D, so that $l_c = O(R_0/D) \gg 1$. From the $R_1 = 0$ extreme to the $D \ll R_0$ extreme the critical l_c increases progressively from 1 to $O(R_0/D)$. For further details, see *Chandrasekhar* [1961]. Finite amplitude convection for $Ra > Ra_c$ has been analyzed by *Busse* [1975].

4.2.1. Rotating Sphere

[104] Rotation of the sphere about Oz destroys the horizontal isotropy of the system, although the eigenvalue problem still separates in longitude ϕ. A marginal mode therefore involves only a single value of m, although an infinite number of l terms arise in the expansion (38) of the solution. Thus $Ra_m(m)$ depends on m alone. Moreover, although $\mathrm{Re}(\lambda) = 0$ (by the definition of the term "marginal"), $\mathrm{Im}(\lambda) \neq 0$, corresponding to a convection pattern that drifts round Oz. If Ω is sufficiently large, the most unstable mode is not axisymmetric, which in view of Cowling's theorem is a hopeful sign for the future of this type of convection in generating a magnetic field; the motions also possesses helicity ($\mathbf{V}\cdot\nabla \times \mathbf{V}$).

[105] The critical mode is the one that minimizes $Ra_m(m)$. Let us consider the case of the full sphere and again focus on high rotation ($E \ll 1$). Then $m_c = O(E^{-1/3})$. This is because, as for the plane layer of section 4.1.2, the rotational constraint is most easily broken by convection cells having dimensions in directions perpendicular to Ω that are of order $E^{1/3}$ times smaller than their $O(R_0)$ length. Using a local stability analysis, *Roberts* [1968] argued that these cells would all lie within a cartridge belt surrounding the z axis (i.e., in a thin cylindrical shell at one particular distance $\sim s_0$ from Oz) and that for these, $Ra_c = O(E^{-4/3})$ as before [see also *Busse*, 1970]. *Soward* [1977] recognized that the local analysis had an unsatisfactory feature, and this was remedied by *Jones et al.* [2000], who found the correct critical mode, which consists of a cartridge belt of cells but at a slightly different distance s_0 from Oz; again Ra_c is $O(E^{-4/3})$, although with a slightly different constant of proportionality. For a recent realization of this form of convection, see Figure 2.

[106] Since the convection is largely confined to a thin cylindrical shell, the convection pattern and critical Rayleigh number are the same for a rapidly rotating spherical annulus as for the full sphere, provided that the inner radius R_1 of the annulus is less than s_0 (which happens to be the case for the Earth). Similar to the plane layer case, spherical convection occurs more easily in the presence of an externally created magnetic field; Ra_c is correspondingly reduced and the scale of the convection is increased, as it was in section 4.1.2.

4.2.2. Ekman Layer and Ekman Pumping

[107] The $2m_c$ cells in the cartridge belt rotate about their axes, which are parallel to Oz. The sense of their rotation is alternately in the prograde and retrograde directions, depending on whether their spin is parallel or antiparallel to $\mathbf{\Omega}$. Looking downward on them from the CMB, their motions resemble the cyclones and anticyclones, respectively, in the Earth's atmosphere. This is not true on the CMB itself, where $\mathbf{V} = \mathbf{0}$ (in the corotating frame). The transition from this state of no motion to the cyclonic or anticyclonic motions underneath

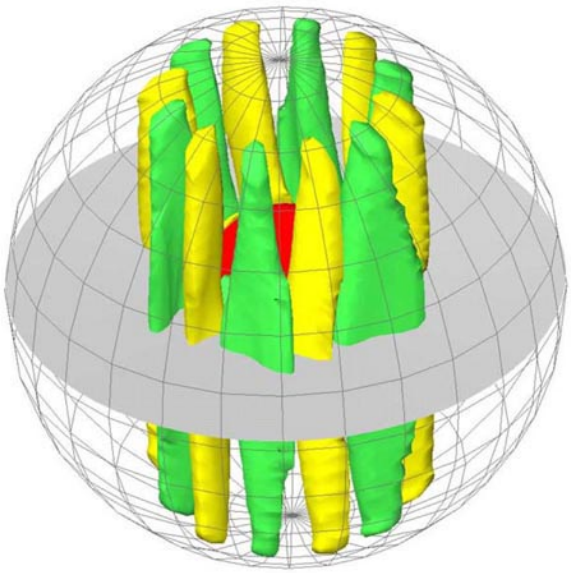

Figure 2. Snapshot of convection cells aligned nearly parallel to the rotational axis, visualized by the isosurfaces of the z component of vorticity **W**. The yellow ($W_z > 0$) and green ($W_z < 0$) surfaces indicate cyclonic and anticyclonic convection cells. Reproduced from *Kageyama and Sato* [1997c], with the permission of the authors and the publisher (American Physical Society).

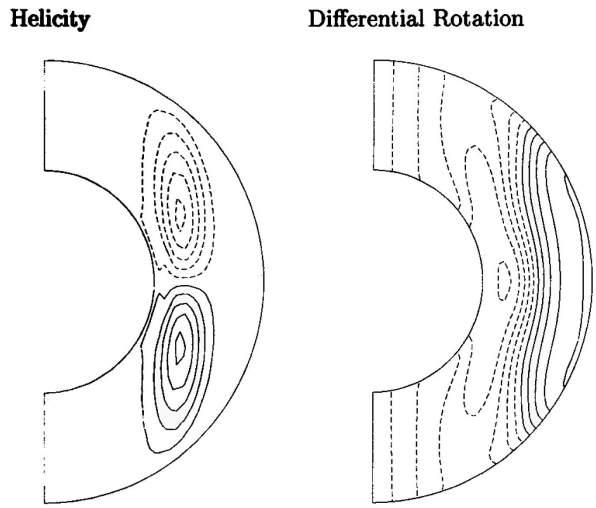

Figure 3. Snapshots of azimuthal averages of (left) the helicity and (right) the differential rotation ω. The sense of rotation is positive (solid contours) for eastward and negative (dashed contours) for westward movement. In this and Figures 4, 12, 13, and 17, solid and dashed contours show positive and negative values, using the usual definition of the quantity. In Figure 17, the zero contours are made prominent by using thick solid or dotted lines. Reproduced from *Kageyama et al.* [1993], with the permission of the authors and the publisher (American Institute of Physics).

is accomplished in a thin boundary layer, known as the *Ekman layer*; its thickness is $\delta_v = O(E^{1/2}R_0)$.

[108] A significant feature of the Ekman layer is the so-called *Ekman suction/pumping*; that is, it pumps fluid downward ($V_r < 0$) or sucks it in from below ($V_r > 0$), depending on whether the radial component of the vorticity, W_r, of the flow beneath is negative or positive, i.e., depending on whether the boundary layer lies above a cyclone or an anticyclone. To satisfy mass conservation, there must be an inflow of fluid from the Ekman layer into the cyclonic cells and an expulsion of fluid into the Ekman layer from the anticyclonic cells. The fluid pumped downward from the two ends of a cyclonic column must spread out laterally as it approaches the equatorial plane, where it helps to supply the fluid required by the upward motion in the neighboring anticyclonic columns. The velocity of pumping/suction is $O(E^{1/2})$ times the vorticity (of order R_0W_r) associated with the spin of the cells about their axes. This means that no matter whether the cells are cyclones or anticyclones, the pumping/suction creates negative helicity in their northern halves and positive in their southern halves (Figure 3). The effect of the helicity on the dynamo process will be considered in section 5.2.

[109] For cartridge belt convection to be the basis of a dynamo its magnetic Reynolds number, Rm, must be finite. We must therefore consider the finite amplitude convection that arises when $Ra > Ra_c$ (with $\mathbf{B} = \mathbf{0}$ as before). For O(1) values of Ra/Ra_c the general morphology of the cartridge belt is unaltered, but the cyclones and anticyclones are no longer on an equal footing, as may be seen from Figure 2, which was actually produced for a case of mildly supercritical convection. The cyclones are narrowed by the Ekman inflow near the poles but widened near the equatorial plane by the outflow there; conversely, the anticyclones are constricted on the equatorial plane by the incoming flow but expanded near the poles by the outgoing Ekman flow.

[110] The nonlinear interactions that arise when $Ra > Ra_c$ create a mean flow that is absent in the critical state. The mean zonal shear is shown on the right-hand side of Figure 3; it is defined by

$$\omega = \bar{V}_\phi(r, \theta)/r \sin\theta, \tag{69}$$

where

$$\bar{V}_\phi = (2\pi)^{-1}\int_0^{2\pi} V_\phi(r, \theta, \phi)d\phi$$

is the zonal average of V_ϕ. This was introduced in section 1.1 when describing the ω effect and will be of interest in section 5. It may be seen from Figure 3 that the mean flow is eastward far from the rotation axis but is westward elsewhere.

5. MAGNETIC FIELD GENERATION

[111] In section 1 we listed the nine groups that have so far published results of 3-D MHD dynamo simula-

tions (Table 1), and we plotted the position of these simulations in the $Ra - E$ plane (Figure 1). This provides a framework for classifying the models. We first summarize our classification scheme and then describe the dynamo mechanisms for typical models which characterize the various classes.

5.1. Classification of 3-D Dynamo Models

[112] Although the parameters so far employed in MHD dynamo simulations are not truly appropriate for the Earth, a wide variety of models have already been explored (Figure 1). We summarize the defining parameters of the models in Table 6; we have reexpressed them using the unified scheme that we developed in section 3.4. There are two main ways of classifying the models: by Ekman number and by Rayleigh number.

[113] First, we define three classes based on Ekman number, E. The first class, which includes KS95, KAK97, and KMH99, is the slow rotators for which E is about 10^{-4} or larger; among these, KAK97 and KMH99 are really slow rotators. Because the Coriolis force is small, these can convect at Rayleigh numbers of only a few times 10^4. The benchmark dynamo ($E = 2.1 \times 10^{-4}$, $Ra = 2.0 \times 10^5$) is a member of this class. The second class, which includes KB97, COG98, SK99, and GBT99, is the *intermediate rotators*, with $E \sim 10^{-5}$. (The COG98 and GBT99 groups also studied slow rotators but emphasized intermediate cases.) The third class of models, which includes GR95 and GR96, is the fast rotators, for which $E < 10^{-6}$. Even $E \sim 10^{-6}$ is more than 2 orders of magnitude larger than is appropriate for the Earth (see Figure 1). Although we may hope that in the future there will be a fourth class (the very fast rotators for which $E \sim 10^{-9}$), this class is currently empty; the fast rotators define the limit of what is computationally practical at the present time.

[114] We may also classify a model by how greatly its Rayleigh number Ra exceeds its critical value Ra_c. The asymptotic theory of rapidly rotating nonmagnetic convection *Jones et al.* [2000] gives $Ra_c = cE^{-4/3}$, where the constant c is 1.13, 4.12, and 8.05 for $Pr = 0.1$, 1, and 10, respectively. The term "criticality" used in Table 6 is Ra/Ra_c based on the $cE^{-4/2}$ measure of Ra_c. The representative points for some of the models plotted in Figure 1 lie below the solid line defined by the theoretical Ra_c (for $Pr = 1$). This is because the theoretical Ra_c is based on one mode of energy supply and one set of boundary conditions, whereas various other conditions were used in some of the models studied. The classification by Rayleigh number is therefore more ambiguous than that based on Ekman number. Nevertheless, we shall use the criticality parameter to measure how strongly a dynamo is driven. It turns out that for all the slow and intermediate rotators, Ra/Ra_c is rather small [$<O(10^2)$]. We shall use values of roughly 1 and 100 to classify models as weakly driven, moderately driven, or strongly driven. The distinction between weakly and moderately driven dynamos is based on the velocity field which is more or less regular in the former but chaotic in the latter (see below and Figures 7, 8, and 9). Among the fast rotators, only GR95 is strongly driven ($RaE^{4/3} > 10^4$); according to our definition the GR96 model is moderately driven.

[115] We discuss magnetic field generation in dynamo models based on three typical examples. Figure 4 compares the azimuthally averaged velocity and magnetic field structures in these three models. The first is the benchmark dynamo, which is typical of a weakly driven, slow rotator. This model is of particular interest because most of the groups listed in Table 1 participated in the benchmark test using this model, and good agreement was found between the reported results [*Christensen et al.*, 2001]. In this model the convection cells maintain a regular form. The solution is quasi-stationary, with a time-independent pattern that drifts steadily in the azimuthal direction as envisaged by *Zhang and Busse* [1988, 1989, 1990] (section 3.1). The second model is SK99 [*Sakuraba and Kono*, 1999], which is an intermediate rotator, driven by forcing of moderate strength. The convection pattern is drastically affected by the magnetic field, and both the velocity and the magnetic fields are more or less chaotic. The basic structure retains, however, something in common with the first group of models, namely, the cartridge belt convection and associated concentrations of magnetic flux. The third model is GR96 [*Glatzmaier and Roberts*, 1996a], which is not as strongly driven as the GR95 model but which is a fast rotator. Because of the dominance of the Coriolis force and the need to dispose of the energy released above the inner core, much of the activity is concentrated within the *tangent cylinder*, i.e., the imaginary cylinder that touches the ICB on its equator. Heat transfer is greatest in regions near the polar caps, and the magnetic field is strongly concentrated there.

[116] Figure 5 displays the energy spectrum in the core for all three models. In each case, the magnetic energy exceeds the kinetic energy. Their ratio depends on how strongly the dynamo is driven; although the magnetic energy is about 10 and 50 times larger than the kinetic energy in the benchmark and SK99 models, it is about 1000 times greater in the GR96 model. Another notable feature of Figure 5 is the rate of decrease of energy with increasing harmonic degree l. In the benchmark model the decay is quite rapid with a reduction of about 10^4 between $l = 1$ and $l = 40$. The SK99 model shows a reduction of only about 10 across this range, even though this model employs a weak hyperdiffusivity. The GR96 models are usually integrated with rather a severe hyperdiffusivity (see section 3.2.3 and Table 6), but the simulation reported by *Roberts and Glatzmaier* [2000a] used no hyperdiffusivity whatever, although numerical resolution required a truncation level of $L = 239$.

5.2. Comparison of Dynamo Behavior in Typical Models

[117] In this section, we describe the MHD processes seen in various dynamo models. We first return to the

Table 6. Comparison of MHD Dynamo Models

Quantity	*Symbol*	*Group*								
		KS95	*GR95*	*GR96*	*KB97*	*KAK97*	*COG98*	*SK99*	*GBT99*	*KMH99*
Density change[a]	$\Delta\rho$	C	B	A	B	B	B	B	B	B
Energy supply[b]		ΔT	Q_0	$Q_0 + \Delta\xi$	ΔT	ΔT	ΔT	ε	ε	ΔT
Radius ratio	R_1/R_0	0.30	0.351	0.351	0.343	0.5	0.351	0, 0.4	0.4	0.4
Rayleigh number	Ra	$0.8–1.1 \times 10^5$	5.4×10^{12}	4.6×10^9	$0.15–2.8 \times 10^8$	$0.5–2.6 \times 10^5$	$0.07–1.5 \times 10^7$	1.0×10^7	$0.1–1.7 \times 10^7$	$6.2–7.7 \times 10^3$
Ekman number	E	2.0×10^{-4}	8.4×10^{-7}	8.2×10^{-7}	$2.0–10 \times 10^{-5}$	$1.9–2.8 \times 10^{-3}$	$6.3–63 \times 10^{-5}$	3.2×10^{-5}	$3.6–21 \times 10^{-5}$	$3.6–36 \times 10^{-3}$
Prandtl number	Pr	0.78–1	5000	725	1	1	1	1	1	1
Magnetic Prandtl number	Pm	10–28	500	725	1	8.3–50	1–5	20	1–50	35
Criticality[c]	$Ra\,E^{4/3}$	0.6–1.7	4.3×10^4	36	70–200	20–130	1.5–29	10	5.6–33	3.4–33
Hyperdiffusivity[d]	ν_1/ν_0-1	no	$0.075l^3$	$0.0375l^3$	$0.05(l-5)^2$	no	no	$(1/20)^3$	no	no
Velocity boundary condition		no-slip	no-slip	no-slip	stress-free	no-slip	no-slip	no-slip	stress-free	no-slip
Magnetic boundary condition at CMB[e]	B_{CMB}	$B_\theta, B_\phi = 0$	H	H	H	H	H	H	H	H
Inner core conductivity[f]	σ_{IC}	∞	σ	σ	σ	0	0	σ	0	0
Numerical method[g]		FDSG	PSM	PSM	PSM	FDPS	PSM	PSM	PSM	PSM
Harmonics in r[h]	L_r		46 + 15	48 + 32		128	33–41	32 + 10	33	4
Harmonics in θ	$L\theta$		21	21–239	40	64	53–85	43	64	16
Harmonics in ϕ	L_ϕ		21	21–239	40	128	96–256	43	64	16
Grids in r	N_r	30–50	49 + 17	31	40	128	33–41	32 + 16		
Grids in θ	N_θ	32–38	32	32	32	64	80–128	64		
Grids in ϕ	N_ϕ	64–128	64	32	32	128	160–256	64		
Time step	Δt		1.5×10^{-6}	15 days		1.25×10^{-5}		2.0×10^{-7}	$\leq 1 \times 10^{-4}$	

[a]Density change: A, anelastic; B, Boussinesq; C, compressive.
[b]Energy supply: ΔT, temperature difference assigned between R_0 and R_1; Q_0, total heat flow at R_0; $\Delta\xi$, buoyancy source given at ICB; ε, distributed heat source.
[c]Criticality: according to *Jones et al.* [2000] the condition for onset of convection is $RaE^{4/3} = 4.12$ for $Pr = 1$.
[d]Hyperdiffusivity: the form $a(l - l_0)^n$ indicates that $\nu = \nu_0$ for $l \leq l_0$ but $\nu = \nu_0[1+a(l - l_0)^n]$ for $l > l_0$.
[e]Magnetic boundary condition at CMB: H, harmonic boundary condition. GR95 assumes that a layer of thickness $0.04D$ above the CMB has the same conductivity as the core. GR96 provide an infinitely thin conductive layer at the CMB to simulate the core-mantle coupling.
[f]Inner core conductivity: inner core is assumed to be perfect conductor (∞) and insulator (0) or has the same conductivity (σ) as the outer core.
[g]Numerical method: FDSG, finite difference in spherical grid; PSM, pseudospectral method in all coordinates; FDPS, finite differencing in r and pseudospectral method in θ,ϕ coordinates.
[h]Harmonics here means Chebyshev coefficients: outer core and inner core harmonic degrees if two numbers are given.

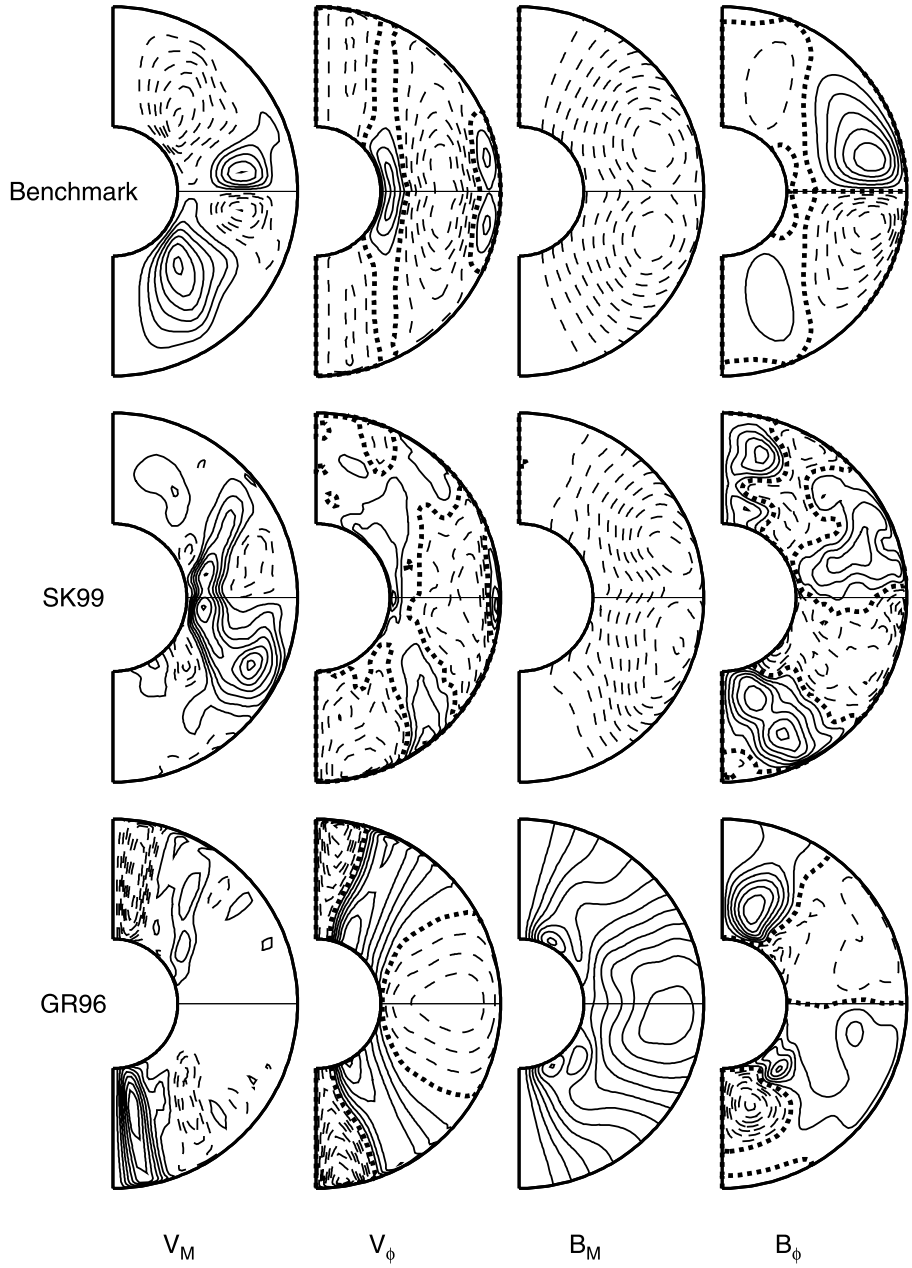

Figure 4. Snapshots of azimuthal averages of meridional and azimuthal components of velocity (V_M, V_ϕ) and magnetic field (B_M, B_ϕ) for (top) the benchmark, (middle) SK99, and (bottom) GR96 models. The positive (negative) contours indicate counterclockwise (clockwise) meridional field lines (V_M and B_M) and eastward (westward) azimuthal fields (V_ϕ and B_ϕ).

supercritical cartridge belt convection described in section 4.2, i.e., the slow to intermediate rotators. The way this convection generates field has, up to now, been studied at low to moderate energies. We describe why it is a successful dynamo. We then turn to more strongly driven dynamos and stress the differences caused by the greater energy available to the system. We shall also touch on some issues that are of general interest to dynamo theorists.

5.2.1. Kinematics of the Cartridge Belt Dynamo

[118] Figure 6 is taken from a cartoon prepared by *Kageyama and Sato* [1997c]. Figure 6a shows the distortion of a westward directed zonal field line (labeled 1), situated just outside but touching the cartridge belt in northern midlatitudes, by the fluid motions in the vicinity of two adjacent cells, the cyclonic cell being to the west of the anticyclonic cell. The flow in the "valley" between the cells is inward (toward Oz) and tends to draw the field line into the valley, as indicated by the curve labeled 2. This stretches the field line against its tension, i.e., $-\mathbf{V}\cdot(\mathbf{J} \times \mathbf{B}) > 0$, corresponding to the creation of magnetic energy from kinetic energy (see section 2.1.1). At the same time, the flow created by Ekman pumping draws the field line upward within the

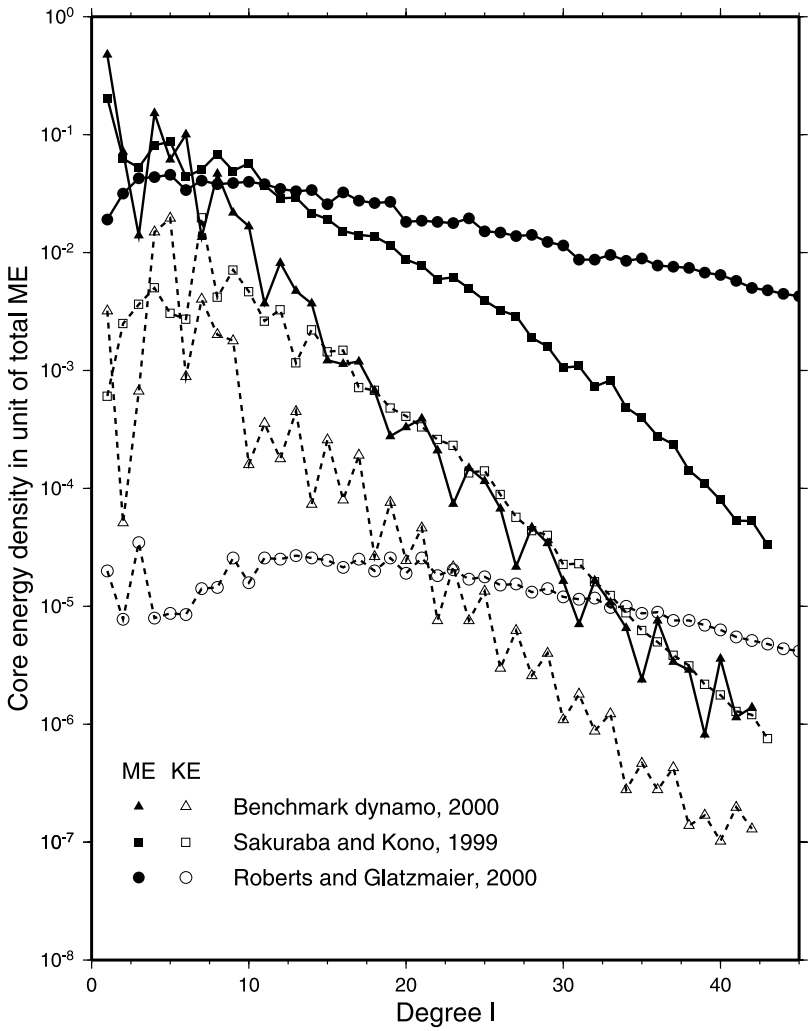

Figure 5. Kinetic (KE) and magnetic (ME) energy densities in the core for the benchmark, SK99, and GR96 models of which the last was calculated without hyperdiffusivity [*Roberts and Glatzmaier*, 2000a]. The abscissa and ordinate indicate the spherical harmonic degree l and the energy contained in each degree, as a fraction of the total magnetic energy.

anticyclone and downward within the cyclone, so giving the field a meridional component in the z direction, as indicated by the curve labeled 3.

[119] A similar process operates in the Southern Hemisphere where, as we show below (Figure 12d), the toroidal field is directed eastward. The curves labeled 1 and 3 in Figure 6a are shown again in Figure 6b together with their partners in the Southern Hemisphere. It may be seen that the two lines of type 3 are in close proximity near the point labeled a, and one can readily imagine that they will reconnect and straighten up to create a magnetic field line lying approximately in a meridional plane and crossing from one hemisphere to the other, as in a dipole field. When we consider the net effect of all the convection cells in the cartridge belt, we see that a complex field has been created from the initial axisymmetric zonal field and that the field has a nonzero mean meridional part. Such processes were considered in section 1.1. They correspond to an α effect that is positive in the Northern Hemisphere of the core and negative in the Southern Hemisphere.

[120] To close the regenerative loop, we must create the mean zonal field from the mean meridional field. *Kageyama and Sato* [1997c] established unequivocally that in the case of their dynamo (KS95), this was brought about by the ω effect of the mean zonal flow, which has a form similar to that shown in Figure 3. This flow is symmetric with respect to the equatorial plane and stretches the meridional field lines (which are of dipole type, see Figure 6) into the ϕ direction, giving them an east to west component in the Northern Hemisphere and a west to east component in the Southern Hemisphere. This is exactly what is required to complete the regenerative loop for the mean field (see section 1.3.1). The dynamo is therefore of $\alpha\omega$-type (see section 1.3), as are the KS95 models and probably the benchmark and SK99 models also (see V_ϕ in Figure 4). However, there is also the possibility that the zonal field required to

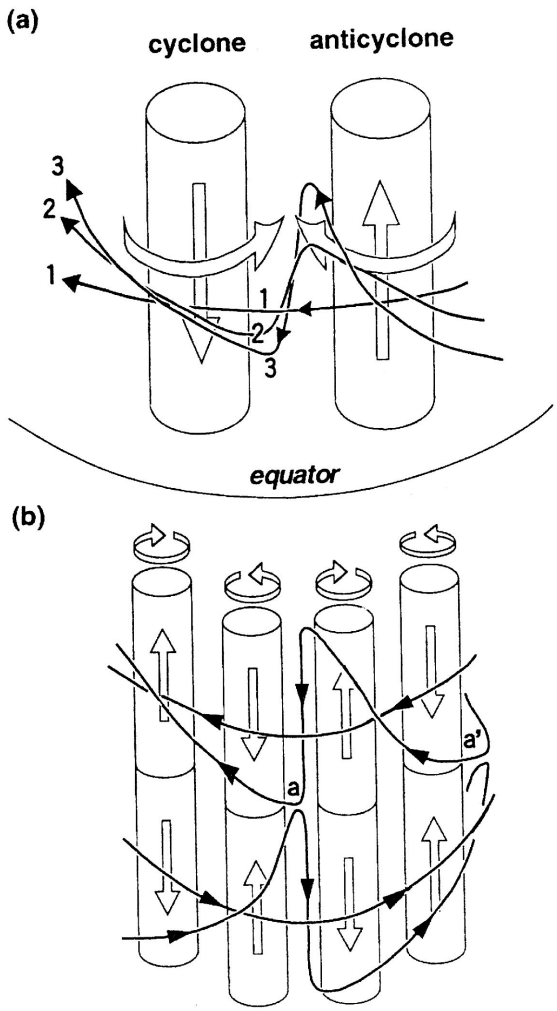

Figure 6. The dynamo mechanism as explained by *Kageyama and Sato* [1997c]. (a) A pair of cyclonic and anticyclonic convection cells with clockwise or anticlockwise rotation is associated with a poleward or equatorward transport (shown by the open arrows), which deform the toroidal magnetic field lines from $1 \rightarrow 2 \rightarrow 3$. (b) Similar deformation of the magnetic field occurs in the Southern Hemisphere but with the opposite sense and finally generates the poloidal field by magnetic reconnection near the points marked *a* and *a'*. Reproduced with the permission of the authors and the publisher (American Institute of Physics).

complete the regenerative loop is created from the meridional field by the α effect (see section 1.3). It appears that the COG model is such an α^2 dynamo [see *Olson et al.*, 1999].

5.2.2. Magnetic Flux Concentration in Cyclones and Anticyclones

[121] Although the signs of the helicity in both cyclonic and anticyclonic columns are the same within a hemisphere, the distribution of magnetic flux in the two types of columns is not the same. As one may guess from the directions of influx and efflux in the columns described in section 4.2, the magnetic flux is concentrated into the anticylones near the equatorial plane, and into the cyclones near the poles. Figures 7–9 compare the complex correspondences between the velocity and magnetic fields for the case of the three typical models. The benchmark model represents a slowly rotating, weakly driven dynamo, the SK99 model is an intermediate rotator with weak to moderate driving, and the GR96 model represents a fast rotator driven by an moderate energy supply (see Figure 1 and Table 6).

[122] Figure 7 shows the axial components of the vorticity (W_z) and the magnetic field (B_z) on the equatorial plane for the three models. For the first two models it is clearly seen that the magnetic flux is strongly concentrated inside the anticyclones (which rotate counterclockwise as seen from the north, i.e., $W_z < 0$). In equatorial latitudes the fluid within the anticyclones moves poleward (see below) and can be supplied only by an inward flow from the outside. This, in turn, draws the magnetic flux into the anticyclones. In the case of the benchmark dynamo the patterns can be seen to have clear fourfold symmetry. In the SK99 model the pattern is more or less chaotic (and changes with time), but the strong magnetic flux is again confined within the anticyclones. On the other hand, there appears to be no immediate correspondence between the patterns of W_z and B_z in the case of the GR96 model; the distribution of W_z shows that there are about four pairs of cyclonic and anticyclonic rolls, but the distribution of B_z does not follow suit. Another difference between the benchmark and SK99 models and the GR96 model is that the direction of the magnetic field is nearly uniform in the former two but strong reversed magnetic flux exists in the latter.

[123] At the surface of the sphere the correspondence between vorticity and field is completely reversed. In the benchmark model (Figure 8a) the positions of the concentrated magnetic flux are displaced by about 30° to the west of their equatorial positions (Figure 7a) and now reside inside the cyclones (clockwise rotation, i.e., $W_z < 0$). In the SK99 model (Figure 8b) the displacements of the concentrations from their equatorial positions are not the same in every case, but their positions again coincide with the cyclones. For the GR96 model (Figure 8c), there seems to be little correspondence between the *convection rolls* and the magnetic flux concentrations. Instead, there is a notable intensification of the of magnetic field near the poles (inside the tangent cylinder).

[124] To demonstrate that the magnetic flux concentration in the anticyclones or cyclones in the cartridge-belt-type dynamos is caused by the convergence of fluid, the flow pattern in the equatorial plane is depicted in Figure 9 (left), where the poleward flux (V_z) is given by contours and the velocity components perpendicular to the rotation axis (V_s and V_ϕ) are shown by arrows. Figure 9 (right) presents the flow pattern inside the Ekman layer ($r = 0.98R_0$); in this case, contours give the radial components (V_r), and arrows give the horizontal (V_θ and V_ϕ) components of the velocity. In the benchmark and

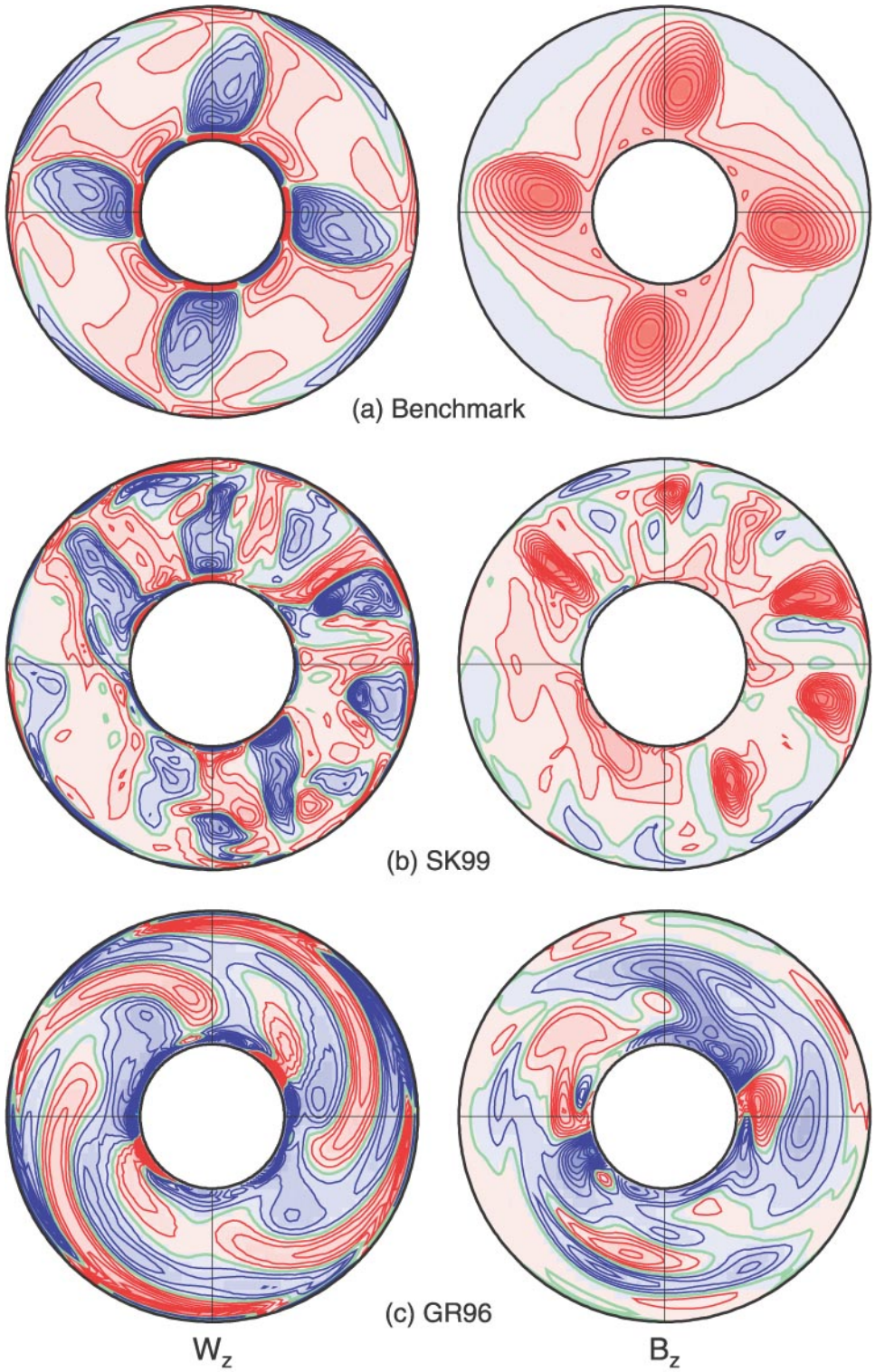

Figure 7. Snapshots of the axial components of the vorticity (W_z) and the magnetic field (B_z) in the equatorial plane, for (a) the benchmark, (b) SK99, and (c) GR96 models. In this and Figures 8, 9, 10, and 16, red (blue) color and contours show positive (negative) values, and green line gives the zero contour. The concentration of the magnetic flux in the anticyclones ($W_z < 0$) is evident in Figures 7a and 7b but is not significant in Figure 7c.

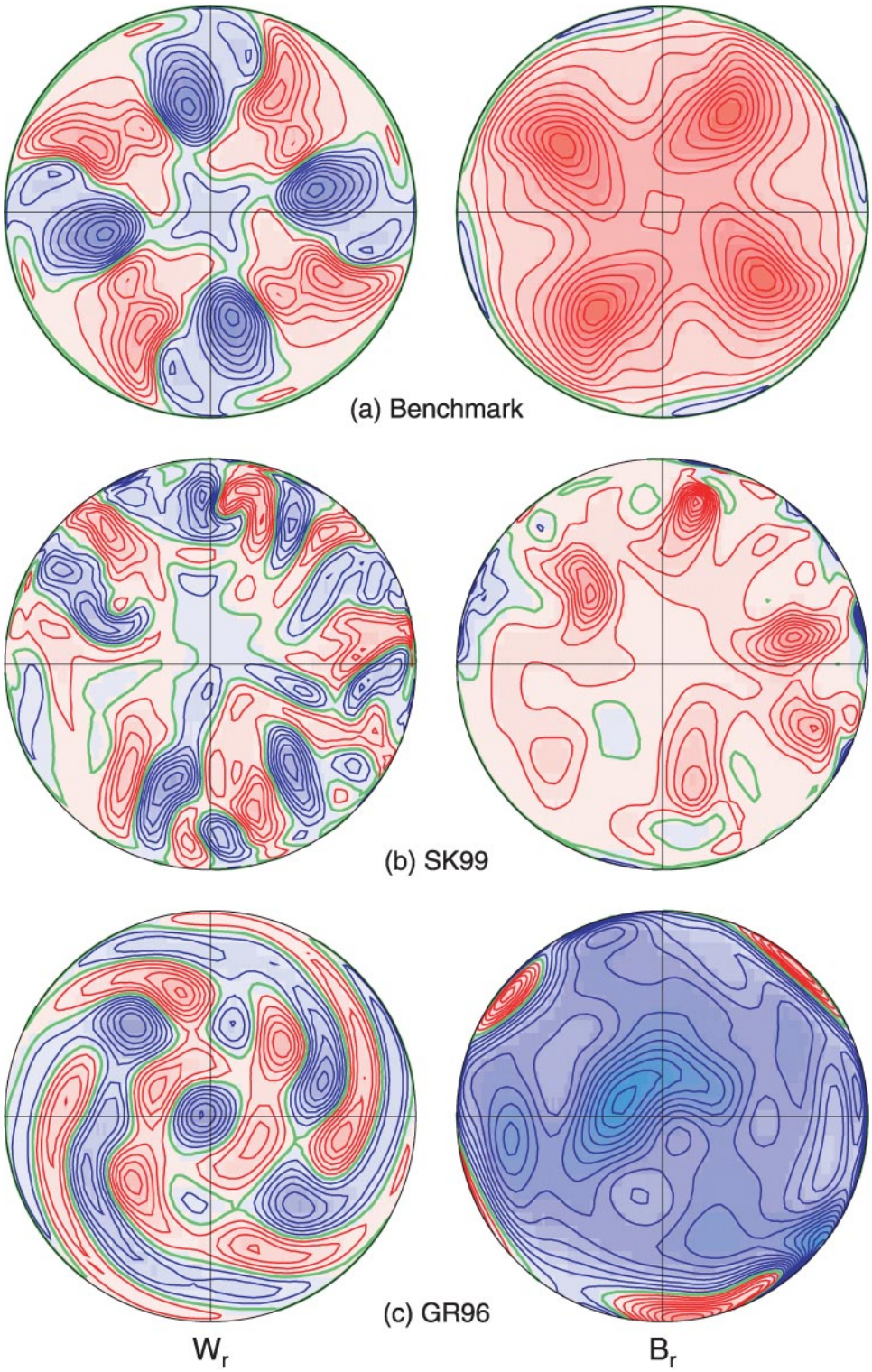

Figure 8. Snapshots of the radial components of the vorticity (W_r) and the magnetic field (B_r) near the CMB for (a) the benchmark, (b) SK99, and (c) GR96 models. The value of B_r is that at the surface, but W_r is given by the value inside the Ekman layer ($r = 0.98R_o$). Contrary to Figure 7, the magnetic flux is concentrated in the cyclones ($W_z > 0$) in Figures 8a and 8b, and near the north pole in Figure 8c. Shown by orthogonal projection centered at the north pole.

SK99 dynamos the counterclockwise and clockwise circulation associated with the cyclones and anticyclones is very clearly seen. The convergence of fluid into anticyclones in the equatorial plane and into cyclones in the Ekman layer can be seen from the ϕ component of velocity near the boundaries of two convection cells. This phenomenon is more evident from the velocity components perpendicular to the plane. For a more

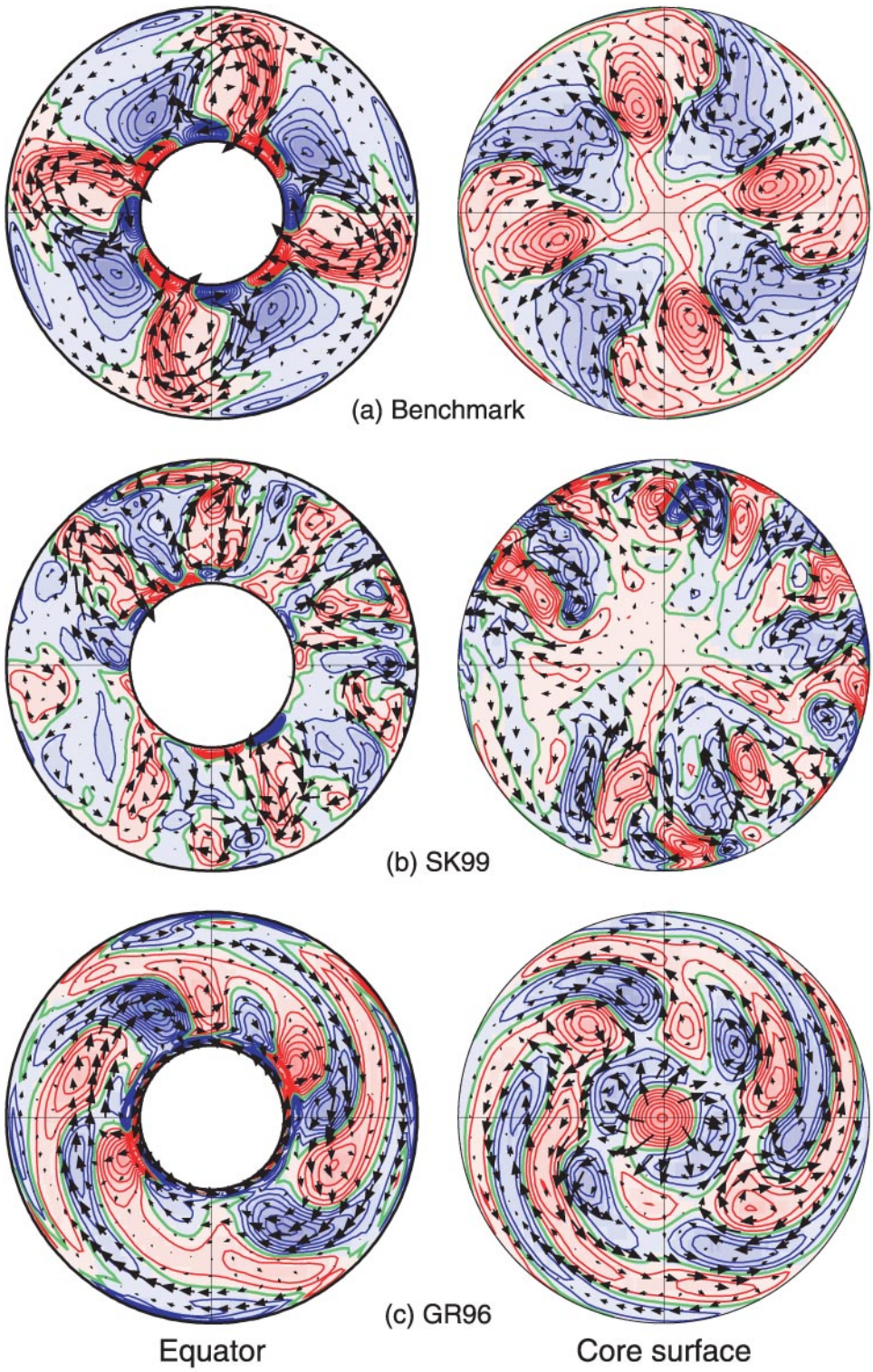

Figure 9. Snapshots of the flow (left) in the equatorial plane and (right) in the Ekman layer below the CMB ($r = 0.98R_0$). Color shade and contours give the flux perpendicular to the plane under consideration (V_z on the left and V_r on the right). Arrows show the velocity component in the plane (V_s and V_ϕ on the left and V_θ and V_ϕ on the right). In the benchmark (Figure 9a) and SK99 (Figure 9b) models, flux converges in the anticyclones (red) in the equatorial plane, and in cyclones (blue) in the Ekman layer. In GR96 model (Figure 9c), a very strong outward flow exists near the pole, which is caused by the strong upward transport in the polar region associated with the thermal wind.

detailed discussion on flux concentration in cartridge-belt-type convection, see *Sakuraba and Kono* [2000].

[125] There is also circulation of the type discussed above in the GR96 model (Figure 9c), but the correspondence between the magnetic flux and cyclones or anticyclones is not so direct in the GR96 model. In this rapidly rotating system the interior of the tangent cylinder plays a more important role than the region outside it. The highly concentrated V_r flux near the north pole and the associated strong outward flow in the Ekman layer indicate this fact for the velocity field, while a strong concentration of magnetic flux is seen near the north pole in Figure 8c.

5.2.3. MHD of the Cartridge Belt Dynamo

[126] When *Ra* is so large that the magnetic Reynolds number, *Rm*, of the flow significantly exceeds the critical value, Rm_c, at which the kinematic dynamo described in the section 5.2.2 becomes marginally possible, a weak seed field will grow until nonlinear terms, and particularly the Lorentz force $\mathbf{J} \times \mathbf{B}$, halt further growth. Here we consider some of the ways in which this saturated solution differs from the nonmagnetic state.

[127] In section 4.1 we saw that in a plane layer the scale of convection in directions perpendicular to Ω is increased by the presence of a magnetic field. The same is true for convection in a spherical annulus, and it brings about a reduction in m_c, corresponding to a reduction in the number of convection rolls. This happens whether the magnetic field is applied, as in section 4.1, or is generated by dynamo action, as here. Figure 10 shows such an example based on the SK99 model, in which the axial component of vorticity W_z in the equatorial plane is compared for three stages of the same simulation. When there is no magnetic field, eight pairs of more or less regularly spaced cyclonic and anticyclonic convection rolls can be seen (Figure 10a). The convection pattern also exhibits a "trailing" effect; the cell is elongated in the direction of rotation. When a magnetic field is generated by dynamo action, the number of cells is progressively reduced as the magnetic field increases. Also the trailing of the cells become less and less clear, indicating that the magnetic field has reduced the zonal shear present in the nonmagnetic system. In Figure 10b the magnetic field is still weak, and the kinetic energy is larger than the magnetic energy, while the magnetic field is fully grown and its energy is ~50 times larger than the kinetic energy in Figure 10c. When the magnetic field becomes strong enough, the symmetry between the cyclones and anticyclones is broken and the anticyclonic rolls (negative W_z) become more dominant (Figure 10c).

[128] It is well known that when the Lorentz force is interpreted through the Maxwell stresses, the magnetic field lines are in tension but repel each other. This means that they resist being concentrated together in the way described in section 5.2.2. They therefore oppose being forced together into the anticyclones in the equatorial plane and into the cyclones near the poles. Figure 11 shows one half of the equatorial section at the same time as in Figure 10c. The strongest concentration of the magnetic field lines is in the anticyclone situated at 180° latitude. There the Lorentz force is strong and points

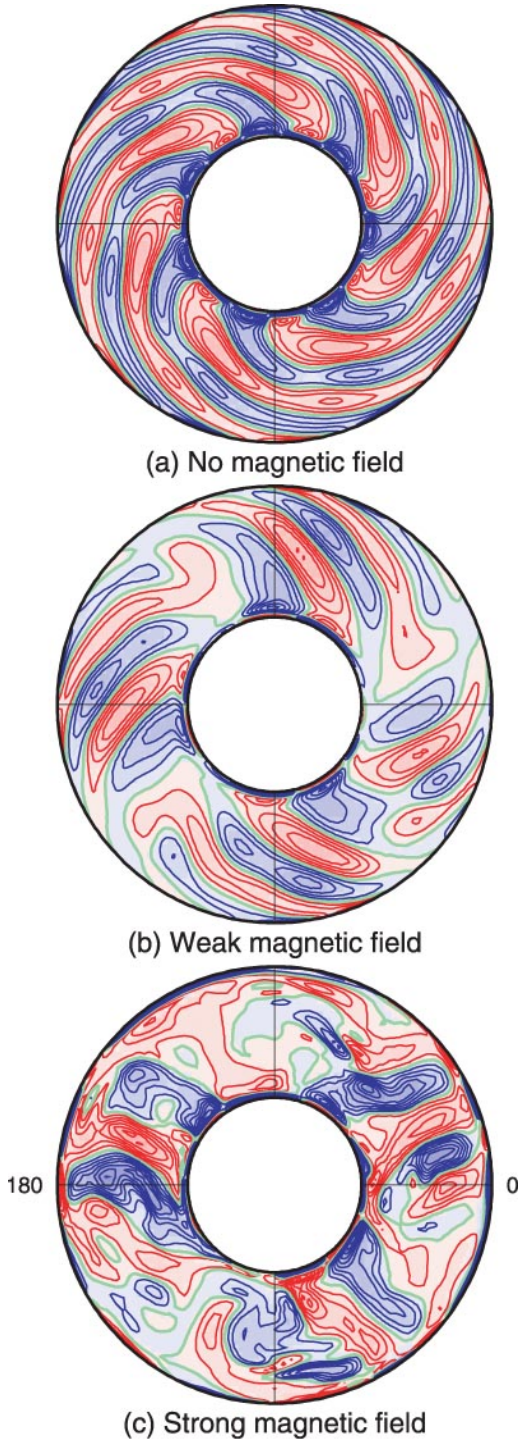

Figure 10. Snapshots showing the effect of magnetic field on the pattern of fluid motions in a convecting spherical shell in the SK99 model, as seen by the axial component of the vorticity (W_z) in the equatorial plane for (a) the nonmagnetic case, (b) the weak magnetic field regime, and (c) the strong magnetic field regime. Note the changes in the number of convection rolls and in the trailing effect.

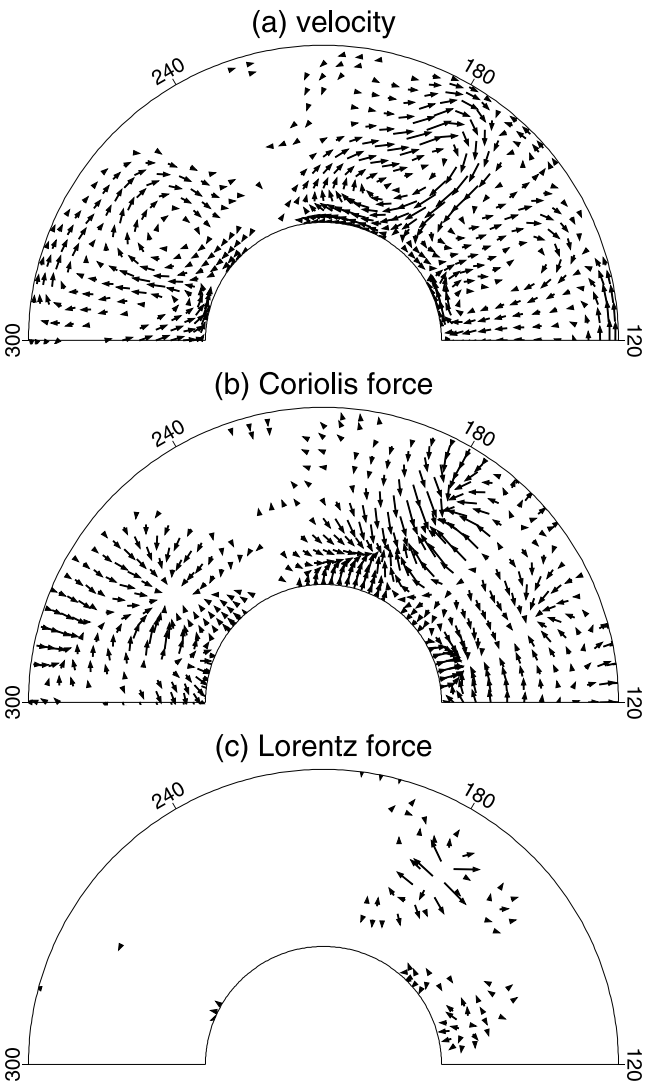

Figure 11. A snapshot of (a) the velocity, (b) the Coriolis force, and (c) the Lorentz force in the equatorial plane based on the SK99 model. This and Figure 12 show the SK99 model at the same moment as in Figures 7–10. Reproduced from *Sakuraba and Kono* [1999], with the permission of the publisher (Elsevier Science BV).

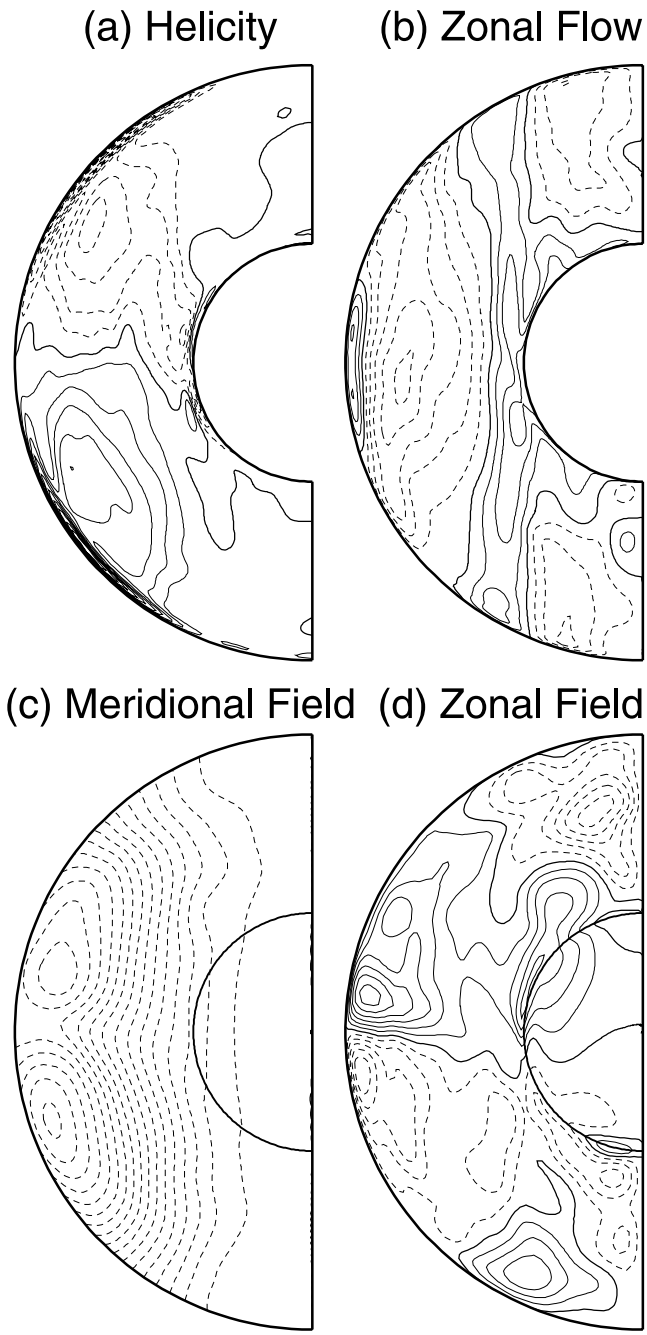

Figure 12. A snapshot of the longitudinally averaged (a) helicity, (b) zonal velocity, (c) meridional, and (d) zonal magnetic field from the SK99 model. Reproduced from *Sakuraba and Kono* [1999], with the permission of the publisher (Elsevier Science BV).

away from the center of the convection cell. This strong outward force is opposed by the Coriolis force which points inward in the case of the anticyclonic cell. To establish this balance, anticyclones should grow in size as the magnetic field becomes stronger [*Sakuraba and Kono*, 1999]. Such a strong effect of the magnetic field on the velocity is not seen in weakly driven dynamos such as the KS95 and benchmark models.

[129] An even more drastic change can be discerned in the structure of the azimuthal shear, ω. When the magnetic field is sufficiently strong, the situation for $\mathbf{B} = \mathbf{0}$ (illustrated by Figure 3) is essentially reversed: the mean flow is westward far from the rotation axis but is eastward elsewhere and, in particular, eastward in the vicinity of the inner core. This again can be attributed to the dominance of anticyclone in the low to middle latitudes [*Sakuraba and Kono*, 1999]. Such a situation is illustrated by Figure 12.

5.3. Strongly Driven Dynamos

[130] In section 4.1.3 we considered the onset of convection in a rapidly rotating plane layer when a magnetic field that owes its existence to sources outside the layer is present. We observed that the critical Rayleigh number is reduced by the magnetic field; when the Elsasser

number $\Lambda = O(1)$, for example, it was $O(E^{-1})$ rather than the much greater $O(E^{-4/3})$ that applies when $\mathbf{B} \equiv \mathbf{0}$. We attributed this to a weakening of the Proudman-Taylor constraint by the magnetic field, so that convection occurs more easily. The situation is not very different when the magnetic field is created within the layer by dynamo action [see *Jones and Roberts*, 2000b]. A system convects more readily if it can create its own dynamo; convection can then occur subcritically at values of Ra much less than the Ra_c for nonmagnetic convection described in sections 4.1.2 and 4.2. In this sense, strongly driven dynamos are far more supercritical than is suggested by the steeper set of lines (based on Ra_c) drawn in Figure 1. This is why the thin lines (of constant Ra_M) were added to Figure 1. However, since convection can generate the field that it needs to overcome the rotational constraint only if it has finite amplitude ($Rm \sim 1$), it cannot be described accurately by marginal theories such as those outlined in sections 4.1.2 and 4.2.

[131] This discussion highlights the fact that the characterization we adopted in section 5.1, in which a dynamo is classified by the size of its Rayleigh number, is not completely satisfactory. When the field is sufficiently strong, the value of $Ra_M \equiv E\,Ra$ may provide a more realistic parameter with which to gauge whether or not the dynamo is strongly driven. Alternatively and perhaps preferably, we might distinguish between different dynamos not (through Ra or $RaE^{4/3}$) by how strongly they are driven but (through Λ) by how large the magnetic fields are that they produce. A dynamo is a "strong field dynamo" if it maintains a field of order, or greater than, $(2\Omega\eta\mu_0\rho_0)^{1/2}$ and is a "weak field dynamo" otherwise. Perhaps the main objection to characterizing a dynamo in this way is that Λ is not known until the numerical integrations have determined how strong the field is that it creates. Although the Lorentz force is as large as, or larger than, the Coriolis force in a strong field dynamo, this does not mean that all vestiges of two dimensionality are lost. The Lorentz force has no naturally preferred direction, but in countering the rotational constraint the magnetic field and Lorentz force acquire a preference for the direction of $\mathbf{\Omega}$. This is ultimately the reason why the magnetic compass needle points north. A strong field dynamo is merely a subcritical state of convection which is available to a sufficiently large body of electrically conducting fluid. According to our definition in section 5.1, it is not necessarily strongly driven.

[132] The fact that a rapidly rotating system lying in an externally produced magnetic field convects when $Ra > Ra_c$, where $Ra_c = O(E^{-1})$ for $\Lambda \sim 1$, suggests (but by no means proves) that the same is true for a strong field dynamo. If this suggestion is correct, as was essentially postulated by *Taylor* [1963], the well-known uncertainty in the viscosity of core fluid may not have important dynamical consequences because $Ra_c = O(E^{-1})$ implies that the temperature gradient β_0 required for convection is independent of ν (see section 4.1.3); also $\Lambda \sim 1$ implies that the field created by the dynamo is independent of ν. Further, from section 4.1.2 one would anticipate that the scale of convection in a strong field dynamo is that of the fluid container; the convection cells are as broad as they are deep. A degree of caution is, however, advisable especially in view of the alternative proposal of *Braginsky* [1975]; if the geodynamo is of model Z type, it will operate only if Ra_M is larger than O(1). The motions in the dynamos described below certainly display striking features on scales much smaller than R_0.

[133] The GR95 and GR96 models are driven more strongly than the SK99 model and appear to be strong field dynamos. The magnetic field energy in the GR95 and GR96 models is usually greater than the kinetic energy density by about 1000; this factor is more typically 50 for the SK99 model. Their magnetic activity is confined more completely than the SK99 model to the interior of the tangent cylinder. They also operate at smaller Ekman numbers (see Figure 1), and this gives them some highly developed two-dimensional features. Figure 13 shows that the helicity and differential rotation are largely confined to the tangent cylinder, as, in fact, are the electric currents. Meridional circulations exist outside the tangent cylinder but are much weaker than the circulations within it. The temperature gradient is also greatest inside this cylinder. The buoyancy force produces an outward flow near and along the rotation axis. The return flow skirts the surface of the tangent cylinder. The meridional flow near the poles is therefore away from the rotation axis but is toward that axis near the equator. This flow is deflected by the Coriolis force to create a strong zonal wind, which is eastward near the inner core and westward near the polar caps. The associated ω effect is very strong, as are the associated magnetic stresses on the inner core (which is electrically conducting in these models) (see section 5.4.1).

[134] From Figures 7–9 we see that the greater thermal forcing of the SK99 model, as compared with the benchmark model, results in some irregularity in its structure. This tendency becomes even more pronounced when the models are driven still more strongly. This is seen with particular clarity in the GR95 and GR96 models, which behave in a very irregular way, and it is no accident that these were the first geodynamo models to undergo polarity reversals [*Glatzmaier and Roberts*, 1995b].

5.4. Other Aspects of Dynamo Mechanisms

5.4.1. Rotation of the Solid Inner Core

[135] On the basis of GR95, *Glatzmaier and Roberts* [1995a] predicted that the inner core of the Earth drifts eastward relative to the mantle at about 1° per year. The reasons were analyzed by *Glatzmaier and Roberts* [1996b]. In short, the drift is an example of Lenz's law. In their models (in which the inner core is electrically conducting) the heat from inside the tangent cylinder is carried mostly by the meridional circulations inside the cylinder. Because of rotation, circulations produce

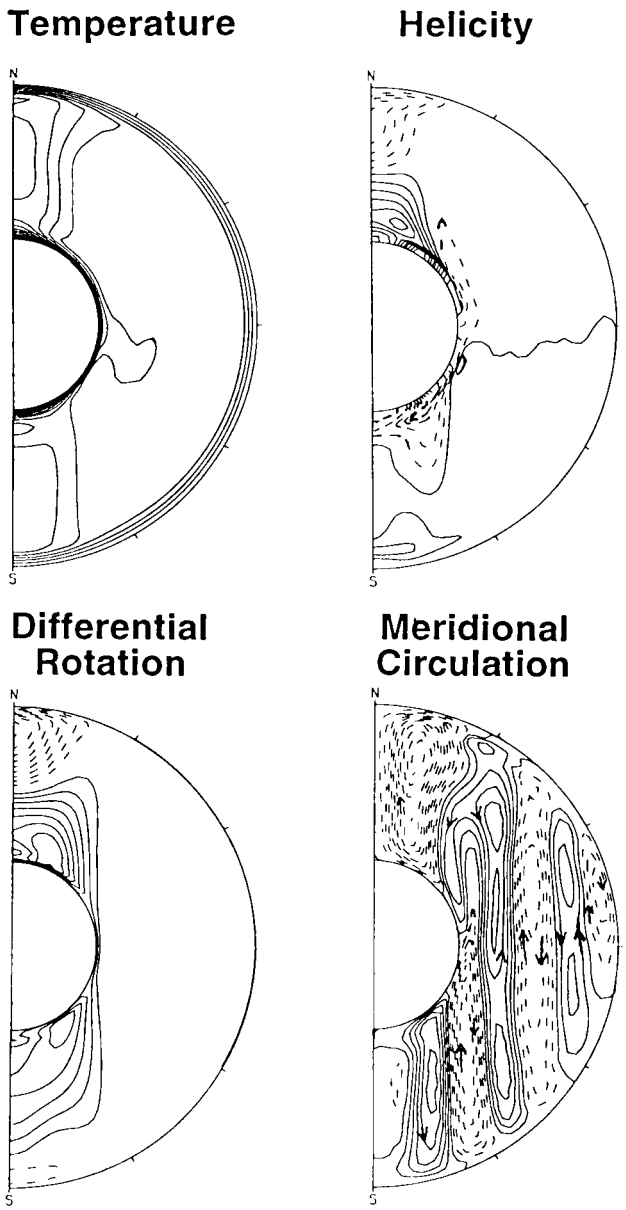

Figure 13. A snapshot of the longitudinally averaged temperature perturbation, helicity, differential rotation, and meridional circulation in the GR95 model. Note the strongly concentrated activity within the tangent cylinder. Reproduced from *Glatzmaier and Roberts* [1995a], with the permission of the authors and the publisher (Elsevier Science BV).

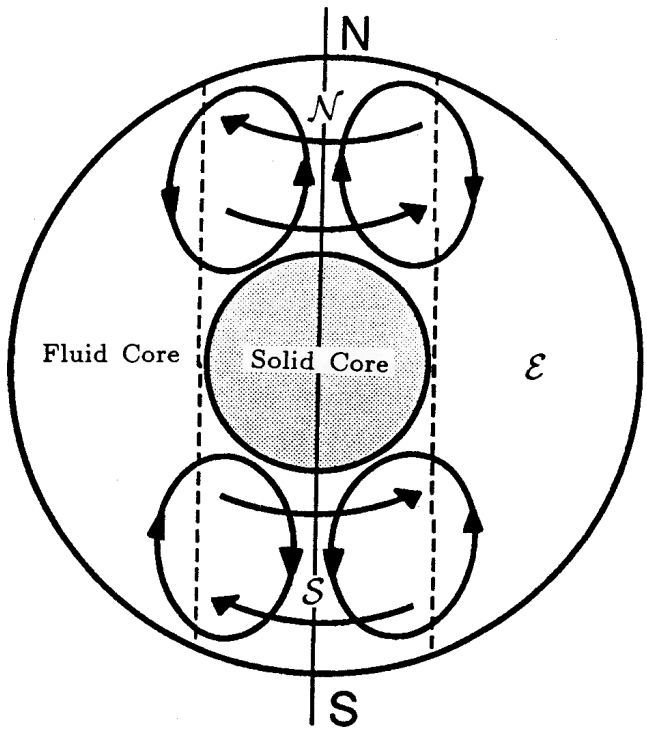

Figure 14. A sketch of the flow pattern in the GR models. The meridional circulations near north and south poles carry heat from the ICB to the CMB. Because of the rotation these induce a strong zonal thermal wind in the directions indicated. The dashed line shows the tangent cylinder. Reproduced from *Glatzmaier and Roberts* [1997], with the permission of the authors and the publisher (Taylor and Francis Ltd).

strong thermal winds, which are zonal and in opposite directions in the deeper and shallower parts of the fluid core (Figure 14). The zonal velocity in the neighborhood of the ICB is eastward, and unless the inner core rotates at a rate very similar to that of the adjacent fluid, a large magnetic couple is speedily brought into play that quickly restores corotation. A similar situation arises in the SK99 models; Figure 12 clearly shows that the zonal flow of the fluid in contact with the ICB is eastward, but in this case a larger effect is caused by the low-latitude part, i.e., outside the tangent cylinder. *Sakuraba and Kono* [1999] attributed this effect to the dominance of anticyclones near the equatorial plane brought about by the approximate balance between Coriolis and Lorentz forces (see Figure 11).

[136] Soon after *Glatzmaier and Roberts'* [1995a] prediction, two groups reported seismic evidence for the superrotation of the solid inner core at about the expected rate [see *Song and Richards*, 1996; *Su et al.*, 1996]. *Buffett* [1996] argued, however, that a strong gravitational couple, produced by the mantle on the solid inner core, will lock the two bodies together in a common motion. The situation is still unclear, but the possibility that new information about the deep Earth may come from a study of the rotational state of the solid inner core is exciting. If gravitational locking defeats Lenz's law, the zonal velocity shear at the inner core boundary will be greater, leading to a larger ω effect there.

[137] The decadal variations in the length of the day are attributed to topographic, magnetic, and viscous couples exerted by the fluid core on the mantle, of which the viscous couple seems to be negligible. Prior to *Buffett's* [1996] discovery the topographic couple was thought to be somewhat larger than the magnetic couple, but the gravitational locking of the inner core to the mantle has reversed this opinion. The inner core has an electrical conductivity that is probably rather larger than

the fluid core, and even though the arm of the torque exerted on the inner core by the magnetic stresses created by the fluid core is so small, it makes (with the gravitational link between the inner core and mantle acting as a catalyst) a significant addition to the torque on the mantle.

5.4.2. Dynamos Operating Between Stress-Free Boundaries

[138] There is insufficient space in this review to describe in any depth the way that convection and field generation is affected by adopting stress-free boundary conditions instead of the no-slip conditions (19). Simulations that use stress-free conditions include KB97, GBT99, and some of the COG98 models.

[139] This issue of boundary conditions is a contentious one. Proponents of stress-free boundary conditions argue that the Ekman layer has a thickness of approximately $\delta_\nu = (\nu/\Omega)^{1/2}$, which is only ~10 cm for the Earth, assuming a molecular kinematic viscosity of 10^{-6} m^2 s^{-1}, or at most 10 m if a turbulent viscosity about equal to η is assumed. It may be hard to believe that such small scales can significantly influence convection and the geodynamo, which operate on lengths of order $D \approx 3000$ km. It may then seem natural to dispense with the Ekman layer entirely by adopting stress-free conditions on the CMB. Nevertheless, there is perhaps a logical inconsistency in adopting the stress-free conditions while, at the same time, retaining a viscosity that is all too large in the bulk of the fluid.

[140] The Ekman layers are very significant in the dynamics of rotating fluids in the absence of a magnetic field. They control the axisymmetric flow (or more precisely its geostrophic part) far from the boundaries. They give rise to the so-called "spin-up" timescale, $\tau_{su} = E^{-1/2}(2\pi/\omega)$, which for $E = 10^{-15}$ is about 3×10^7 days ~80,000 years and which, though correspondingly less for larger E, is in the range of interesting geomagnetic timescales. Roughly speaking, τ_{su} is the time taken by a rapidly rotating fluid to respond to changes in the angular velocity of its container (assumed axisymmetric); it is an approximate measure of the importance of the (viscous) coupling of the geostrophic part of the core flow to the mantle. Potentially, the replacement of the no-slip conditions by the stress-free conditions has very serious repercussions in the nonmagnetic case.

[141] When a magnetic field is present, the situation is less clear, since topographic and magnetic coupling across boundaries may relegate viscous coupling to oblivion. Even if the mantle were electrically insulating, the strong magnetic coupling between the inner and outer cores would (via the gravitational coupling between inner core and mantle) create a torque between the outer core and mantle (see section 5.4.1). The most stringent test of the effects of boundary conditions is to exclude gravitational and topographic coupling together with electrical conduction in the mantle and to retain only viscous coupling at the core-mantle boundary (which arises only in the no-slip case). On this basis, comparisons between the no-slip and no-stress cases were made by *Kuang and Bloxham* [1997] and *Roberts and Glatzmaier* [2000b]. These suggest that the models behave rather similarly, although the effect of the tangent cylinder appears to be more pronounced in the case of the no-slip boundaries. In explication, we may recall (section 5.1) that although Ekman pumping/suction at the ends of the cyclonic and anticyclonic convection columns is effective in producing helicity and an α effect, the sloping ends of the columns create flow along the columns and also an associated α effect.

[142] Figure 15 focuses on a small area of the phase space shown in Figure 1 in which two groups (COG98 and GBT99) undertook extensive parameter searches. They selected different modes of energy supply. *Christensen et al.* [1999] specified the temperature difference between the boundaries; *Grote et al.* [2000] selected a uniformly distributed heat source. In spite of these differences, the stress-free boundaries and no-slip boundaries gave similar results (Figure 15b). Only results for no-slip boundaries are reported by the COG98 group, but these seem not very different from the stress-free results of GBT99 (Figure 15a). Although the dipole models, and the points where no dynamo was found, are the focus of Figure 15, the existence of quadrupolar dynamos and the discovery of the bizarre "hemispherical dynamos" (jointly shown as "other" on Figure 15) are of some theoretical interest.

6. COMPARISON WITH THE OBSERVED GEOMAGNETIC FIELD

[143] The prime aim of geodynamo simulations is to understand the mechanisms that generate the geomagnetic field and its variation with time. A second and very significant ambition is to use this understanding to enhance knowledge of the Earth's interior. Both these objectives require that detailed comparisons be made between the results of the simulations and the observed data on the strength and character of the geomagnetic field in both the recent and remote past. Such comparisons, which require a proper appreciation of the limitations imposed by the data, are made below and have also been the principal thrust of a recently published review by a French group [*Dormy et al.*, 2000].

6.1. Problems Associated With the Observed Data

[144] Observations may be conveniently assigned to one of three time windows: the recent field (10^1–10^2 years), the archeomagnetic field (10^2–10^4 years), and the paleomagnetic field ($>10^4$ years). These intervals span the characteristic timescale of the dynamo, which we may take to be the free decay time of the dipole, about 1.5×10^4 years in the Earth's core.

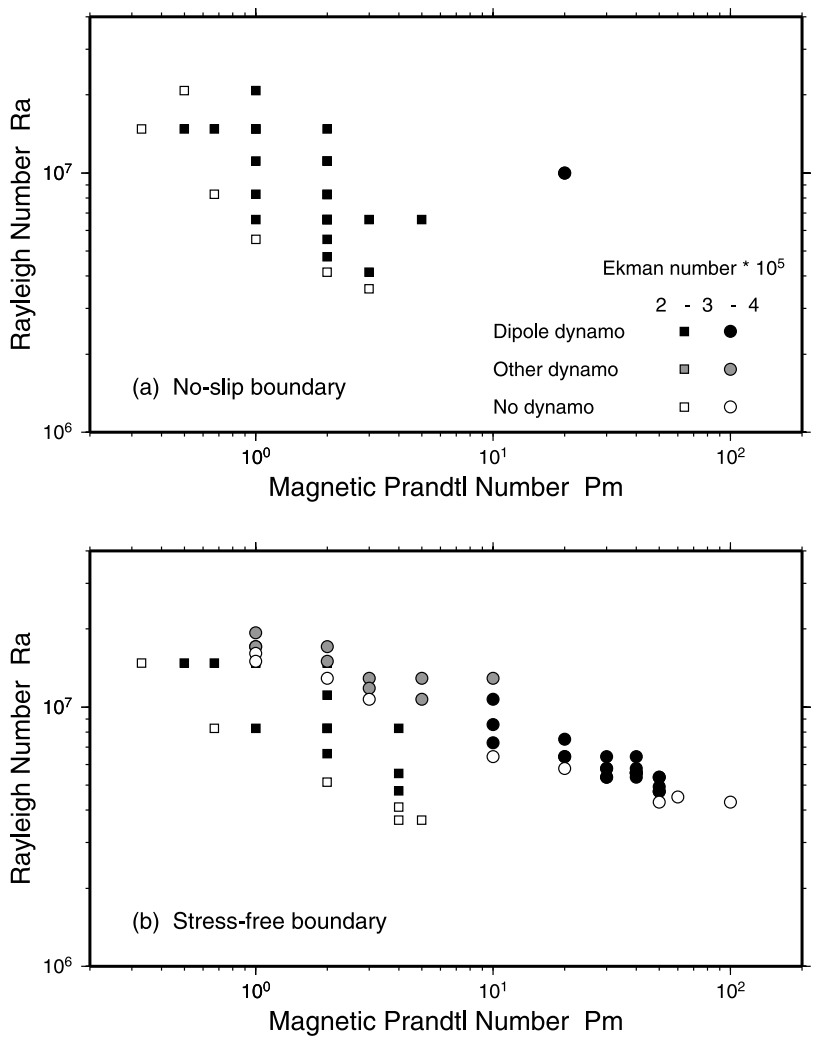

Figure 15. A "phase diagram" for dynamos with Ekman number in the range of (2–4) $\times$ 10^{-5}. Squares and circles indicate models with Ekman numbers in the ranges of 2–3 and 3–4 times 10^{-5}. Most of the data are either from *Christensen et al.* [1999] (squares) or *Grote et al.* [2000a] (circles). Dynamos producing fields of dipole type are distinguished from failed dynamos and from other types of dynamo (quadrupolar or hemispherical).

6.1.1. Instrumental Observations

[145] The recent field is quite accurately known. It is measured very precisely by magnetic observatories, by magnetic surveys, and by satellites such as Magsat or Ørsted [*Olsen et al.*, 2000]. The most severe limitation inherent to this type of data is their brief time span. Systematic instrumental observations of the global magnetic field commenced only in the nineteenth century when C. F. Gauss organized an international cooperation in magnetic observations [e.g., *Langel*, 1987]. Even if the values of the inclination and/or declination that were measured prior to the time of Gauss are included (which are accurate to within a degree or so; see the recent compilation of *Jackson et al.* [2000]), the total time interval covered by the data is a mere four centuries. To learn about the field over longer time intervals, we must necessarily rely on data of much lower accuracy supplied by the indirect observations.

6.1.2. Observation of the Past Magnetic Field

[146] Although different time windows are their targets, archeomagnetic and paleomagnetic data are obtained by essentially the same procedures: the measurement of the *natural remanent magnetization (NRM)* of either natural objects such as rocks or man-made artifacts such as pottery. The main distinction between the two categories is the resolution in age. For times less than about 2×10^4 years in the past, there is good age control, through old documents, archaeology, stratigraphy, or ^{14}C and other dating techniques. Data from different locations can be compared reasonably well because uncertainties in age are only about 100 years or less. Such accuracy is unattainable in paleomagnetic studies.

[147] Paleomagnetic data come mainly from two different sources: volcanic rocks (e.g., lavas) and sediments. The acquisition of magnetization by volcanic rocks (ther-

moremanent magnetization, TRM) is well understood [*Néel*, 1949]; it can be reproduced and studied in the laboratory. The main problem is that the intervals between eruptions are very irregular. Even when samples are collected from a section that includes tens or even hundreds of lava flows (good examples are found in places like Iceland and Hawaii), there is no way to accurately estimate the length of time between successive eruptions. They may erupt in quick succession (at intervals of less than 100 years), but there may be quiescent intervals in which eruptions are separated by 10^4 years or more. Accordingly, data from volcanic rocks are mainly used to infer statistical properties of the magnetic field. Within the limitations imposed by this lack of age control, volcanic data supply very reliable information, especially about field directions in the past. Volcanic rocks also provide an excellent medium with which to study the intensity of the magnetic field. Regrettably, however, analysis is still limited by a paucity of reliable data [*Kono et al.*, 2000a].

[148] Data from sediments provide continuous readings of past changes in the magnetic field in the form of depositional remanent magnetization (DRM). As long cores are obtained routinely by the Ocean Drilling Program (ODP), new and interesting data sets continually become available. These cores are usually dated by magnetostratigraphic methods, but independent age estimates can often be made on the basis of microfossil zonation or oxygen isotope stages. Thus magnetic phenomena that require temporal resolution, such as reversals, have been studied almost exclusively using sedimentary data. Unfortunately, the process through which sediments acquire and retain their magnetic remanence is incompletely understood. In particular, it is well known that the intensity of magnetization is controlled not only by the Earth's magnetic field but also by environmental changes, such as the chemistry of the ocean water and the productivity of biota [*Tauxe*, 1993]. This means that when we detect a variation in the remnant intensity, it is not absolutely clear if this reflects a genuine change in the intensity of the magnetic field or merely records a shift in, for instance, the climate.

[149] Recently, curves of the relative paleointensity variation over the past 200 kyr [*Guyodo and Valet* 1996] and then for the past 800 kyr [*Guyodo and Valet* 1999] have been generated. This was achieved by a careful comparison of good quality sedimentary data from the world's oceans. The prospects seem excellent that sedimentary data will provide a description of past magnetic field variations that is temporally well resolved.

6.1.3. Problem of Resolution

[150] Another important limitation of magnetic data from all time windows is that they inevitably sample the field at the Earth's surface, which is remote from the sources of magnetism, which lie in the core. The amplitude of the lth harmonic of the geomagnetic field decreases with distance r from the geocenter as r^{-l-2}. Accordingly, only harmonics of degree 12 or less in the signal from the core can be discerned at the Earth's surface, the remainder being swamped by sources of permanent magnetism in the crust. In other words, only features of the surface field with a wavelength of roughly 3000 km or greater are relevant to the geodynamo; shorter wavelengths have nothing to do with the dynamo process [*Langel and Estes*, 1982].

[151] This obstacle is illustrated in Figure 16, which compares the radial magnetic field produced by the dynamo model of SK99 at the CMB with the same field at the Earth's surface [see also *Roberts and Glatzmaier*, 2000a]. At the CMB the magnetic fields constructed from the low-degree harmonics ($L = 6, 12$) alone show marked differences from those produced at higher resolution ($L = 24, 43$). There are even some features which look different at $L = 24$ and at $L = 43$ (e.g., in the Southern Hemisphere near the center of the panels). At the surface of the Earth, on the other hand, it is already difficult to distinguish between the models truncated at $L = 6$ and $L = 12$. Figure 16 forcibly demonstrates the difficulty of deducing from the surface field the true nature of the core surface field and inference of the core surface flow.

6.2. Field Structure Seen From Recent Observations

[152] We will now describe some of the characteristics of the geomagnetic field obtained from the recent observations and compare them with what we see in some of the dynamo models. We include only properties that throw light onto the basic nature of the geodynamo.

6.2.1. Dominance of the Axial Dipole

[153] The geomagnetic field is usually expressed by the geomagnetic potential Ψ,

$$\Psi = R_E \sum_l \sum_m \left(\frac{R_E}{r}\right)^{l+1} P_l^m(\cos\theta)\,(g_l^m \cos m\phi + h_l^m \sin m\phi), \tag{70}$$

where g_l^m, h_l^m are Gauss coefficients, R_E is the radius of the Earth, and P_l^m is the Legendre function. If it is assumed that the mantle is an insulator, this expansion gives the field everywhere outside the core as $\hat{\mathbf{B}} = -\nabla\Psi$. Gauss coefficients are related to the core field through the boundary condition (48) at the CMB:

$$S_l^m(R_0) = \frac{1}{l}\left[\frac{(1+\delta_{m0})2\pi}{2l+1}\right]^{1/2}\left(\frac{R_E}{R_0}\right)^{l+2}(g_l^m - ih_l^m). \tag{71}$$

The factor in brackets arises from differences in definition: completely normalized spherical harmonics (equation (39)) are mostly used in studying core MHD, but Schmidt-normalized Legendre functions, which are only partially normalized, are employed in analyzing geomagnetic data:

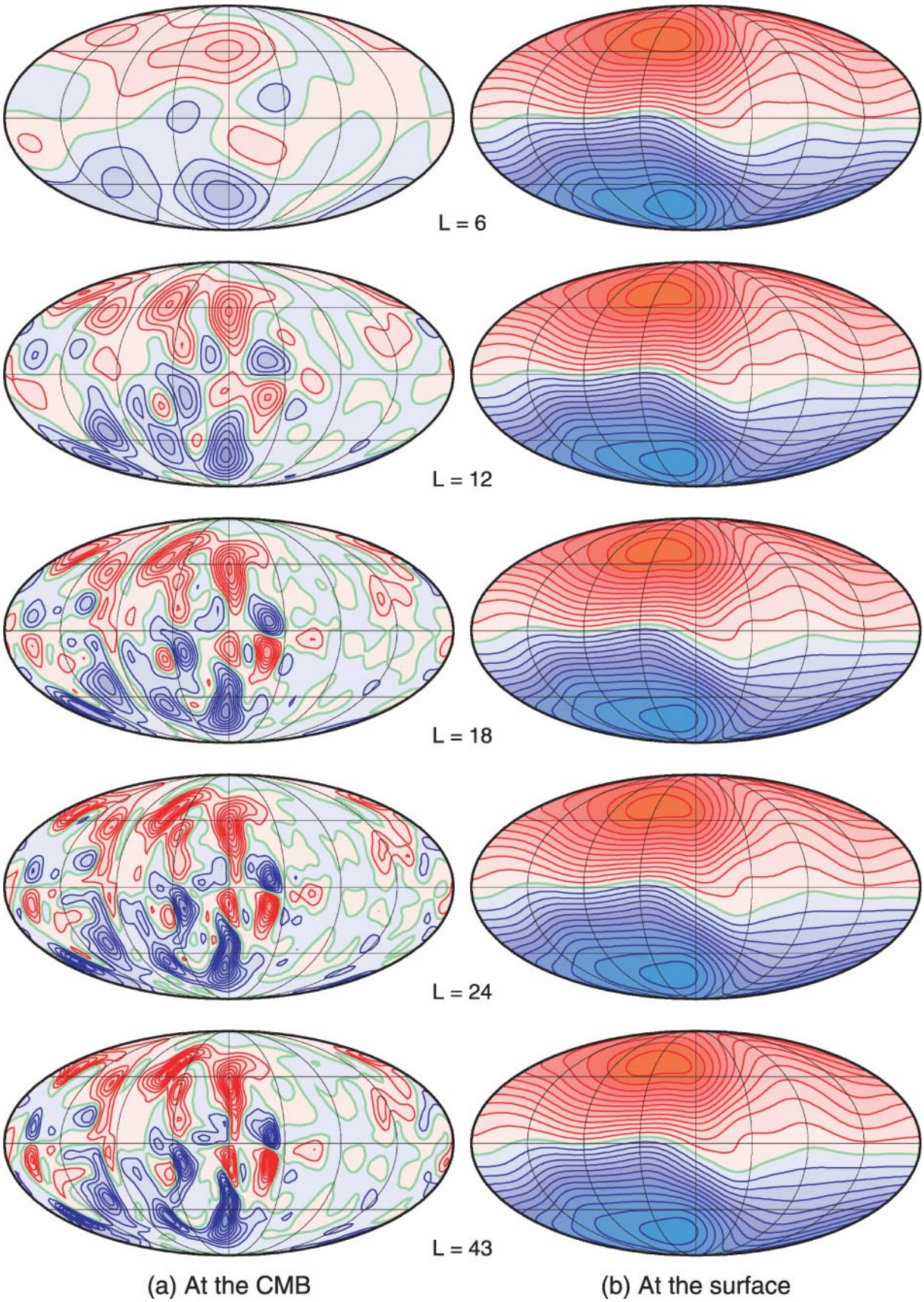

Figure 16. Examples of the radial component of the magnetic field as seen (a) at the CMB and (b) on the surface of the Earth for various truncation levels L. The contour intervals are the same for all the panels in Figure 16a, which is 50 times that used in Figure 16b. Note the very small change in Figure 16b.

$$\int\int P_l^m(\cos\theta)\,P_{l'}^{m'}(\cos\theta)\begin{pmatrix}\cos m\phi\\ \sin m\phi\end{pmatrix}\begin{pmatrix}\cos m'\phi\\ \sin m'\phi\end{pmatrix}$$

$$\cdot \sin\theta d\theta d\phi = \frac{4\pi}{2l+1}\,\delta_{ll'}\delta_{mm'}. \qquad (72)$$

[154] About 90% of the magnetic field energy at the surface of the Earth is due to its dipole moment, and the axial dipole component g_0^1 is responsible for most of that [*Langel and Estes*, 1982]. The dominance of the axial dipole throughout geological time is perhaps the most fundamental property of the geomagnetic field. The precise field morphology prior to the Mesozoic is hard to recover not only because of the paucity of data but also because of the effects of plate motions. Nevertheless, the paleomagnetic data are consistent with the hypotheses that the geomagnetic field was generally dipolar and (when independent information is available) that the dipole axis was very close to the rotational axis [see, e.g., *Merrill et al.*, 1996].

[155] Almost all the MHD dynamo models so far reported, including all those listed in Table 1, create dipole-dominated fields. In this, they are in satisfactorily agreement with observation.

6.2.2. Westward Drift

[156] One of the best known features of the secular variation of the geomagnetic field is the westward drift of some of the surface features. This was at first modeled by a westward motion of the field as a whole at a speed of a few tenth of a degree per year [*Bullard et al.*, 1950]. This description has given way to a more recent view in which the surface field has both stationary and drifting features [*Yukutake and Tachinaka*, 1969]. The most prominent drifting features are strong and tend to be flux patches reminiscent of sunspots [*Bloxham et al.*, 1989]. Perhaps the drifting features are intrinsic to the dynamo mechanism, while the fixed ones may be the result of inhomogeneities in the structure or thermal state of the lower mantle.

[157] *Kono et al.* [2000b] examined the surface field of the SK99 model and discovered that there are strong foci of magnetic flux near 50° (and 20°) north or south, which migrate either to the west or to the east. There did not seem to be much preference in the directions of motion; the eastward drift occurred with about the same probability as the westward drift. They also found that these flux concentrations tend to appear and disappear rather randomly; the average lifetime of a typical focus is about 1000–2000 years. Another interesting finding was that because of the strong attenuation of short wavelengths with distance, flux concentrations of this type might not be observable at the Earth's surface (see Figure 16). Consequently, they concluded that drifting features seen on the Earth's surface may not directly correspond to anything significant at the CMB.

[158] Figure 17 compares the longitudinal drift of the radial geomagnetic field at the equator during the last 400 years [*Jackson et al.*, 2000] with the drift of the radial field produced by the homogeneous model of *Glatzmaier et al.* [1999] during a period of 5000 years. Most of the core surface features in the model drift to the west (in agreement with the observations), and the same features can be correlated with what is seen at the surface of the Earth. The zonal flow in the GR95 and GR96 simulations is dominantly eastward, but the magnetic field pattern drifts westward; this is true even at the surface of the inner core. The westward drift in such strongly driven models is clearly a wave phenomenon. Because these models are strongly stochastic, the dominant longitudinal wave number of the field changes with time, as the wave pattern repeatedly forms, breaks down, and reforms, a vacillation that may be related to the finite lifetimes of secular variation foci.

[159] The character of a diagram of the type shown in Figure 17 depends on the time interval selected and the latitude chosen for the display. It appears, however, that the typical morphology of the *Glatzmaier et al.* [1999] model shown in Figure 17 differs from that of the SK99 model analyzed by *Kono et al.* [2000b]. The magnetic flux is more strongly concentrated in the SK99 simulation than in most of the GR95 and GR96 simulations, perhaps because of the fact that stronger hyperdiffusivity (section 3.2.3) and a rather low truncation level ($L = 21$) were employed in the latter models. Very intense flux concentrations were, however, created by the highly resolved model of *Roberts and Glatzmaier* [2000a]. This suggests that westward drift may depend sensitively on the computer model used to derive it and therefore that comparisons between observed and simulated westward drifts may provide a basis for preferring one simulation over another as a model of the geodynamo.

6.2.3. Magnetic Power Spectrum

[160] The energy density (also often called the "power") of a potential field of degree l on the surface of a sphere of radius r, within which the field is generated, may be written in terms of Gauss coefficients as [*Lowes*, 1974]

$$R_l(r) = \left(\frac{R_E}{r}\right)^{2(l+2)}(l+1)\sum_{m=0}^{l}[(g_l^m)^2+(h_l^m)^2]. \qquad (73)$$

The dependence of R_l on the harmonic degree l is usually referred to as the *geomagnetic spectrum*. Global measurements by the Magsat satellite showed that R_l decreases exponentially with increasing l with an exponent that is small at the CMB. In other words, it could be represented by a white source lying only slightly beneath the CMB [*Langel and Estes* 1982]. Although this property has only been established for the present-day mag-

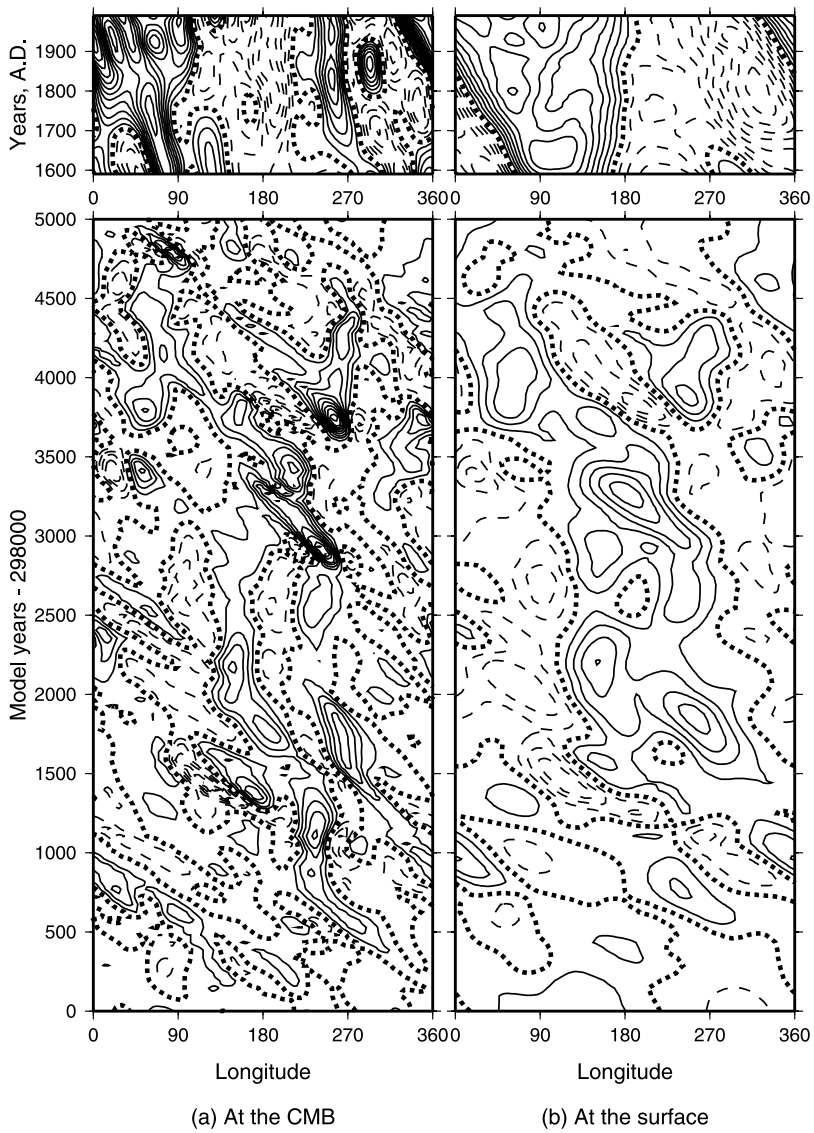

Figure 17. Time-latitude section of the radial component of the magnetic field at the equator for (bottom) the homogeneous model of *Glatzmaier et al.* [1999] compared with (top) the geomagnetic field in the last 400 years [*Jackson et al.* 2000]. The left and right sections show the patterns at the CMB and at the surface of the Earth, respectively. Note that for the top panel the time axis is expanded 2.5 times.

netic field, it is often speculated that it is a fundamental property of the geomagnetic field throughout geologic time (e.g., see section 6.3.2 and *Constable and Parker* [1988]).

[161] The spectra implied by some dynamo models also support this idea [*Glatzmaier and Roberts*, 1995b; *Kono et al.*, 2000b]. Figure 18 compares the present-day magnetic power spectrum obtained by Ørsted satellite [*Olsen et al.*, 2000] with the ones obtained from several dynamo models. Although the spectra for the dynamo models were derived only from "snapshots," they are not much altered if the snapshots were taken at different times (provided, of course, they are not taken during a reversal). It may be seen that the decay of the power is quite rapid both for the benchmark model as well as for the two GR96 models, but the reasons are rather different. The benchmark model is forced rather weakly, so that R_l decreases strongly and systematically; the GR models are (hyper)diffused rather strongly, resulting in a rapid decrease in R_l beyond $l \approx 10$.

[162] In contrast, the power spectrum for the SK99 model (for which only a weak hyperdiffusivity was required) does not decay as quickly. This is also true of the highly resolved *Roberts and Glatzmaier* [2000a] model, which employed no hyperdiffusivity whatever. One interesting feature of Figure 18 is that in all the models as well as in the observed field, the power residing in the quadrupole field ($l = 2$) is much less than in the dipole. In fact, there is a tendency for the power to drop quite sharply at $l = 2$ and to recover at a higher degree ($l = 3$ or larger). This may be another important property of Earth-type dynamos, but we still lack com-

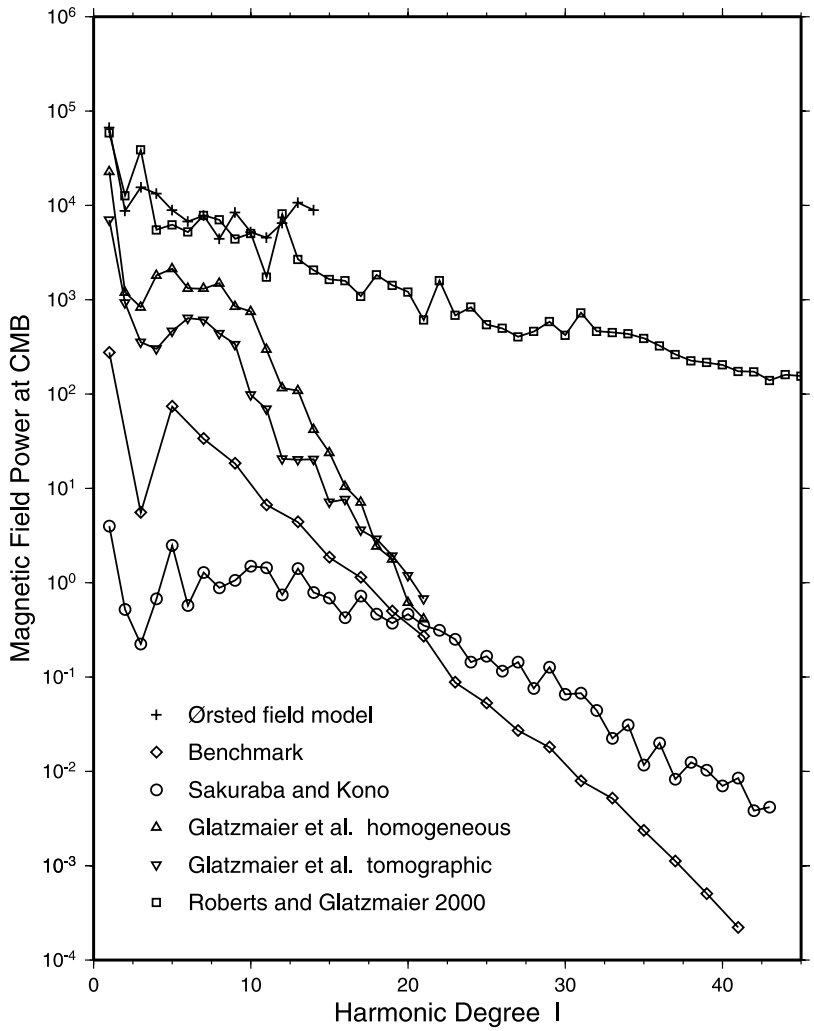

Figure 18. Magnetic field power at the core surface. "Ørsted" refers to the present field measured by the satellite [*Olsen et al.* 2000]. The remainder are from various MHD dynamo simulations. The power is given in μT^2 for Ørsted and the three GR96 models and in arbitrary units for the SK99 and benchmark models.

pelling evidence for, and a good explanation of, this phenomenon.

6.3. General Field Structures in the Long Term

[163] We shall now concern ourselves with characteristics mostly revealed by analyses of the paleomagnetic field. They are statistical properties but seem to be quite robust. Any dynamo model with ambitions to simulate the geomagnetic field must replicate these properties.

6.3.1. Strength of the Dipole Moment

[164] It is known that during the last 5 or 10 Myr the strength of the magnetic dipole follows a normal distribution, having a mean and standard deviation of 8.9 and 3.5×10^{22}A m^2, respectively [*Kono and Tanaka*, 1995b]. Within the experimental uncertainties, both the normal and reversed polarity data can be fitted by the same distribution. It is of particular interest that the mean value is not significantly different from the present-day value of 8×10^{22}A m^2. *McFadden and McElhinny* [1982] argue that the fit of the data to a lognormal distribution is closer. *Selkin and Tauxe* [2000] suggest that the mean would be reduced if only very reliable data were used. Very extensive paleointensity determinations on a Hawaiian drill core [*Laj and Kissel*, 1999] suggest, however, that the dipole moment really does follow a normal distribution and also that the mean is similar to the one determined by *Kono and Tanaka* [1995b].

[165] Figure 19 compares the distribution of the axial dipole moment (g_1^0) derived from paleomagnetic data with those of three MHD dynamo models. It is clearly seen from Figure 19a that the observed distribution in each of the normal and reversed polarities is unimodal and has a similar shape. In the final analysis, it is this fact that justifies the geodynamo hypothesis (section 2.1). Nondynamo sources of magnetic field would favor one polarity over the other and would create an asymmetry that is conspicuously absent from Figure 19a.

[166] In discussing the geomagnetic data we shall from now on adopt the geodynamo hypothesis. Consequently,

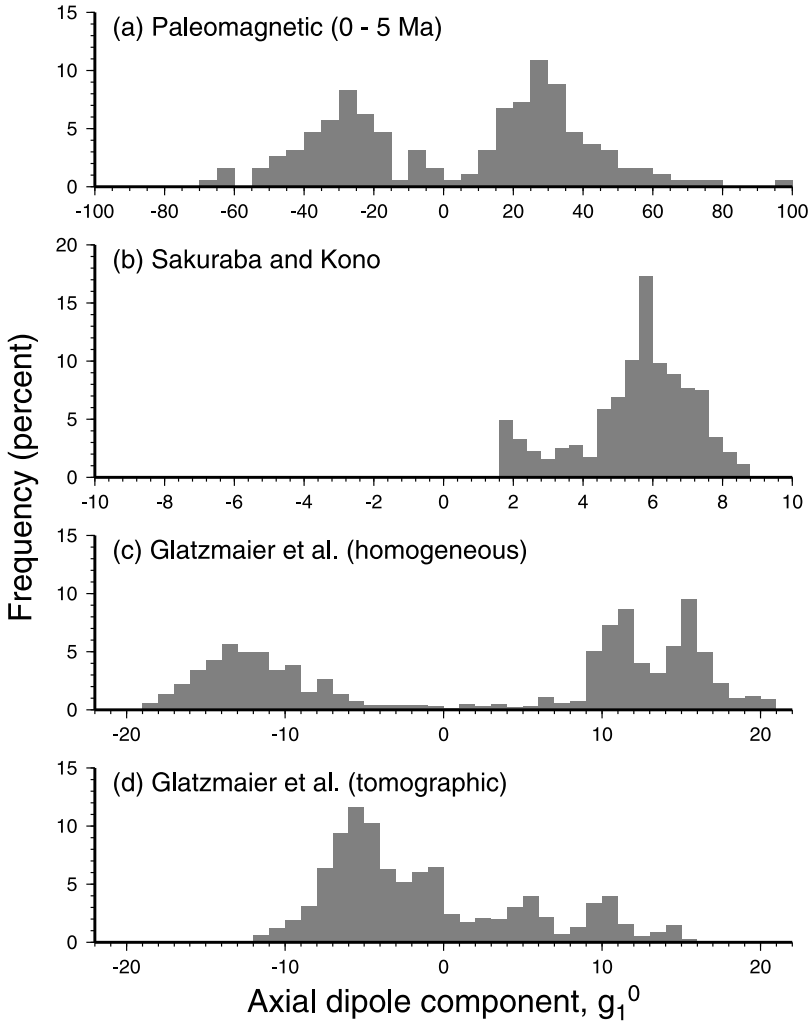

Figure 19. Distribution of the axial dipole moment g_1^0 during (a) the last 5 Myr according to paleomagnetic observations [*Kono and Tanaka*, 1995b], (b) about 5×10^4 years according to the SK99 model [*Kono et al.*, 2000b], and about 3×10^5 years according to (c) the homogeneous and (d) the tomographic models of *Glatzmaier et al.* [1999].

we shall assume that that all statistical properties of the observed geomagnetic field that are linear in **B** are zero, any deviation from this being attributed to insufficient data. This must also be true of the fields created by the dynamo models, but here we face a difficulty with statistical sampling. The models are computationally expensive, and it is rarely possible to integrate them for long enough to put the normal and reversed states on an equal statistical footing. Indeed, some models reverse rarely or not at all, so that "long enough" can mean "for ever"! These are models in which the distributions for normal and reversed polarity overlap very little, or not at all. For example, the benchmark dynamo is quasi-stationary, and its unimodal distribution is therefore a single "spike" (a delta function), at the constant value of g_1^0 that it steadily maintains. The degree of overlap of the normal and reversed distributions is related to the frequency of reversals [*Kono*, 1972]. Such an overlap is seen in Figure 19a. Figure 19b concerns the SK99 model. This maintained only one polarity, but it seems doubtful from the form of its distribution that it is truly unimodal. More likely it is a reversing dynamo that, because it was integrated for only about 50,000 years, did not have sufficient time to reach the other polarity state even once.

[167] Figures 19c and 19d focus on the two MHD models on which *Glatzmaier et al.* [1999] concentrated most of their attention: the "homogeneous" model and the "tomographic" model. These underwent polarity reversals, but their distributions of g_1^0 are quite different from each other and from that of the Earth. Small values of g_1^0 are practically absent from the homogeneous model but are quite abundant for the tomographic model, for which there is little distinction (in terms of the frequency of occurrence) between "typical" values of g_1^0 and "abnormally low" ones. In this respect, the tomographic distribution differs substantially from those of the paleofield and the homogeneous model, but the

latter distributions themselves differ significantly from one another in other ways. The two well-populated parts of the distribution generated by the homogeneous model are well separated and are not similar to each other in shape. Their large separation suggests that this model spends most time in stable polarity states which are not seriously threatened by the possibility of reversal. This also explains the pronounced differences in the shapes of the normal and reversed distributions in Figure 19c; even though this model was integrated for more than 550,000 years of simulated time, this was insufficient to make the two distributions very similar.

[168] The tomographic model is driven at the core-mantle boundary by a heat flux that is asymmetric with respect to the Northern and Southern Hemispheres. It is important to reiterate that this asymmetry does not introduce any bias that favors the normal over the reversed state or vice versa; $\mathbf{B}$ and $-\mathbf{B}$ are equally good solutions of the equations governing the convective dynamo, irrespective of differences in the thermal forcing or, indeed, differences in the internal structure of the Earth. The asymmetry of Figure 19d merely indicates that the 300,000 years over which this model was integrated was again insufficient to establish statistical symmetry between the polarities. This does not mean that geomagnetic data are incapable of detecting inhomogeneities in the structure of the Earth. However, future studies of "magnetic tomography" must rely on quadratic properties of $\mathbf{B}$, such as the power spectrum studied in section 6.2.3, or correlations between $\mathbf{B}$ at different times or places or between Gauss coefficients.

[169] None of the three dynamo models featured in Figure 19 reproduces the Earth's g_1^0 distribution well, and all the models listed in Table 1 are equally unsatisfactory in this respect. It therefore seems likely that the distribution of g_1^0 will prove useful in testing the credibility of every new model as a viable geodynamo, though only if the model is integrated for a long enough time for convincing statistics to be assembled.

[170] *Prévot et al.* [1990] observed that the intensity in the lower Mesozoic was smaller, by a factor of 2–3, than it was before or after. They called this the "Mesozoic dipole low." This also features in the recent paleointensity data compilation of *Tanaka et al.* [1995] and appears to be robust. *Kono and Tanaka* [1995b] pointed out that throughout the time during which paleointensity data are available (a period of ~3 Gyr), the intensity seems to lie within a rather narrow range, in which the maximum and minimum differ only by a factor of ~4. They suggest that the geodynamo mechanism operated in essentially the same way for more than 3 Gyr. This view conflicts with that of *Hale* [1987], who argued that a sudden increase in the dipole moment occurred about 3 Gyr ago, coinciding with the birth of the inner core. *Sakuraba and Kono* [1999] compared two simulations that were identical except that one has an inner core, and the other does not. Although there were differences in the working mechanism of the two dynamos, the fields they created, as seen at the outer boundary, were very similar in both form and magnitude. The model was, however, integrated over too short a time for dogmatic claims to be made. For another exploration of the effects of varying the core radius, see *Roberts and Glatzmaier* [2001]. Decisive examination of questions of this type will undoubtedly be a target in future geodynamo research.

6.3.2. Paleosecular Variation

[171] As noted earlier, by their nature, data from volcanic rocks are best suited for statistical treatment. In paleomagnetism the most popular method of analysis of paleosecular variation (PSV) used to be that developed by *Cox* [1970]. In this method the mean directions of magnetization of individual lava flows are converted to the position (θ_p, ϕ_p) of the *virtual geomagnetic pole (VGP)* by

$$\cos\theta_p = \cos\theta\cos p + \sin\theta\sin p\cos D$$
$$\sin(\phi_p - \phi) = \sin p\sin D/\sin\theta_p, \tag{74}$$

where θ and ϕ are the colatitude and longitude of the sampling site, I and D are the inclination and declination of the magnetic field, and p is the magnetic colatitude given by the dipole formula $\cot p = \frac{1}{2}\tan I$. The angular standard deviation (ASD) of the VGPs is then calculated from

$$\mathrm{ASD} = \sqrt{\frac{1}{N-1}\sum_i^N \Delta_i^2}, \tag{75}$$

where N is the number of lavas and Δ_i is the angular distance of the ith pole from the mean pole position. *Cox* [1970] showed that the ASD is mainly determined by the latitude of the sampling site, increasing monotonically from about 14° at the equator to ~20° at 70°N or 70°S.

[172] A very different approach for the study of PSV was suggested by *Constable and Parker* [1988]. They proposed that over a sufficiently long time interval, Gauss coefficients (apart from the axial dipole term g_1^0) behave as normally distributed variates having zero means and variances independent of the order m of the harmonic. Appealing to the geomagnetic power spectra derived from satellites (see section 6.2.3), they further supposed that the expectation values of the power spectrum (equation (73)) at the core surface is exactly flat. (Strictly speaking, this implies that the total magnetic energy outside the core is infinite. In reality, the spectrum is slightly "pink" at the CMB, as seen in section 6.2.3.)

[173] The assumptions of *Constable and Parker* [1988] lead to a unique form for the variances of the individual Gauss coefficients:

$$\sigma_l^2 = \frac{(R_0/R_E)^{2l}\alpha^2}{(l+1)(2l+1)}, \tag{76}$$

where α is a constant, to which they assigned a value of 27.7 μT (which is quite similar to the present-day value of 30 μT). As equation (76) implies that all Gauss coefficients (after suitable normalization) are distributed in the same way (i.e., the normal or Gaussian distribution), they called their proposal the "giant Gaussian model." Ideally, this model can describe the changes in Gauss coefficients by only two parameters (the mean of g_1^0 and α). However, it was found necessary to assign a nonzero mean to g_2^0 and a variance σ_1^2 for dipole coefficients which is different from the value given by equation (76) [*Constable and Parker*, 1988]. Their original model was further modified later to account for the dependence of the ASD of the VGPs on latitude [*Johnson and Constable*, 1997]. Nevertheless, it can be truly said that their model provides a fresh approach to PSV studies. Its viability can be quantitatively assessed by using paleomagnetic data. It is also well suited for comparison with the results of dynamo simulations.

[174] Figure 20 shows the distributions of Gauss coefficients of degrees 1 and 2 for the homogeneous and tomographic models of *Glatzmaier et al.* [1999]; similar diagrams were provided for the SK99 model by *Kono et al.* [2000b]. (Distributions for the axial dipole were already given in Figure 19 and are not included again in Figure 20.) It may be seen that all the coefficients follow a unimodal distribution which can be approximated very well by a normal distribution. Apart from g_2^0 in the tomographic model, all the coefficients have means that are not statistically different from zero. Furthermore, as predicted by the giant Gaussian model, the distributions depend only on the degree l of the spherical harmonic and not on its order m. In short, the models of *Glatzmaier et al.* [1999] seem to satisfy the assumptions of the giant Gaussian model rather well.

[175] *Kono and Tanaka* [1995a] showed that the original giant Gaussian model cannot reproduce the ASD—latitude relation deduced from the paleomagnetic data. They further demonstrated that the paleomagnetic observations can be explained most naturally by assigning a greater variance to the (2,1) harmonics (i.e., g_2^1 and h_2^1) than the giant Gaussian model envisages. Interestingly, the SK99 dynamo model exhibits this greater variance [see *Kono et al.*, 2000b]. The *Glatzmaier et al.* [1999] simulations give very similar variances for all the degree 2 coefficients (Figure 20), so they are more consistent with the original giant Gaussian model than is the real Earth! (It should perhaps also be mentioned that the (3,2) harmonics provide another, though much less likely, way of explaining the behavior of the ASD.)

[176] Figure 21 compares the ASD—latitude relations derived from the paleomagnetic data with those simulated by three dynamo models. While the two models of *Glatzmaier et al.* [1999] give essentially constant values of the ASD, the SK99 model (with its larger (2,1) variances) exhibits a strong latitude dependence that somewhat resembles the observations [*Kono and Tanaka* 1995a]. The similarity between the observation (Figure 21b) and the behavior of the SK99 model (Figure 21c) may be just a coincidence; the model was integrated for a time equivalent to only about 50,000 years. Nevertheless, by highlighting deviations from too idealized symmetric states, characterizations of the geomagnetic field of this kind may provide useful insights into the geodynamo mechanism and may motivate more realistic geodynamo simulations.

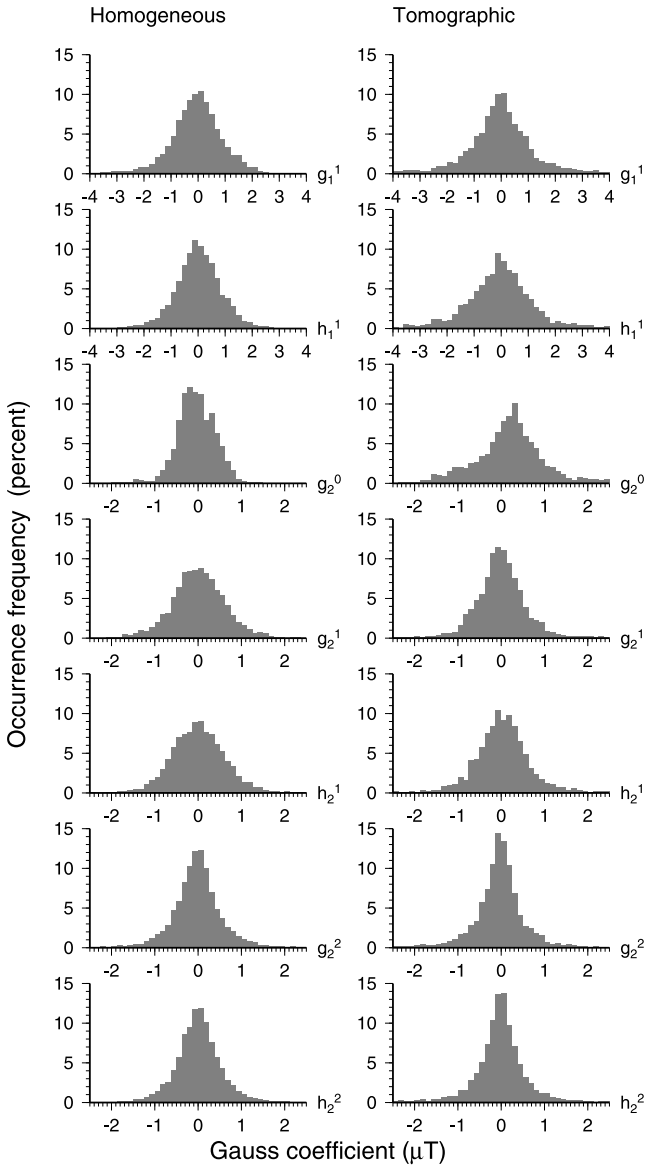

Figure 20. Distributions of Gauss coefficients of degrees 1 and 2 (except for the g_1^0 coefficients, which were shown in Figure 19) for the homogeneous and tomographic models of *Glatzmaier et al.* [1999], for the same time interval as Figure 19. All the coefficients except g_2^0 of the tomographic model can be approximated by zero-mean normal distributions dependent only on the degree l.

6.3.3. Departure From Axial Dipole Field

[177] It is well known that the Earth's surface magnetic field is approximately that of a dipole located at the

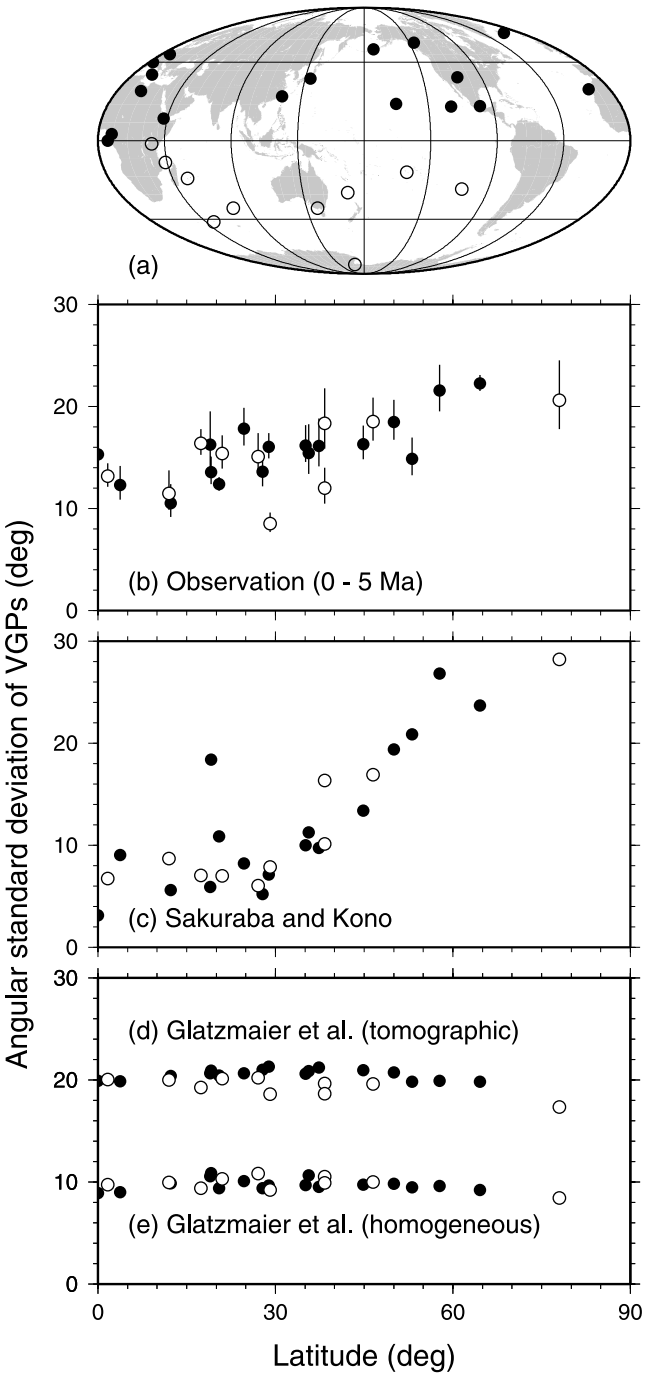

Figure 21. Angular standard deviation (ASD) of the VGPs from observation and from dynamo models. (a) The sites where PSV data are available for the last 5 Myr (from the database of *Quidelleur et al.* [1994]). Dependence of ASD on latitude as derived from (b) the paleomagnetic observation, (c) the *Sakuraba and Kono* [1999] model, and (d) the tomographic and (e) the homogeneous models of *Glatzmaier et al.* [1999]. Note that the ASD is calculated for the sites shown in Figure 21a. Solid (open) circles denote sites in the Northern (Southern) Hemisphere.

center of the core, with its axis aligned with the rotational axis. This observation is extended to the *geocentric axial dipole (GAD) hypothesis*, by which we assume that the suitable average of the field of the Earth in the past is exactly that of the axial dipole at the geocenter. This is the basic postulate of paleomagnetism. Data analysis has shown that the GAD hypothesis is a good approximation for the last 200 Myr or so. It is difficult to test the hypothesis prior to about 200 Ma, however, because all ocean floor of that age has been destroyed by subduction.

[178] The GAD hypothesis is an idealization and does not hold perfectly, however. *Wilson* [1970] discovered that the distribution of the younger Cenozoic VGPs is not centered at the north pole but is shifted to the far side of the north pole as seen from the sampling site. Paleomagnetic data from other sampling sites subsequently confirmed this. The phenomenon can be explained by supposing that the axial dipole is located not at the geocenter but is displaced slightly, by ~100 km, to the north. Equivalently, it can be interpreted by a combination of the axial dipole and quadrupole, $g_1^0 + g_2^0$. Because this feature is seen in both polarities, it can be concluded that g_1^0 and g_2^0 are correlated. Figure 20 shows that the mean of the g_2^0 distribution is nonzero for the tomographic model of *Glatzmaier et al.* [1999]. It is difficult to judge if this feature corresponds to the "dipole offset" seen in paleomagnetism; the sampling period for the tomographic model is not quite long enough to satisfy the geodynamo hypothesis, as seen from the asymmetric distribution of g_1^0 in Figure 19d (see also sections 2.1 and 6.3.1). Even so, it may represent a feature which persists quite a long time, as may be the case for the observed dipole offset itself. The relation between model and field behaviors can better be judged after carrying out a long enough integration of the model; if we find that the mean of g_2^0 changes sign with that of the axial dipole, we can conclude that a heterogeneous boundary condition can also cause the dipole offset.

[179] There are observations that indicate that the GAD hypothesis may be poor approximation for older fields [*Kent and Smethurst*, 1998]. The distribution of the inclination (actually its absolute value $|I|$) is not compatible with the GAD hypothesis. *Bloxham* [2000a, 2000b] proposed an explanation based on a dynamo model which, like the earlier models of *Glatzmaier et al.* [1999], assumed that the heat flow at the CMB is inhomogeneous, i.e., varies with horizontal position on the CMB. More explicitly, he found that by supposing that the heat flux from the core is a combination of a uniform flow together with a flow that varies with colatitude as $P_2(\cos\theta)$, he could simulate the proposed distribution of $|I|$ prior to 250 Ma. His model is perhaps the first that has been designed with the specific aim of explaining a single feature of the paleomagnetic observations. Such studies will become more common in the future.

6.4. Magnetic Reversals

[180] Geomagnetic reversals are the marvels of geomagnetism, one of the most spectacular phenomena in the whole of geophysics. Although the details of the

reversal process are still incompletely understood, the occurrence of reversals is well documented by volcanic rocks, by sediments, and especially by oceanic magnetic anomalies [*Cande and Kent*, 1995]. Since the seafloor is younger than 200 Ma, the reversal history is less well known for the lower Mesozoic and earlier ages [*Opdyke and Channell*, 1996].

[181] The first reversal of polarity in a MHD dynamo model was presented by *Glatzmaier and Roberts* [1995a, 1995b]. An extensive study was performed by *Glatzmaier et al.* [1999] to examine the conditions that control the occurrence and the nature of reversals. This work reached provocative conclusions that were pursued by *Coe et al.* [2000] in a very detailed study of the simulated reversal process.

[182] It appears that the polarity reversals are realized only in strongly driven dynamo models, which (as we have seen) require either very high levels of truncation or the injection of hyperdiffusivity. Some doubts were expressed that the reversals of the GR95, GR96, and *Glatzmaier et al.* [1999] models were direct consequences of the hyperdiffusivity they assumed and would not occur if it were removed. These doubts were laid to rest by *Ochi et al.* [1999], who reported the occurrence of two reversals in their compressible model (KS95) which does not employ hyperdiffusivity. They had, however, to integrate the equations for quite a long time and to increase *Ra* beyond the value assumed in the original simulation of *Kageyama et al.* [1995].

[183] Reversals are a quite complex phenomenon. In the reversals observed in the MHD dynamo simulations, each occurrence seems to show some unique property. It is therefore difficult to cover every aspect of this diverse phenomenon. What we discuss in the following is only a brief summary of the problems posed by reversals. Interested readers are referred especially to the work of *Coe et al.* [2000].

6.4.1. Normal and Reversed Polarities

[184] Several analyses of paleomagnetic data have attempted to establish differences between the states of normal and reversed polarity, but these have been uniformly unsuccessful or unconvincing. The present consensus in the paleomagnetic community is that the geomagnetic field has no significant preference for one polarity over the other [*Merrill et al.*, 1996]. This is no surprise to dynamo theorists, since it merely confirms the validity of the geomagnetic dynamo hypothesis (see section 2.1).

6.4.2. Reversal Frequency

[185] The geomagnetic reversal timescale is very well established for the last 160 Myr. The reversal frequency in the last 20 Myr or so is ~ 5 Myr^{-1} but steadily decreases as we go back in time. Between about 85 and 125 Ma, there was a long interval without any reversal whatever. This is the Cretaceous Long Normal (CLN) superchron. Going backward in time from the CLN, it is found that the reversal frequency increases from zero to about its present value over a time span of ~ 40 Myr. It has been suggested that the CLN reflects a state of the geodynamo that differs fundamentally from the geodynamo in ordinary times [*McFadden and Merrill*, 1995]. Further back in time, another very long reversed state existed during the Permian [*Opdyke and Channell*, 1996]. Perhaps this indicates that a process exists, having a characteristic time constant of about 10^8 years, that takes the dynamo from a frequently reversing state to a nonreversing state and back. Dynamo simulations covering such long intervals of time have not yet been performed. *Glatzmaier et al.* [1999] did, however, examine the effects on the geodynamo of different heat flow boundary conditions at the CMB and found these were very significant. This provided concrete support for the popular notion that changes in the lower mantle, occurring on the timescale of convective overturning in the mantle, affect the workings of the core dynamo and change the reversal frequency.

6.4.3. Reversal Morphology

[186] In the last 20 Myr or so, a magnetic reversal occurred on average once every 200 kyr [*Cande and Kent*, 1995]. A magnetic reversal is generally of short duration compared with the intervals of time between reversals, during which the field remains in a normal or reversed polarity state. During a reversal, the field decreases substantially to 1/5 or even 1/10 of its prereversal intensity. There is no unique or satisfactory way of defining the duration of a reversal. Even if we defined it to be, for example, the time taken by the VGP to move from within 10° of one geographic pole to within 10° of the other, the answer would depend on the site from which the observations were made. Even if this were not the case, the MHD simulations suggest that no two reversals are the same and are not completed in the same time [*Coe et al.*, 2000]. It is not surprising therefore that on the basis of the change in field direction, estimates of geomagnetic transition times mostly lie in a wide range, from 2000 to 5000 years. The weakening and recovery of the intensity may take longer than the reversal in field direction [*Merrill et al.*, 1996]. A transition time estimated from the drop in field intensity therefore tends to be longer.

[187] It is difficult to understand the global characteristics of a reversal because it is rare that detailed records for the same reversal are available from different parts of the world. (For some recent reversals, however, multiple data are becoming available [see *Love and Mazaud*, 1997].) Consequently, a reversal is studied mostly through the VGP path that pertains to a single site. These paths are in many cases quite complex. A reversal is not a smooth movement of the VGP from the vicinity of one pole to the neighborhood of the other. There may be periods of extremely rapid movement [*Coe and Prévot*, 1989]. Prior to the reversal proper, an aborted reversal, known as a "kickback event," may occur; some-

times, in a so-called "cryptochron," one reversal is quickly followed by another that restores the original polarity [*Cande and Kent*, 1995]. In some cases the VGP remains at an intermediate position for a prolonged period of time [*Hoffman*, 1991].

[188] Figure 22 is reproduced from *Glatzmaier et al.* [1999], who examined how the frequency and morphology of polarity reversals are altered when the total heat flowing from the core to the mantle is assigned on the CMB in different ways. Some assignments made reversals frequent events (e.g., Figure 22c); others seemed to discourage reversals (e.g., Figure 22e). These findings suggest that slow changes in the lower mantle temperature distribution, due to plate tectonics and mantle overturning, may account for the existence of long intervals of one polarity (e.g., the Cretaceous Long Normal) and may also explain why during other periods (e.g., the Cenozoic) reversals are quite frequent events.

[189] In Figure 22, the "homogeneous" (Figure 22g) and "tomographic" (Figure 22h) models are of special interest; this is why some of their characteristics have already been described above. The tomographic model was so named because by choice of heat flux over the CMB it attempts to form a link with a study of seismic tomography from which the temperature distribution in the Earth's lower mantle was inferred. During the simulated time over which this model was integrated, the field reversed twice, but the morphology of the reversals was somewhat dissimilar to that of geomagnetic reversals. The homogeneous model assumes that the outward heat flux is uniform over the CMB, a very simple boundary condition which, however, led to reversals that seem to be consistent with the paleomagnetic observations [*Coe et al.*, 2000].

[190] It is clear that the study of magnetic reversals is still incomplete, but exciting times lie ahead. As multiple data from worldwide sites become available, paleomagnetism will tell us what really happens to the field during a reversal, and this information will help to guide dynamo theorists toward models that are consistent with the data.

6.5. Other Observations

[191] There are a host of other paleomagnetic observations that may in the future play a significant role in guiding dynamo modelers. Some of these are not yet sufficiently well established. Others are based on observations whose relevance to the geodynamo is hard to judge at this time, and they will remain hard to evaluate until dedicated studies are undertaken by dynamo simulators. Some of them are described below because of their potential importance in understanding dynamo process.

6.5.1. Longitudinal Preference in the VGP Paths

[192] The longitudinal preference phenomenon is perhaps one of the best known in geomagnetism, and it is also one of the most controversial. It was pointed out by *Laj et al.* [1991] that the reversal VGP paths inferred from Quaternary and early Tertiary sedimentary records lie in preferred bands, one centered on the Americas and the other about 180° in longitude away. *Prévot and Camps* [1993] did not find any such preference from past lava flows in Iceland.

[193] Researchers in favor of preferred bands suggest that they may be related to the anomalously low velocity region in the lower mantle centered on the Pacific discovered by seismic tomography [e.g., *Su et al.*, 1994]. There is no doubt that the mantle controls core dynamics through the boundary conditions it imposes at the CMB, but whether this explains the preferred VGP path is still an open question. *Coe et al.* [2000] performed a very detailed analysis of the reversals experienced by the homogeneous and tomographic models of *Glatzmaier et al.* [1999]. In the case of the tomographic model they found that the low-latitude VGP path tended to be confined to one sector. Figure 23 shows the heat flow pattern assumed for the tomographic model and the density of VGPs obtained by this dynamo model. It can be seen that the transitional VGPs seem to be concentrated on two latitude bands, remarkably reminiscent of the observation by *Laj et al.* [1991]. However, this may again be just a coincidence. A more detailed study is needed before we can conclude that the lower mantle controls the VGP paths.

6.5.2. Sawtooth Pattern in Intensity

[194] *Valet and Meynadier* [1993] found that in some sediment cores covering the last few million years the intensity of magnetization changed in a peculiar sawtooth pattern and that magnetic reversals and excursions occurred when the intensity was smallest. According to their ideas, after the polarity reversal, the field quickly attained its largest magnitude and then starts to weaken again. *Valet and Meynadier* [1993] interpret this phenomenon by supposing that the dynamo weakens until it reaches a transitional state but after undergoing a reversal or an excursion it climbs to a high-energy state before starting to weaken again. Whether this process truly represents a change in the magnetic field intensity is controversial. Also, *Kono and Tanaka* [1995b] observe that this interpretation conflicts with the observed normal distribution of the dipole moment, since an increase in intensity linear in time produces a flat distribution of intensity (or dipole moment).

6.5.3. Excursions as Aborted Reversals

[195] The normal polarity of the Earth's field has persisted throughout the last 790 kyr [*Cande and Kent*, 1995], but there have been reports of numerous occasions on which the field direction deviated by a large amount from its usual direction and may in some cases have nearly reversed [*Champion et al.*, 1988]. These short-lived ($\sim 10^3$ years) deviations are called the *magnetic excursions*. They are usually defined as states in which the VGP deviates from the pole by more than 45°.

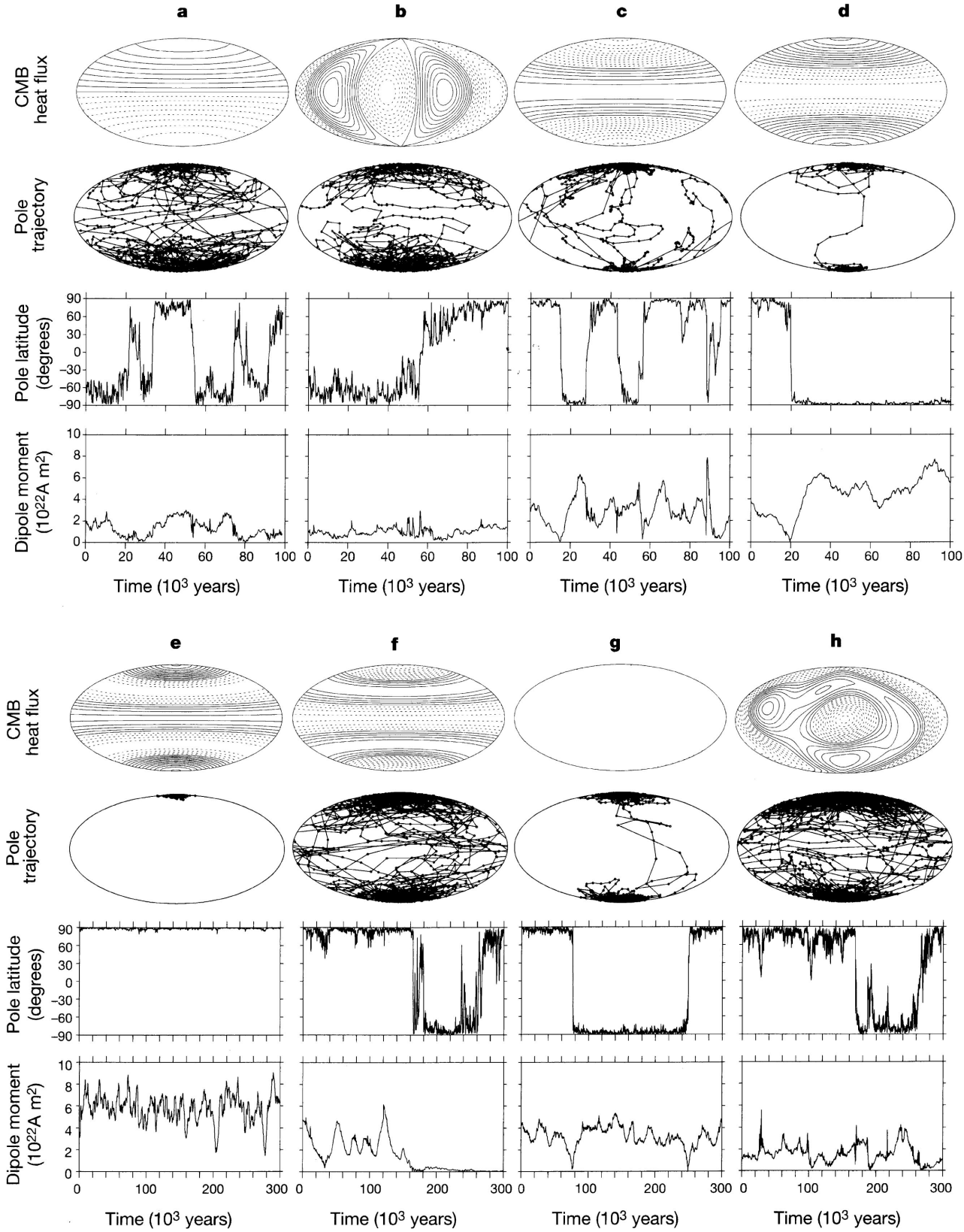

Figure 22. Results of eight dynamo simulations reproduced from *Glatzmaier et al.* [1999]. For each model the pattern of the CMB heat flux, the trajectory of the VGPs during reversals, and the evolutions of the VGP latitude and dipole moment with time are shown from top to bottom. The heat flow patterns for the models (except the tomographic model) are a combination of a uniform heat flux corresponding to the spherical harmonics (l, m) = (0,0) and heat fluxes proportional to (a) (1,0), (b), (2,2), (c) and (d) (2,0), and (e) and (f) (4,0); (g) in the case of the homogeneous model, there are no further harmonics. (h) Model assumes a heat flux based on an interpretation of results from studies of the seismic tomographic model of the lower mantle. Reproduced with the permission of the authors and the publisher (Nature Publishing Company).

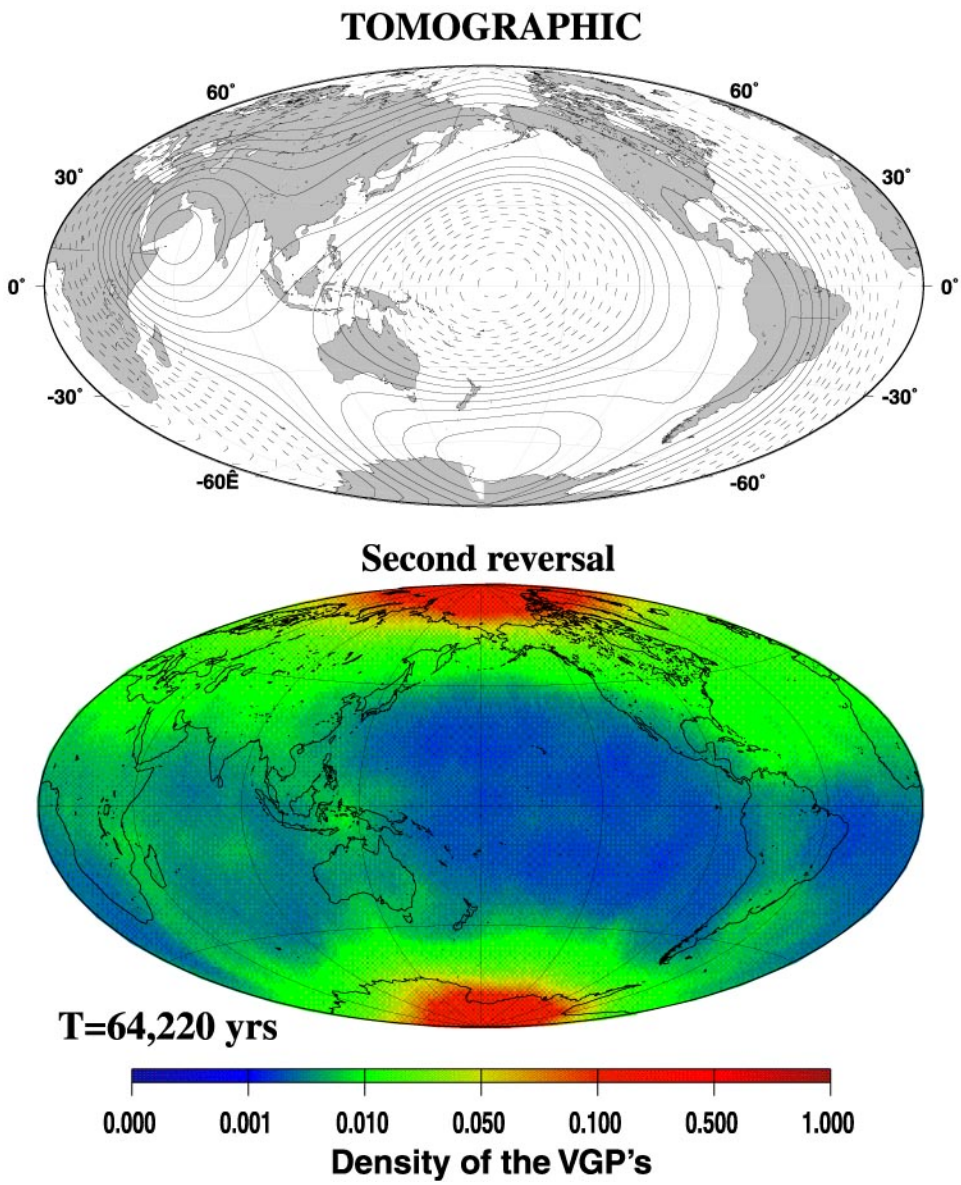

Figure 23. Correlation between the boundary conditions and the VGP distribution in a model of *Glatzmaier et al.* [1999]. (top) Heat flow pattern assumed at the CMB and (bottom) VGP density calculated for a period including the second of the two polarity reversals observed in their "tomographic model." Reproduced from *Coe et al.* [2000], with the permission of the authors and the publisher (the Royal Society of London).

It is often argued that excursions are aborted reversals. *Glatzmaier and Roberts* [1995b] proposed that excursions are reversal attempts in the outer core that were not completed because the inner core did not have time to respond. This idea is based on the observation by *Hollerbach and Jones* [1993] that because of its long time constant, the inner core tends to suppress rapid changes in the outer core. The time constant of the fluid core is determined by convection and is short (~100 years), while that of the inner core is its magnetic diffusion time, which is quite long (~1500 years). While the explanation of *Glatzmaier and Roberts* [1995b] is certainly a possibility, it would be premature to believe it. Reliable observations of excursions are almost exclusively from the present Brunhes chron. During earlier chrons the short duration of excursions makes reliable observations quite difficult.

7. SUMMARY AND CONCLUSIONS

[196] We have reviewed recent simulations that are three-dimensional, truly nonlinear, magnetohydrodynamic (MHD) models of the geodynamo. These have already considerably advanced understanding of mechanism generating the Earth's magnetic field in a way that was not thought possible even a few years ago. Some of their more significant implications are summarized below.

1. For the first time, the dynamo process has been modeled without making arbitrary or artificial assumptions; the physics is complete. The basic equations are fully self-consistent and include all nonlinear interactions. In this respect, these integrations can be said to be "first principles calculations."

2. In dynamos that are driven weakly or driven mod-

erately strongly, the fluid motion is of cartridge belt type, in which convection cells are aligned approximately with the rotation axis and are almost uniformly spread around a cylindrical surface centered on that axis. These cells appear as pairs of cyclones and anticyclones, and in addition to this circulation around their axes, there are convective flows along the axes associated both with the Ekman suction/pumping in the boundary layers at the CMB and the sloping ends of the cells where they meet the CMB.

3. The cyclones rotate anticlockwise as seen from the north and are associated with an equatorward flow. In the anticyclones the situation is reversed (clockwise rotation with poleward flow). Consequently, both the cyclones and anticyclones have negative (positive) helicity in the Northern (Southern) Hemisphere, which helps to stretch and twist the magnetic field to convert toroidal field into poloidal, a process that in the past has been parameterized by the α effect.

4. The converging flows in the Ekman boundary layer at the CMB as well as in the equatorial region tend to concentrate magnetic flux within the cyclones (at the CMB) or anticyclones (at the equator). This process is significant in intensifying the magnetic field and is limited by the Maxwell stresses of the field itself, which try to spread the magnetic field lines apart.

5. In strongly driven dynamos the interesting dynamic and magnetic activity is largely confined to the interior of the tangent cylinder. This is because of the large amount of heat that has to be carried outward. The thermal winds in the north and south polar regions play a very important role in generating the highly concentrated magnetic field in the polar regions. This is in striking contrast to the less strongly driven dynamos in which the concentrations of magnetic flux are found at about 50°N or about 50°S and are associated with the cartridge belt convection.

The dynamo simulations have opened up the possibility of making comparisons between the behaviors of models and the observations of recent and paleomagnetic fields. Although these comparisons are currently at a rudimentary level, it is hoped that ultimately, at some time in the future when models are created that reproduce all known facts about the geomagnetic field past and present, such comparisons will allow new facts about the Earth's internal structure and dynamics to be confidently inferred. This is because it is obviously possible to probe all characteristics of a model in a way that will never be possible for the real Earth. Some of the more significant results of comparisons between the existing models and the Earth are listed below.

6. Almost all the dynamo models reported so far create a strong axial dipole component (g_1^0). More precisely, the field harmonics define a power spectrum of approximately power law form, but the dipole lies "above" this spectrum; the quadrupolar contribution ($l = 2$) tends to lie below the spectrum. Both these characteristics are in encouraging agreement with the present Earth's field.

7. Other dipole and nondipole components seem to behave in a stochastic way, so that in a long run, their magnitudes follow normal distributions with zero mean. Such features were already anticipated from studies of the paleomagnetic field. The harmonics of the same degree l seem to have similar statistical properties.

8. An important exception to the above rule, seen both in the observations and in the behavior of the SK99 model, concerns the anomalously large amplitude of the $m = 1$ harmonics for $l = 2$. However, the coincidence may be a merely due to the short integration time of the SK99 model.

9. Some of the models showed that under certain inhomogeneous boundary conditions the axial quadrupole (g_2^0) or octupole (g_3^0) may be significantly correlated to the axial dipole (g_1^0). This is similar to the "dipole offset" observed by paleomagnetists.

10. A few models underwent magnetic reversals, which represent perhaps the most important characteristic of the Earth's magnetic field. In particular, *Glatzmaier et al.* [1999] showed that the frequency as well as the morphology of reversal depends strongly on the boundary conditions at the CMB. Some of their models gave reversals which are, in many ways, surprisingly similar to the paleomagnetically observed ones [see *Coe et al.*, 2000].

The remarkable progress in dynamo simulations is likely to continue for many years to come. There are some obstacles that may, however, not easily be surmounted. In closing this review, we shall point out some of the more important of these.

11. To attain the parameter range appropriate for the real Earth in dynamo simulations is a truly formidable task that no computer will be able to overcome in the near future. For example, consider the difficulty of resolving an Ekman layer of thickness 10 cm (or even 10 m) at the surface of a core 3500 km in radius! The increased spatial resolution necessitates the concomitant expense of very small time steps in the integrations. The large Rayleigh number and very small Ekman number of the Earth's core will pose severe obstacles for many years to come. Lacking an explosive growth in computer technology, one can hope for theoretical development or innovation in numerical methods that either can parametrize the physics well or can drastically diminish the computational load of small Ekman number calculations (see section 2.2.4).

12. Even if difficulty 11 were overcome, the correspondence between the simulations and the real Earth would remain imperfect until the physical properties of the core become better known than they are at present. However, we confidently expect that advances in seismology and mineral physics, including high-pressure experimentation and first principles calculations, will gradually fulfill the needs of geodynamo simulators.

13. In trying to compare the simulations with the observations, we became strongly aware of the inadequacy of the available data in many respects. Some of the shortcomings are inevitable: such as bad time resolution in paleomagnetic data or the geometrical factor R_E/R_0 defining the signal level at the surface of the Earth, which prohibits the

direct observation of small-scale features at the surface of the core. We felt, however, that many of the remaining problems can be solved. In particular, the paleomagnetic data do not yet have high enough quality nor a tolerable distribution in space or time. To make fruitful comparisons with simulation results, a dedicated effort will be required on the paleomagnetic side to obtain data that are sufficiently reliable and complete. We believe that the paleomagnetic community will rise to the challenge.

[197] In this review, comparisons were made mostly between the dynamo models and magnetic observations. Observations related to the core (and lowermost mantle) from other branches of geophysics are not so abundant nor easy to compare with dynamo models at present, but it can be hoped that comparison with these will become possible in the near future. For instance, length of day changes and polar wander on timescales of 100 years or longer or seismic signals related to core oscillation (the Slichter mode) are some of the candidates which can provide tests for geodynamos. For such comparisons, it goes almost without saying that the quality of the observed data will be of prime importance.

APPENDIX A: NOTATION AND CORE VALUES

[198] The symbols with the meaning and typical values appropriate for the core are summarized in Table A1.

Table A1. Notation and Typical Values Applicable to the Core[a]

Symbol	*Meaning*	*Definition*	*Value*	*Unit*
α	thermal expansion coefficient		10^{-5}	K^{-1}
α^{ξ}	compositional expansion coefficient			dimensionless
β	temperature gradient	$\partial T/\partial r$	1×10^{-12}	$K\ m^{-1}$
ε	generation of heat in a unit volume			$K\ s^{-1}$
ζ	radius ratio (inner core versus outer core)	R_1/R_0	0.351	dimensionless
η	magnetic diffusivity	$1/\mu_0\sigma$	2	$m^2\ s^{-1}$
Θ	temperature perturbation	$T - \bar{T}$	10^{-3}	K
κ	thermal diffusivity	$k/\rho\ c_p$	5×10^{-6}	$m^2\ s^{-1}$
Λ	Elsasser number	$B^2/2\Omega\ \mu_0\rho\eta$	O(10)	dimensionless
μ_0	permeability of vacuum		$4\pi \times 10^{-7}$	$H\ m^{-1}$
ν	kinematic viscosity		10^{-6}	$m^2\ s^{-1}$
ξ	fraction of light elements			dimensionless
ρ	density		$9.9–12.2 \times 10^3$	$kg\ m^{-3}$
σ	electric conductivity		4×10^5	$S\ m^{-1}$
ψ	magnetic potential (for external field)			T m
Ω	rotation rate of the mantle		7.27×10^{-5}	s^{-1}
$\mathbf{B}$	magnetic field		3×10^{-3}	T
$\hat{\mathbf{B}}$	magnetic field outside the core	$-\nabla\ \psi$	10^{-4}	T
C	codensity			dimensionless
c_p	heat capacity at constant pressure		840	$J\ kg^{-1}\ K^{-1}$
D	spherical shell thickness	$R_0 - R_1$	2.26×10^6	m
E	Ekman number	$\nu/2\Omega R_0^2$	10^{-15}	dimensionless
ε	Electromotive force	$\mathbf{V} \times \mathbf{B}$		V
G	gravitational constant		6.67×10^{-11}	$kg^{-1}\ m^3\ s^{-2}$
g	gravity		10.7–4.4	$m\ s^{-2}$
H	helicity	$\mathbf{V}\nabla \times \mathbf{V}$		$m\ s^{-2}$
$\mathbf{J}$	electric current	$\nabla \times \mathbf{B}\ \mu_0$		A
k	thermal conductivity		6×10^{-6}	$J\ m^{-1}\ s^{-1}\ K^{-1}$
P	pressure		$136–329 \times 10^9$	Pa
Pm	magnetic Prandtl number	ν/η	5×10^{-6}	dimensionless
Pr	Prandtl number	ν/κ	0.2	dimensionless
Q	dissipation			$W\ m^{-3}$
q	diffusivity ratio	κ/η	2×10^{-7}	dimensionless
R_0	radius of the outer core		3.48×10^6	m
R_1	radius of the inner core		1.22×10^6	m
R_E	radius of the Earth		6.37×10^6	m
Ra	Rayleigh number	$\alpha_0\beta_0 g_0 R_0^4/\nu\kappa$	10^{30}	dimensionless
Rm	magnetic Reynolds number	VR_0/η	$O(10^2)$	dimensionless
T	temperature		5000	K
$\mathbf{V}$	velocity		4×10^{-4}	$m\ s^{-1}$
$\mathbf{W}$	vorticity	$\nabla \times \mathbf{V}$		s^{-1}

[a]Subscript 0 and 1 are used to indicate values at the CMB and the ICB; β is the estimated superadiabatic temperature gradient in the core, which is different from the one used in the Boussinesq approximation [*Braginsky and Roberts*, 1995]. All diffusivities and Prandtl numbers are based on molecular values. The use of turbulent diffusivities, of the order of η, is probably more appropriate when studying core MHD; see *Braginsky and Meytlis* [1990].

GLOSSARY

α effect: The process through which a small-scale motion and a small-scale magnetic field create a large-scale electromotive force of the form $\alpha\langle\mathbf{B}\rangle$, where $\langle\mathbf{B}\rangle$ is the large-scale magnetic field. Close correlation between the α effect and helicity is noted.

Convection roll: An elongated convective cell, having the axis nearly parallel to the rotation axis, and occurring in convection in a rapidly rotating sphere or spherical shell.

Cowling's theorem: A theorem stating that a purely axisymmetric magnetic field cannot be sustained by dynamo action.

Critical Rayleigh number: The Rayleigh number (Ra_c) at which a convective system becomes marginally unstable. Convection takes place if the Rayleigh number Ra exceeds Ra_c.

Cyclone (anticyclone): A flow in a rotating fluid, associated a low (high) pressure, that has an anticlockwise (clockwise) circulation as seen from the north. The vorticity of such a system is parallel (antiparallel) to the angular velocity of the system.

Ekman layer: A boundary layer in the fluid adjacent to a solid surface in a highly rotating system, i.e., a system in which the Ekman number E is small.

Ekman suction/pumping: The flow into (out of) an Ekman boundary layer, created by anticyclonic (cyclonic) flow beneath the boundary layer.

Free convection: Convection which takes place in a fluid when the isothermal surfaces are necessarily oblique to gravity. Then convection must occur (unless the Rayleigh number is zero). This stands in contrast to situations where a motionless state can exist in which the isothermal surfaces are perpendicular to gravity. Then a critical Rayleigh number must be exceeded before convection can occur.

Geocentric axial dipole (GAD) hypothesis: A hypothesis that the magnetic field of the Earth can, when averaged over some long enough interval and excluding the rare cases of magnetic reversals and excursions, be well approximated by a field produced by a dipole located at the geocenter and aligned with the rotational axis.

Geodynamo hypothesis: The hypothesis that the Earth's magnetic field is produced by the dynamo action in the conducting liquid core, and not from other sources such as thermoelectric or electrochemical emfs, or permanent magnetism.

Geomagnetic spectrum: The dependence of the power R_l of the magnetic field on harmonic degree l. This depends on distance from the geocenter and is known, for the accessible values of l, to be nearly flat at the core-mantle boundary.

Helicity: The scalar product of velocity and vorticity ($\mathbf{V}\cdot\nabla\times\mathbf{V}$), which is positive (negative) if the streamlines of the flow spiral in a right-handed (left-handed) sense.

Hyperdiffusivity: A diffusivity that increases with decreasing wavelength. For example, hyperviscosity for horizontal scales of spherical convection may be defined by $\nu = \nu_0(1 + al^3)$, where ν_0 and a are constants and l is the spherical harmonic degree.

Intermediate dynamo: A two-dimensional MHD dynamo in which only the axisymmetric field and flow are considered, the field being prevented from collapse by an α effect.

Kinematic dynamo: A solution of the electrodynamic equations for a specified motion in a simply connected body of fluid conductor (such as a sphere or spherical shell) that maintains a magnetic field.

Magnetic excursion: A large swing in the direction of the paleomagnetic field (usually defined by the VGPs which deviate from the rotational axis by more than 45°) which almost reaches the reversed polarity but eventually returns to the original polarity. It is interpreted as either a very large amplitude secular variations or as an aborted reversal.

MHD dynamo: A homogeneous dynamo satisfying the full magnetohydrodynamic equations for a specified energy source (e.g., thermal or compositional buoyancy) and maintaining a magnetic field.

Model Z: An intermediate dynamo for a highly rotating fluid in which the zonal flow is so large that its Ekman pumping creates in the bulk of the fluid a significant meridional flow. A characteristic of the solution (which led its name) is that the meridional field created is almost parallel to the polar (z) axis, except near boundaries.

Natural remanent magnetization (NRM): Permanent magnetization carried by rocks, sediments, or artifacts such as bricks. They may have been acquired by cooling from high temperature (thermoremanent magnetization, *TRM*), by deposition (depositional remanent magnetization, *DRM*), or by other mechanisms.

ω effect: The process of stretching the meridional component of the magnetic field into zonal direction through the differential rotation in the fluid core.

Polarity reversal: The magnetic field of the Earth, which is, for most of the time, either in *normal* or *reverse* state. In the normal (reverse) state the VGP stays near the north (south) pole. A rapid transition from normal to reverse states, or vice versa, is called the polarity reversal and takes ~4000 years.

Proudman-Taylor theorem: A theorem that states that the slow, steady motion of a rotating, inviscid, incompressible fluid is two-dimensional with respect to the axis of rotation. It is therefore independent of the coordinate parallel to that axis. This provides what is called a rotational constraint.

Rayleigh-Bénard convection: Convection in a layer of uniform fluid of constant thickness and of infinite horizontal extent. A state of convective instability is created by maintaining the bottom of the layer at a higher temperature than that at the top.

Secular variation (SV): The fluctuations of the Earth's magnetic field over time spans of several decades or

longer. The long term ($>10^4$ years) fluctuations define the paleosecular variation (*PSV*).

Tangent cylinder: An imaginary cylinder drawn parallel to the angular velocity vector, and touching the inner core boundary on its equator.

Taylor state: An MHD dynamo for a rapidly rotating fluid in which inertial forces are negligible and in which viscous forces and Ekman layers play no essential role.

Virtual geomagnetic pole (VGP): A hypothetical dipole located at the center of the Earth which would produce the observed magnetic field direction at a specified site. Magnetic reversals are most often studied by the VGP paths corresponding to transitional directions.

[199] **ACKNOWLEDGMENTS.** We are grateful to Rob Coe, Gary Glatzmaier, Chris Jones, Akira Kageyama, Ataru Sakuraba, Hisayoshi Shimizu, and Keke Zhang for providing simulation data, programs, figures, and discussion. This review is based on material presented at the 8th SEDI symposium held in Exeter in the summer of 2000. The bulk of this review was written while M.K. was a guest of the Institute of Geophysics and Planetary Physics (IGPP), UCLA. He is grateful to the IGPP for the hospitality and to Mombusho for the travel grant that made this visit possible. We thank the publishers who permitted us to reproduce the figures in their journals; American Physical Society (Figures 2 and 6), American Institute of Physics (Figure 3), Elsevier Science B.V. (Figures 11, 12, and 13), Taylor and Francis (Figure 14), Nature Publishing Group (Figure 22), and the Royal Society of London (Figure 23). Other figures are newly drawn for this review with the use of the free software GMT, developed by *Wessel and Smith* [1991]. This work was partially supported by a grant-in-aid from Japan Society for Promotion of Science (12304024) awarded to M.K. P.H.R. thanks the NSF for support under grant EAR0074015.

REFERENCES

Backus, G., A class of self-sustaining dissipative spherical dynamos, *Ann. Phys., 4*, 372–447, 1958.

Backus, G., Poloidal and toroidal fields in geomagnetic field modeling, *Rev. Geophys., 24*, 75–109, 1986.

Bloxham, J., Core-mantle interactions and the palaeosecular variation, *Philos. Trans. R. Soc. London, Ser. A, 358*, 1171–1179, 2000a.

Bloxham, J., Sensitivity of the geomagnetic axial dipole to thermal core-mantle interactions, *Nature, 405*, 63–65, 2000b.

Bloxham, J., D. Gubbins, and A. Jackson, Geomagnetic secular variation, *Philos. Trans. R. Soc. London, Ser. A, 329*, 415–502, 1989.

Braginsky, S. I., Kinematic models of the Earth's hydromagnetic dynamo, *Geomagn. Aeron., 4*, 732–747, 1964. (*Geomagn. Aeron.*, Engl. Transl., *4*, 571–583, 1964.)

Braginsky, S. I., Nearly axially symmetric model of the hydromagnetic dynamo of the Earth, I, *Geomagn. Aeron., 15*, 149–156, 1975. (*Geomagn. Aeron.*, Engl. Transl., *15*, 122–128, 1975.)

Braginsky, S. I., and V. P. Meytlis, Local turbulence in the Earth's core, *Geophys. Astrophys. Fluid Dyn., 55*, 71–87, 1990.

Braginsky, S. I., and P. H. Roberts, A model-Z geodynamo, *Geophys. Astrophys. Fluid Dyn., 38*, 327–349, 1987.

Braginsky, S. I., and P. H. Roberts, Equations governing convection in Earth's core and the geodynamo, *Geophys. Astrophys. Fluid Dyn., 79*, 1–97, 1995.

Buffet, B. A., Gravitational oscillation in the length of day, *Geophys. Res. Lett., 23*, 2279–2282, 1996.

Bullard, E. C., The magnetic field within the Earth, *Proc. R. Soc. London, Ser. A, 197*, 433–453, 1949.

Bullard, E. C., and H. Gellman, Homogeneous dynamos and terrestrial magnetism, *Philos. Trans. R. Soc. London, Ser. A, 247*, 213–278, 1954.

Bullard, E. C., C. Freedman, H. Gellman, and J. Nixon, The westward drift of the Earth's magnetic field, *Philos. Trans. R. Soc. London, Ser. A, 243*, 67–92, 1950.

Busse, F. H., Thermal instabilities in rapidly rotating systems, *J. Fluid Mech., 44*, 441–460, 1970.

Busse, F. H., Patterns of convection in spherical shells, *J. Fluid Mech., 72*, 67–85, 1975.

Busse, F. H., Homogeneous dynamos in planetary cores and in the laboratory, *Annu. Rev. Fluid Mech., 32*, 383–408, 2000.

Cande, S. C., and D. V. Kent, Revised calibration of the geomagnetic polarity timescale for the Late Cretaceous and Cenozoic, *J. Geophys. Res., 100*, 6093–6095, 1995.

Champion, D. E., M. A. Lanphere, and M. A. Kuntz, Evidence for a new geomagnetic reversal from lava flows in Idaho: Discussion of short polarity reversals in the Brunhes and late Matuyama polarity chrons, *J. Geophys. Res., 93*, 11,667–11,680, 1988.

Chandrasekhar, S., *Hydrodynamic and Hydromagnetic Stability*, 654 pp., Oxford Univ. Press, New York, 1961.

Christensen, U., P. Olson, and G. A. Glatzmaier, A dynamo model interpretation of geomagnetic field structures, *Geophys. Res. Lett., 25*, 1565–1568, 1998.

Christensen, U., P. Olson, and G. A. Glatzmaier, Numerical modeling of the geodynamo: A systematic parameter study, *Geophys. J. Int., 138*, 393–409, 1999.

Christensen, U.R., et al., A numerical dynamo benchmark, *Phys. Earth Planet. Inter., 128*, 25–34, 2001.

Coe, R. S., and M. Prévot, Evidence suggesting extremely rapid field variation during a geomagnetic reversal, *Earth Planet. Sci. Lett., 92*, 292–298, 1989.

Coe, R. S., L. Hongre, and G. A. Glatzmaier, An examination of simulated geomagnetic reversals from a palaeomagnetic perspective, *Philos. Trans. R. Soc. London, Ser. A, 358*, 1141–1170, 2000.

Constable, C. G., and R. L. Parker, Statistics of the geomagnetic secular variation for the past 5 m.y., *J.Geophys. Res., 93*, 11,569–11,581, 1988.

Cowling, T. G., The magnetic field of sunspots, *Mon. Not. R. Astron. Soc., 94*, 39–48, 1934.

Cox, A., Latitude dependence of the angular dispersion of the geomagnetic field, *Geophys. J. R. Astron. Soc., 20*, 253–269, 1970.

Davidson, P. G., *An Introduction to Magnetohydrodynamics*, 431 pp., Cambridge Univ. Press, New York, 2001.

Dormy, E., J.-P. Valet, and V. Courtillot, Numerical models of the geodynamo and observational constraints, *Geochem. Geophys. Geosyst., 1*(Article), 2000GC000062 [23,981 words], 2000.

Dudley, M. L., and R. W. James, Time-dependent kinematic dynamos with stationary flows, *Proc. R. Soc. London, Ser. A, 425*, 407–429, 1989.

Dziewonski, A. M., and D. L. Anderson, Preliminary reference Earth model, *Phys. Earth Planet. Inter., 25*, 297–356, 1981.

Elsasser, W. M., Induction effects in terrestrial magnetism, 1, Theory, *Phys. Rev., 69*, 106–116, 1946.

Fearn, D. R., and G. Morrison, The role of inertia in hydro-

dynamic models of the geodynamo, *Phys. Earth Planet. Inter., 128*, 75–92, 2001.

Gilman, P. A., Dynamically consistent nonlinear dynamos driven by convection in a rotating spherical shell, II, Dynamos with cycles and strong feedbacks, *Astrophys. J. Suppl. Ser., 53*, 243–268, 1983.

Gilman, P. A., and J. Miller, Dynamically consistent nonlinear dynamos driven by convection in a rotating spherical shell, *Astrophys. J. Suppl., 46*, 211–238, 1981.

Glatzmaier, G. A., Numerical simulation of stellar convective dynamos, I, The model and method, *J. Comput. Phys., 55*, 461–484, 1984.

Glatzmaier, G. A., Numerical simulations of stellar convective dynamos, II, Field propagation in the convection zone, *Astrophys. J., 291*, 300–307, 1985a.

Glatzmaier, G.A., Numerical simulations of stellar convective dynamos, III, At the bottom of the convection zone, *Geophys. Astrophys. Fluid Dyn., 31*, 137–150, 1985b.

Glatzmaier, G. A., and P. H. Roberts, A three-dimensional convective dynamo solution with rotating and finitely conducting inner core and mantle, *Phys. Earth Planet. Inter., 91*, 63–75, 1995a.

Glatzmaier, G. A., and P. H. Roberts, A three-dimensional self-consistent computer simulation of a geomagnetic field reversal, *Nature, 377*, 203–209, 1995b.

Glatzmaier, G. A., and P. H. Roberts, An anelastic evolutionary geodynamo simulation driven by compositional and thermal convection, *Physica D, 97*, 81–94, 1996a.

Glatzmaier, G. A., and P. H. Roberts, Rotation and magnetism of Earth's inner core, *Science, 274*, 1887–1891, 1996b.

Glatzmaier, G. A., and P. H. Roberts, Simulating the geodynamo, *Contemp. Phys., 38*, 269–288, 1997.

Glatzmaier, G. A., R. S. Coe, L. Hongre, and P. H. Roberts, The role of the Earth's mantle in controlling the frequency of geomagnetic reversals, *Nature, 401*, 885–890, 1999.

Grote, E., F. H. Busse, and A. Tilgner, Convection-driven quadrupolar dynamos in rotating spherical shells, *Phys. Rev. E, 60*, R5025–R5028, 1999.

Grote, E., F. H. Busse, and A. Tilgner, Regular and chaotic spherical dynamos, *Phys. Earth Planet. Inter., 117*, 259–272, 2000a.

Grote, E., F. H. Busse, and A. Tilgner, Effects of hyperdiffusivities on dynamo simulations, *Geophys. Res. Lett., 27*, 2001–2004, 2000b.

Gubbins, D., Numerical solutions of the kinematic dynamo problem, *Philos. Trans. R. Soc. London, Ser. A, 274*, 493–521, 1973.

Guyodo, Y., and J.-P. Valet, Relative variations in geomagnetic intensity from sedimentary records: The past 200,000 years, *Earth Planet. Sci. Lett., 143*, 23–36, 1996.

Guyodo, Y., and J.-P. Valet, Global changes in geomagnetic intensity during the past 800 thousand years, *Nature, 399*, 249–252, 1999.

Hale, C. J., Palaeomagnetic data suggest link between the Archaean-Proterozoic boundary and inner-core nucleation, *Nature, 329*, 233–237, 1987.

Herzenberg, A., Geomagnetic dynamos, *Philos. Trans. R. Soc. London, Ser. A, 250*, 543–583, 1958.

Hoffman, K. A., Long-lived transitional states of the geomagnetic field and the two dynamo families, *Nature, 354*, 273–277, 1991.

Hollerbach, R., A spectral solution of the magneto-convection equations in spherical geometry, *Int. J. Numer. Methods Fluids, 32*, 773–797, 2000.

Hollerbach, R., and C. A. Jones, Influence of the Earth's inner core on geomagnetic fluctuations and reversals, *Nature, 365*, 541–543, 1993.

Howard, R. F., and B. J. Labonte, Surface magnetic fields during the solar activity cycle, *Sol. Phys., 74*, 131–145, 1981.

Ishihara, N., and S. Kida, Axial and equatorial magnetic dipoles generated in a rotating spherical shell, *J. Phys. Soc. Jpn., 69*, 1582–1585, 2000.

Jackson, A., A. R. T. Jonkers, and M. R. Walker, Four centuries of geomagnetic secular variation from historical records, *Philos. Trans. R. Soc. London, Ser. A, 358*, 957–990, 2000.

Jault, D., Model Z by computation and Taylor's condition, *Geophys. Astrophys. Fluid Dyn., 79*, 99–124, 1995.

Johnson, C., and C. G. Constable, The time averaged geomagnetic field: Global and regional biases for 0–5 Ma, *Geophys. J. Int., 131*, 643–666, 1997.

Jones, C. A., Convection-driven geodynamo models, *Philos. Trans. R. Soc. London, Ser. A, 358*, 873–897, 2000.

Jones, C. A., and P. H. Roberts, The onset of convection at large Prandtl number in a rotating layer, II, Small magnetic diffusion, *Geophys. Astrophys. Fluid Dyn., 93*, 173–226, 2000a.

Jones, C. A., and P. H. Roberts, Convection-driven dynamos in a rotating plane layer, *J. Fluid Mech., 404*, 311–343, 2000b.

Jones, C. A., A. M. Soward, and A. I. Mussa, The onset of thermal convection in a rapidly rotating sphere, *J. Fluid Mech., 405*, 157–179, 2000.

Kageyama, A., and T. Sato, Velocity and magnetic field structures in a magnetohydrodynamic dynamo, *Phys. Plasmas, 4*, 1569–1574, 1997a.

Kageyama, A., and T. Sato, Dipole field generation by an MHD dynamo, *Plasma Phys. Controlled Fusion, 39*, A83–A91, 1997b.

Kageyama, A., and T. Sato, Generation mechanism of a dipole field by a magnetohydrodynamic dynamo, *Phys. Rev. E, 55*, 4617–4626, 1997c.

Kageyama, A., K. Watanabe, and T. Sato, Simulation study of a magnetohydrodynamic dynamo: Convection in a rotating spherical shell, *Phys. Fluids, 5*, 2793–2805, 1993.

Kageyama, A., T. Sato, and the Complexity Simulation Group, Computer simulation of a magnetohydrodynamic dynamo, II, *Phys. Plasmas, 2*, 1421–1431, 1995.

Katayama, J. S., M. Matsushima, and Y. Honkura, Some characteristics of magnetic field behavior in a model of MHD dynamo thermally driven in a rotating spherical shell, *Phys. Earth Planet. Inter., 111*, 141–159, 1999.

Kent, D. V., and M. Smethurst, Shallow bias of paleomagnetic inclinations in the Paleozoic and Precambrian, *Earth Planet. Sci. Lett., 160*, 391–402, 1998.

Kida, S., and H. Kitauchi, Thermally driven MHD dynamo in a rotating spherical shell, *Prog. Theor. Phys., 130*, 121–136, 1998a.

Kida, S., and H. Kitauchi, Chaotic reversals of dipole moment of thermally driven magnetic field in a rotating spherical shell, *J. Phys. Soc. Jpn., 67*, 2950–2951, 1998b.

Kida, S., K. Araki, and H. Kitauchi, Periodic reversals of magnetic field generated by thermal convection in a rotating spherical shell, *J. Phys. Soc. Jpn., 66*, 2194–2201, 1997.

Kitauchi, H., and S. Kida, Intensification of magnetic field by concentrate-and-stretch of magnetic flux lines, *Phys. Fluid, 10*, 457–468, 1998.

Kono, M., Mathematical models of the Earth's magnetic field, *Phys. Earth Planet. Inter., 5*, 140–150, 1972.

Kono, M., and P. H. Roberts, Rayleigh number for geodynamo simulations, *Phys. Earth Planet. Inter., 128*, 13–24, 2001.

Kono, M., and H. Tanaka, Mapping the Gauss coefficients to the pole and the models of paleosecular variation, *J. Geomagn. Geoelectr., 47*, 115–130, 1995a.

Kono, M., and H. Tanaka, Intensity of the geomagnetic field in geological time: A statistical study, in *The Earth's Central Part: Its Structure and Dynamics*, edited by T. Yukutake, pp. 75–94, Terrapub, Tokyo, 1995b.

Kono, M., H. Tanaka, and H. Tsunakawa, Spherical harmonic

inversion of paleomagnetic data: The case of linear mapping, *J. Geophys. Res., 105*, 5817–5833, 2000a.

Kono, M., A. Sakuraba, and M. Ishida, Dynamo simulation and paleosecular variation models, *Philos. Trans. R. Soc. London, Ser. A, 358*, 1123–1139, 2000b.

Krause, F., and K.-H. Rädler, *Mean-Field Magnetohydrodynamics and Dynamo Theory*, 271 pp., Akademie, Berlin, 1980.

Kuang, W., and J. Bloxham, An Earth-like numerical dynamo model, *Nature, 389*, 371–374, 1997.

Kuang, W., and J. Bloxham, Numerical dynamo modeling: Comparison with the Earth's magnetic field, in *The Core-Mantle Boundary Region, Geodyn. Ser.*, vol. 28, edited by M. Gurnis et al., pp. 197–208, AGU, Washington, D. C., 1998.

Kuang, W., and J. Bloxham, Numerical modeling of magnetohydrodynamic convection in a rapidly rotating spherical shell: Weak and strong field dynamo action, *J. Comput. Phys., 153*, 51–81, 1999.

Kumar, S., and P. H. Roberts, A three-dimensional kinematic dynamo, *Proc. R. Soc. London, Ser. A, 344*, 235–258, 1975.

Kutzner, C., and U. Christensen, Effects of driving mechanisms in geodynamo models, *Geophys. Res. Lett., 27*, 29–32, 2000.

Laj, C., and C. Kissel, Geomagnetic field intensity at Hawaii for the last 420 kyr from the Hawaii Scientific Drilling Project core, Big Island, Hawaii, *J. Geophys. Res., 104*, 15,317–15,338, 1999.

Laj, C., A. Mazaud, R. Weeks, M. Fuller, and E. Herrero-Bervera, Geomagnetic reversal paths, *Nature, 351*, 447, 1991.

Langel, R. A., The main field, in *Geomagnetism*, vol. 1, edited by J. A. Jacobs, pp. 249–512, Academic, San Diego, Calif., 1987.

Langel, R. A., and R. H. Estes, A geomagnetic field spectrum, *Geophys. Res. Lett., 9*, 250–253, 1982.

Larmor, J., How could a rotating body such as the Sun become a magnet, *Rep. Br. Assoc. Adv. Sci., 1919*, 159–60, 1919.

Lesieur, M., and O. Metais, New trends in large-eddy simulations of turbulence, *Annu. Rev. Fluid Mech., 28*, 45–82, 1996.

Love, J. J., and A. Mazaud, A database for the Matuyama-Brunhes magnetic reversal, *Phys. Earth Planet. Inter., 103*, 207–245, 1997.

Lowes, F. J., Spatial power spectrum of the main geomagnetic field, and extrapolation to the core, *Geophys. J. R. Astron. Soc., 36*, 717–730, 1974.

Malkus, W. V. R., Precession as the cause of geomagnetism, *Science, 160*, 259–264, 1968.

Matsushima, M., Expression of turbulent heat flux in the Earth's core in terms of a second moment closure model, *Phys. Earth Planet. Inter., 128*, 137–148, 2001.

Matsushima, M., T. Nakajima, and P. H. Roberts, The anisotropy of local turbulence in the Earth's core, *Earth Planets Space, 51*, 277–286, 1999.

McFadden, P. L., and M. W. McElhinny, Variations in the geomagnetic dipole, 2, Statistical analysis of VDMs for the past 5 million years, *J. Geomagn. Geoelectr., 34*, 163–189, 1982.

McFadden, P. L., and R. T. Merrill, Fundamental transitions in the geodynamo as suggested by paleomagnetic data, *Phys. Earth Planet. Inter., 91*, 253–260, 1995.

Meneveau, C., and J. Katz, Scale-invariance and turbulence models for large-eddy simulation, *Annu. Rev. Fluid Mech., 32*, 1–32, 2000.

Merrill, R. T., M. W. McElhinny, and P. L. McFadden, *The Magnetic Field of the Earth: Paleomagnetism, the Core, and the Deep Mantle*, 527 pp., Academic, San Diego, Calif., 1996.

Moffatt, H. K., *Magnetic Field Generation in Electrically Conducting Fields*, 343 pp., Cambridge Univ. Press, New York, 1978.

Néel, L., Theorie du trainage magnetique des ferromagnetique en grain fins avec applications aux terres cuites, *Ann. Géophys., 5*, 99–136, 1949.

Ochi, M. M., A. Kageyama, and T. Sato, Dipole and octopole field reversals in a rotating spherical shell: Magnetohydrodynamic dynamo simulation, *Phys. Plasmas, 6*, 777–787, 1999.

Olsen, N., et al., Ørsted initial field model, *Geophys. Res. Lett., 27*, 3607–3610, 2000.

Olson, P., U. Christensen, and G. A. Glatzmaier, Numerical modeling of the geodynamo: Mechanisms of field generation and equilibration, *J. Geophys. Res., 104*, 10,383–10,404, 1999.

Opdyke, N. D., and J. E. T. Channell, *Magnetic Stratigraphy*, 346 pp., Academic, San Diego, Calif., 1996.

Parker, E. N., Hydromagnetic dynamo models, *Astrophys. J., 122*, 239–314, 1955.

Pekeris, C. L., Y. Accad, and B. Shkoller, Kinematic dynamos and the Earth's magnetic field, *Philos. Trans. R. Soc. London, Ser. A, 275*, 425–461, 1973.

Prévot, M., and P. Camps, Absence of preferred longitude sectors for poles from volcanic records of geomagnetic reversals, *Nature, 366*, 53–57, 1993.

Prévot, M., M. E.-M. Derder, M. McWilliams, and J. Thompson, Intensity of the Earth's magnetic field: Evidence for a Mesozoic dipole low, *Earth Planet. Sci. Lett., 97*, 129–139, 1990.

Quidelleur, X., J.-P. Valet, V. Courtillot, and G. Hulot, Long-term geometry of the geomagnetic field for the last five million years: An updated secular variation database, *Geophys. Res. Lett., 21*, 1639–1642, 1994.

Roberts, P. H., On the thermal instability of a rotating-fluid sphere containing heat sources, *Proc. R. Soc. London, Ser. A, 263*, 93–117, 1968.

Roberts, P. H., Dynamo theory of geomagnetism, in *World Magnetic Survey 1957–1969*, edited by A. J. Zmuda, *IAGA Bull. 28*, pp. 123–131, IUGG Publ. Off., Paris, 1971.

Roberts, P. H., and G. A. Glatzmaier, A test of the frozen-flux approximation using a new geodynamo model, *Philos. Trans. R. Soc. London, Ser. A, 358*, 1109–1121, 2000a.

Roberts, P. H., and G. A. Glatzmaier, Geodynamo theory and simulations, *Rev. Mod. Phys., 72*, 1081–1123, 2000b.

Roberts, P. H., and G. A. Glatzmaier, The geodynamo, past, present and future, *Geophys. Astrophys. Fluid Dyn., 94*, 47–84, 2001.

Roberts, P. H., and C. A. Jones, The onset of convection at large Prandtl number in a rotating layer, I, Finite magnetic diffusion, *Geophys. Astrophys. Fluid Dyn., 92*, 289–325, 2000.

Sakuraba, A., and M. Kono, Effect of the inner core on the numerical solution of the magnetohydrodynamic dynamo, *Phys. Earth Planet. Inter., 111*, 105–121, 1999.

Sakuraba, A., and M. Kono, Effect of a uniform magnetic field on nonlinear magnetoconvection in a rotating fluid spherical shell, *Geophys. Astrophys. Fluid Dyn., 92*, 255–287, 2000.

Sarson, G. R., and C. A. Jones, A convection driven geodynamo reversal model, *Phys. Earth Planet. Inter., 111*, 3–20, 1999.

Sarson, G. R., C. A. Jones, and A. W. Longbottom, Convection driven geodynamo models of varying Ekman number, *Geophys. Astrophys. Fluid Dyn., 88*, 225–259, 1998.

Selkin, P. A., and L. Tauxe, Long-term variations in palaeointensity, *Philos. Trans. R. Soc. London, Ser. A, 358*, 1065–1088, 2000.

Shimizu, H., and D. E. Loper, Time and length scales of buoyancy-driven flow structures in a rotating hydromagnetic fluid, *Phys. Earth Planet. Inter., 104*, 307–329, 1997.

Song, X. D., and P. G. Richards, Observational evidence for differential rotation of the Earth's inner core, *Nature, 382*, 221–224, 1996.

Soward, A. M., On the finite amplitude thermal instability of a rapidly rotating fluid sphere, *Geophys. Astrophys. Fluid Dyn., 9*, 19–74, 1977.

St. Pierre, M. G., On the local nature of turbulence in Earth's outer core, *Geophys. Astrophys. Fluid Dyn., 83*, 293–306, 1996.

Steenbeck, M., and F. Krause, The generation of stellar and planetary magnetic fields by turbulent dynamo action, *Z. Naturforsch. A, 21*, 1285–1296, 1966.

Steenbeck, M., F. Krause, and K.-H. Rädler, A calculation of the mean electromotive force in an electrically conducting fluid in turbulent motion, under the influence of Coriolis forces, *Z. Naturforsch. A, 21*, 369–376, 1966.

Stevenson, A. F., and S. J. Wolfson, Calculations on the 'dynamo' problem of the Earth's magnetic field, *J. Geophys. Res., 71*, 4446–4447, 1966.

Su, W. J., R. Woodward, and A. M. Dziewonski, Degree 12 model of shear velocity in the mantle, *J. Geophys. Res., 99*, 6945–6980, 1994.

Su, W. J., A. M. Dziewonski, and R. Jeanloz, Planet within a planet: Rotation of the inner-core of Earth, *Science, 274*, 1883–1887, 1996.

Tanaka, H., M. Kono, and H. Uchimura, Some global features of paleointensity in geological time, *Geophys. J. Int., 120*, 97–102, 1995.

Tauxe, L., Sedimentary records of relative paleointensity of the geomagnetic field: Theory and practice, *Rev. Geophys., 31*, 319–354, 1993.

Taylor, J. B., The magnetohydrodynamics of a rotating fluid and the Earth's dynamo problem, *Proc. R. Soc. London, Ser. A, 274*, 274–283, 1963.

Valet, J.-P., and L. Meynadier, Geomagnetic field intensity and reversals during the past four million years, *Nature, 366*, 234–238, 1993.

Vanyo, J.P., A geodynamo powered by luni-solar precession, *Geophys. Astrophys. Fluid Dyn., 59*, 209–234, 1991.

Walker, M. R., and C. F. Barenghi, Accurate numerical computations of Taylor integrals, *Geophys. Astrophys. Fluid Dyn., 87*, 173–191, 1998.

Wang, T.-M., N. P. Sheeley, and A. G. Nash, A new solar cycle model including meridional circulations, *Astrophys. J., 383*, 431–442, 1991.

Wessel, P., and W. H. F. Smith, Free software helps map and display data, *Eos Trans. AGU, 72*, 441, 445–446, 1991.

Wilson, R. L., Permanent aspects of the Earth's non-dipole magnetic field over upper tertiary times, *Geophys. J. R. Astron. Soc., 19*, 417–437, 1970.

Yukutake, T., and H. Tachinaka, Separation of the Earth's magnetic field into the drifting and the standing parts, *Bull. Earthquake Res. Inst. Univ. Tokyo, 47*, 65–97, 1969.

Zhang, K.-K., and F. H. Busse, Finite amplitude convection and magnetic field generation in a rotating spherical shell, *Geophys. Astrophys. Fluid Dyn., 44*, 33–53, 1988.

Zhang, K.-K., and F. H. Busse, Convection driven magnetohydrodynamic dynamos in rotating spherical shells, *Geophys. Astrophys. Fluid Dyn., 49*, 97–116, 1989.

Zhang, K.-K., and F. H. Busse, Generation of magnetic fields by convection in a rotating spherical fluid shell of infinite Prandtl number, *Phys. Earth Planet. Inter., 59*, 208–222, 1990.

M. Kono, Institute for Study of the Earth's Interior, Okayama University, Yamada 827, Misasa, Tottori-ken 682-0193, Japan. (mkono@misasa.okayama-u.ac.jp)

P. H. Roberts, Institute of Geophysics and Planetary Physics, University of California, Los Angeles, CA 90095-1567, USA. (roberts@math.ucla.edu)